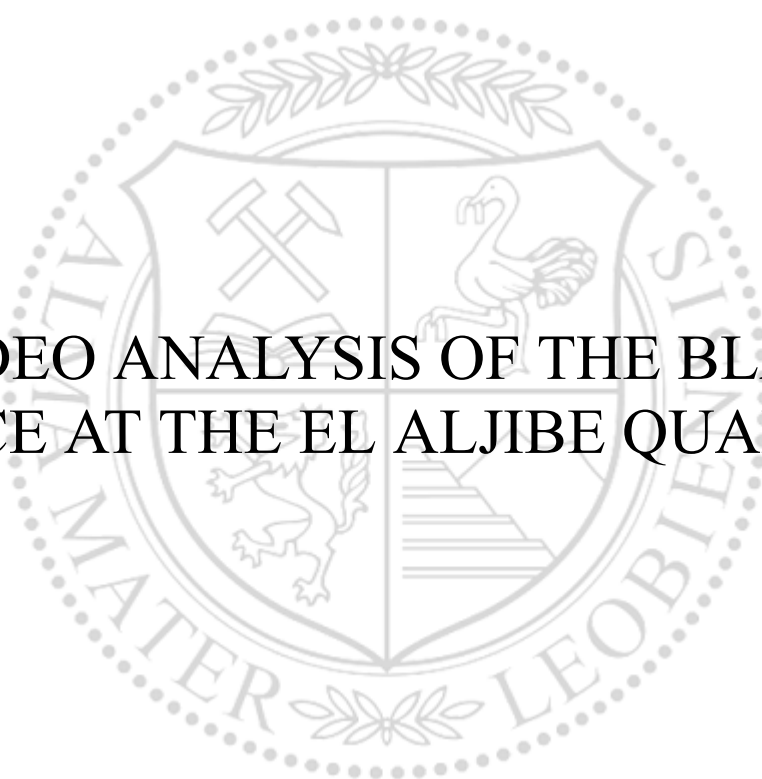




Montanuniversitaet Leoben

Master's Thesis

**VIDEO ANALYSIS OF THE BLAST
FACE AT THE EL ALJIBE QUARRY**



Maria del Pilar Franco Garcia

February 2022

**ESCUELA TÉCNICA SUPERIOR DE INGENIEROS DE MINAS Y
ENERGÍA**

International joint master's degree programme:

ADVANCED MINERAL RESOURCES DEVELOPMENT

&

MASTER UNIVERSITARIO EN MINERÍA SOSTENIBLE

**VIDEO ANALYSIS OF THE BLAST FACE AT THE EL ALJIBE
QUARRY**

Author:

María del Pilar Franco García

Supervisors:

Pablo Segarra Catasús

Santiago Gómez Mateos

**Department of Geological and Mining Engineering – ETSI Minas y
Energía**

AGRADECIMIENTOS

Han pasado dos años desde que comencé este máster. Tiempo que me ha permitido poder vivir una gran aventura. Primero viviendo fuera de casa, en Leoben (Austria). Un lugar perdido por el mundo y del que he acabado enamorada. Y después estudiando en la universidad de Freiberg (Alemania), que por la pandemia del COVID-19 ha tenido que ser a distancia. Pero, sobre todo, he tenido la suerte de haber vivido la mejor experiencia de mi vida rodeada de gente maravillosa. Algunas que me llevan acompañando toda la vida y otras que he conocido por el camino. Quiero aprovechar este espacio darles las gracias.

En primer lugar, quiero dar las gracias a mis dos tutores, Santiago Gómez y Pablo Segarra. A Santi, gracias por ayudarme con mis bloqueos con el MATLAB, con mis dudas y con mis momentos de no poder más con el proyecto. A Pablo, como ya dije en el TFG, gracias por hacerme progresar y por querer siempre sacar lo mejor de mí. Gracias a los dos por toda vuestra dedicación conmigo.

A la gente maravillosa que he conocido gracias al máster y con la que he compartido la aventura de mi vida: Mislav, Kristin, Adriana, Diogo, Dasha, Elena...

A mis amigos de Madrid, por soportarme desde la distancia y por estar ahí en los momentos no tan buenos que he podido vivir.

A mi Núcleo: Carlota, Elena, Javi G, Jorge, Fer y Jero. Sé que con vosotros he encontrado amigos de los de verdad. Os habéis convertido en familia y espero que lo que unió Leoben dure toda nuestra vida. ¡Qué suerte tuve al encontrarlos!

A Javi, mi hogar, mi alma gemela. Gracias por compartir conmigo todas aquellas noches de charleteo y Cola Cao. Gracias por todas las risas, abrazos, besos, planes y locuras que han venido después. Gracias por apoyarme en todas las decisiones que he tomado hasta ahora y por hacer de tu vida la mía. Gracias por hacerme tan feliz.

Por último, gracias a toda mi familia, por preocuparse por mí y por el empujoncito hacia delante cuando lo he necesitado. En especial GRACIAS a mis padres Dulce y Juan Carlos. Gracias por ayudarme a cumplir mis objetivos y mis sueños sin importar lo que cuesten. Gracias por ser mi apoyo incondicional.

Muchas gracias a todos.

TABLE OF CONTENTS

RESUMEN	VII
ABSTRACT	VIII
REPORT	1
1 Introduction	1
1.1 Objective and scope	1
1.2 Background.....	1
2 Description of the blasts	4
2.1 Location of the blasts in the quarry	4
2.2 Geometric measurements.....	5
2.3 Set-up of the blasts and its high-speed video.....	8
3 Transformation system and rock coordinates transformations.....	11
3.1 Rock coordinate transformation.....	15
4 Determination of the position of each fragment in relation to the plane YZ	18
4.1 Burden matrix and borehole coordinates	18
4.2 Projection of 3D points of the BM and targets onto the YZ reference plane.	
23	
5 Trajectory determination for each fragment.....	26
5.1 Adjusting trajectories.....	26
5.2 3D Model.....	31
5.3 Burden and height of each rock	33
6 Response time.....	33
7 Correlation between parameters.....	35
8 Response time and initial velocity analysis.....	38
8.1 Analysis of response time	39
8.2 Analysis of initial velocity.....	41
8.3 Analysis of ejection angle (α)	43
9 Conclusions.....	46
10 References and Bibliography.....	47

ABBREVIATIONS	51
List of measured parameters	51
APPENDIX A: Position of reference targets used to film the blasts ...	55
APPENDIX B: Trajectory of the rocks measured from the video	60
APPENDIX C: Trajectory of the rocks from the transformation system	68
APPENDIX D: Burden matrix and profiles for each blast obtained from software Quarry X.....	76
1 Burden matrix.....	76
2 Profiles	79
APPENDIX E: MATLAB Code.....	86
1 Main code	86
2 Function: myfun	99
3 Function: funveloc2	99
4 Function: funtrayect2.....	101
5 Function: fundist3.....	103
6 Function: fundist4.....	107
7 Analysis of response time, initial velocity and ejection angle (α)	111
8 Correlations.....	115
9 Azimuth calculation.....	116
10 Initial velocity as a quadratic function	117

TABLE OF CONTENTS: Tables

Report

Table 1: Summary of geometrical data I (Segarra P. , et al., 2018) and (Segarra P. , et al., 2019).....	6
Table 2: Summary of geometrical data II (Segarra P. , et al., 2018) and (Segarra P. , et al., 2019).....	6
Table 3: Data for calculation of specific consumption of each blast.....	7
Table 4: Specific consumption of borehole for each blast.	7
Table 5: Setups of the camera for the twelve blasts (Segarra P. , et al., 2018) and (Segarra P. , et al., 2019).....	11
Table 6: Borehole selected for each blast and its length and its azimuth.....	12
Table 7: Model coefficients $c1^*$, $c2^*$, $b1, 1^*$, $b1, 2^*$, $b2, 1^*$, $b2, 2^*$	15
Table 8: Approximated time when the rock starts to move.....	16
Table 9: Mean diameter for each rock measured in the video.....	17
Table 10: Ejection angle formed by the initial velocity components ($^{\circ}$) and initial velocity for rocks of each blast (m/s)	28
Table 11: minimum error of the trajectory adjustment for rocks of each blast (m)	29
Table 12: Burden and height for rocks of each blast*	33
Table 13: Response time for rocks of each blast, with $w = 1t2$	34
Table 14: Initial parameters of each rock	35
Table 15: Results from analysis of model 1 for response time	39
Table 16: Other parameters for each blast.....	40
Table 17: Results from analysis of model 2 for response time	41
Table 18: Results from analysis of model 1 for initial velocity	42
Table 19: Results from analysis of model 2 for initial velocity	43
Table 20: Results from analysis of model 1 for ejection angle	44
Table 21: Results from analysis of model 2 for ejection angle	45

Appendix A

Table A_1: Absolute coordinates of the targets for each blast.....	55
Table A_2: Local coordinates obtained from the video (U_C) versus field coordinates measured in YZ local plane (U_R) versus local coordinates obtained from the transformation system (\hat{U}_R)	57

Appendix B

Table B_1: Trajectory of rocks from the video of blast 4	60
Table B_2: Trajectory of rocks from the video of blast 6	61
Table B_3: Trajectory of rocks from the video of blast 8	62
Table B_4: Trajectory of rocks from the video of blast 10	64
Table B_5: Trajectory of rocks from the video of blast 11	65
Table B_6: Trajectory of rocks from the video of blast 12	66

Appendix C

Table C_1: Trajectory of rocks from the transformation system of blast 4	68
Table C_2: Trajectory of rocks from the transformation system of blast 6	69
Table C_3: Trajectory of rocks from the transformation system of blast 8	70
Table C_4: Trajectory of rocks from the transformation system of blast 10	72
Table C_5: Trajectory of rocks from the transformation system of blast 11	73
Table C_6: Trajectory of rocks from the transformation system of blast 12	74

TABLE OF CONTENTS: Figures

Report

Figure 1: Location of “El Aljibe” quarry.....	3
Figure 2: Ultramylonite (a), orthomylonite (b), prothomylonite (c) and cataclasite (d) from “El Aljibe” quarry. Source: (Fueyo & de la Cuadra, 2016).....	4
Figure 3: Orthophoto of the quarry showing the pit (left) and the processing plant; right: highwall faces of the twelve blasts; DS1 and DS2 refer to the first and second campaign, respectively (Bernardini, Paredes, Sanchidrian, Segarra, & Gomez).....	5
Figure 4: Correlation plot between specific consumption (q) and burden mean (B_{mean}), Spacing (S_p) and Bench height (H_b)	8
Figure 5: Location of an external detonator (B4). Source: (Navarro, Segarra, & Castedo, 2018).....	9
Figure 6: Reference targets. a) procedure to locate the reference targets in blast. b) plane formed by these targets in which rock motion is tracked.	9
Figure 7: High-speed camera " FastCam Sa 3", model 120k C2, manufactured by Photron used for the recording of blasting (Photron Limited, 2014)	10
Figure 8: Transformation system between coordinates in the field and coordinates in the video. Red crosses indicate the position of the targets. Source: (Navarro, Segarra, & Castedo, 2018).....	13
Figure 9: Skewing over Y axis. Source: (Navarro, Segarra, & Castedo, 2018)	14
Figure 10: Analysis of rock trajectory in blast B8 with Photron Fastcam Viewer software. Source: (Segarra P. , et al., 2019)	17
Figure 11: Burden matrix transformation scheme with respect to borehole coordinates for an idealized vertical hole.	20
Figure 12: 3D plot of BM and borehole selected for each blast.....	22
Figure 13: Projection on the plane of the targets for each blast.	24
Figure 14: Profile of the burden for each blast ($D_2=0$).....	25
Figure 15: Forces acting on the gravity centre of the rock. Source: (Segarra P. , et al., 2003).....	26
Figure 16: Trajectories of fragment rock measured for each blast.....	30
Figure 17: 3D plot of each blast.	32
Figure 20: Correlation plot for parameters from Table 14	36

Figure 21: Initial velocity vs. rock height to bench height ratio (0 and 100 % corresponds to the toe and crest, respectively)	37
--	----

Appendix D

Figure D_1: Burden matrix of blast 4.....	76
Figure D_2: Burden matrix of blast 6.....	76
Figure D_3: Burden matrix of blast 8.....	77
Figure D_4: Burden matrix of blast 10.....	77
Figure D_5: Burden matrix of blast 11.....	78
Figure D_6: Burden matrix of blast 12.....	78
Figure D_7: Profile of blast 4	79
Figure D_8: Profile of blast 6	80
Figure D_9: Profile of blast 8	81
Figure D_10: Profile of blast 10	82
Figure D_11: Profile of blast 11	83
Figure D_12: Profile of blast 12	84

RESUMEN

El objetivo principal de este TFM es determinar un modelo matemático para la estimación del movimiento del frente de 6 voladuras llevadas a cabo en la cantera de “El Aljibe” en Almonacid de Toledo (Toledo, España) dentro del proyecto SLIM (Sustainable Low Impact Mining) financiado por la Comisión Europea dentro del programa de investigación e innovación con convenio de subvención No. 730294.

Para cada una de las voladuras se han transformado los datos obtenidos a partir de grabaciones con una cámara de alta velocidad en coordenadas referidas a un plano perpendicular al frente de voladura, utilizando como puntos de referencia las coordenadas de unos sacos medidos *in situ* en la cantera. También, se ha realizado un ajuste de las trayectorias de las rocas, obteniendo las velocidades iniciales, y un ajuste aproximado del tiempo que tardan los fragmentos en moverse, desde el inicio de la detonación del explosivo cargado en el barreno, es decir, del tiempo de respuesta. Las velocidades iniciales y tiempos de respuesta se han ajustado con un modelo matemático en función de parámetros de voladura y de la posición de los blancos. También se ha estudiado la correlación entre parámetros para cada voladura.

Además se ha desarrollado una metodología para obtener las trayectorias en 3D utilizando un mapa del frente topografiado con un perfilómetro.

Todos los cálculos y análisis se han desarrollado utilizando el lenguaje de cálculo técnico MATLAB.

ABSTRACT

The main objective of this master's thesis is to determine a mathematical model for the estimation of the blast front advance of the blasting carried out in the "El Aljibe" quarry in Almonacid de Toledo (Toledo, Spain) within the SLIM (Sustainable Low Impact Mining) project funded by the European Commission within the Horizon 2020 research and innovation program under grant agreement No. 730294.

For each of the blasts, the data obtained from recordings with a high-speed camera were transformed into coordinates referring to a plane perpendicular to the blast face, using as reference points the coordinates of bags measured in situ in the quarry. Also, an adjustment of the rock trajectories has been carried out, obtaining the initial velocities, and an approximate adjustment of the time it takes for the fragments to move from the start of the detonation of the explosive loaded in the blast hole, i.e. the response time. The initial velocities and response times have been adjusted with a mathematical model as a function of blasting parameters and the position of the targets. The correlation between parameters for each blast has also been studied.

In addition, a methodology has been developed to obtain 3D trajectories using a map of the front topographed with a profilometer.

All calculations and analyses have been developed using the MATLAB technical computing language.

**VIDEO ANALYSIS OF THE BLAST FACE AT THE EL
ALJIBE QUARRY**

DOCUMENT 01: REPORT

REPORT

1 Introduction

1.1 Objective and scope

The objective of this work is to estimate trajectories of rock fragments ejected from face movement due to blasting and their corresponding initial velocities, ejection angles, and response times with a mathematical model. Also, to obtain a 3D model of each of the blasts. Blasts were carried out at the "El Aljibe" quarry in two different campaigns. The first campaign was carried out between May and September 2017. These blasts are identified as B1 to B6. The second campaign took place between December 2018 and March 2019. The blasts were identified as B7 to B12 and were in the same area as those of the first campaign.

An analysis of the recordings collected with a high-speed camera and processed with Photron FASTCAM Viewer 3.0 software (2006), is provided. All calculations have been performed in MATLAB software (The MathWorks, Inc., 2021). The "APPENDIX E: MATLAB Code" shows all the lines of code for the calculations used.

1.2 Background

Rock breakage from blasting occurs so rapidly that the details of the phenomenon cannot be observed by the unaided eye. High-speed motion pictures offer a means of slowing down the blasting action so that the process can be observed and studied (Blair, 1960). According to (Segarra P. , et al., 2003), the analysis of the rock movement with video recording is a useful tool in blast design, serving as a general check of the explosive effect on the rock; inefficiencies in loading, stemming, and timing, become easily apparent from the inspection of the recorded images. The knowledge of the response time of the rock, which can be derived from the recorded images, provides guidance to choose an in-row delay for a certain cooperation between adjacent holes.

According to (Segarra Catasus, 2004), movement analysis of the high-speed video recordings allows the trajectories of the blast rocks to be obtained. This provides information on the movement and makes it possible to determine the different velocities and distributions of the rock along the trajectory. A trajectory model is fitted to the path of the rock and the initial velocity of the rock are obtained so that the calculated trajectory fits as closely as possible to the measurement. Existing formulas for predicting response

time and initial velocity are analysed and, if necessary, a detailed analysis is performed to determine the main blasting parameters affecting the rock movement. Determining the response time of the rock mass can be used to choose the delay for a given degree of cooperation between adjacent holes.

Although there are not many studies on face movement, it has been investigated by (Chiappetta, Bauer, Dailey, & Burchell, 1983); (Chiappetta & Mammele, 1987); (Chiappetta, 1998), (Chiappetta, Vanderberg, & Schrag, 2001); (Mishra & Gupta, 1990) and (Oñederra & Esen, 2003)). Simple formulae are developed from experimental data in production blasts for predicting both the initial velocity (Chiappetta, Bauer, Dailey, & Burchell, 1983) and the response time of the rock, i.e. time from the explosive initiation in the borehole to the first evidence of rock motion in front of it has been determined (Oñederra & Esen, 2003)

High-speed imaging is also used in fields other than mining, such as the study of explosive volcanic eruptions to measure the movement of volcanic ejecta by reconstructing pyroclast trajectories. High speed imaging is also used for studying explosive volcanic eruptions to measure volcanic ejecta motion by reconstructing pyroclasts trajectories (e.g. (Gaudin, et al., 2016)

1.2.1 European Project SLIM

This work is developed in the context of the Project SLIM “Sustainable Low Impact Mining solution for the exploitation of small mineral deposits based on advanced rock blasting and environmental technologies”, funded by the European Commission within the Horizon 2020 research and innovation program under grant agreement No. 730294.

The SLIM project has been funded by the European Commission within the Horizon2020 Programme has been launched in 2016 (SLIM, 2021). This initiative involves thirteen European partners from Austria, Denmark, Sweden, France and Spain and include the validation of technologies developed in quarries and mines located in Toledo and Granada (Spain), and in Eisenerz (Austria). SLIM will be developed for four years and has a global budget of 6,979,200 EUR.

The project’s structure and scope are built upon a full user driven strategy for the development of a new sustainable selective low-impact technological solution for mining

of small mineral deposits (including those with chemically complex ore-forming phases) to increase the supply of raw materials from European sources.

To achieve that, the different actions of SLIM include a comprehensive characterisation of explosive technologies and their behaviour on small mineral deposits. Simultaneously, it will undertake an exhaustive analysis on rock fragmentation and kinematics in order to develop the technology to measure muckpile properties and define a new dynamic modelling system. Interaction rock/explosive pre- and post-blast will be considered.

Once the technical development is underway, it will be deployed on-site on some mining sites (upstream) and validated on the corresponding processing plants (downstream), so as to ensure both its superior technical performance and its integration capacity within the mining and processing value chains.

1.2.2 “El Aljibe” quarry

The quarry in which the experimental work was carried out is called “El Aljibe”. It is located near the town of Almonacid de Toledo (Toledo, Spain); 103 km from Madrid. The company Benito Arnó e Hijos is the owner of the quarry. See Figure 1.

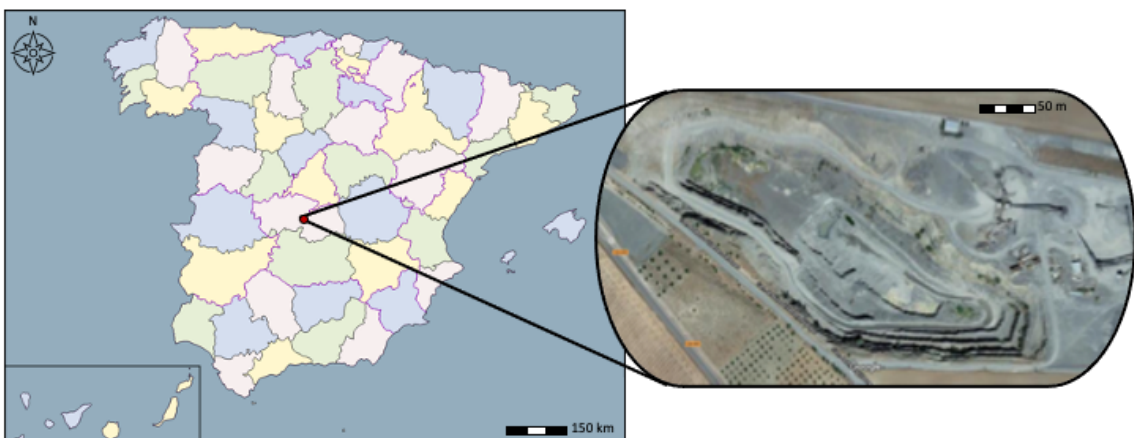


Figure 1: Location of “El Aljibe” quarry

“El Aljibe” quarry is an open pit where a mylonitic deposit is mined. The mylonite is a fine-grained metamorphic rock formed by mylonitization, a type of dynamic metamorphism in which the grain size of a rock is diminished by ductile shearing (shear stress resulting in plastic deformation in the material).

Due to the geotechnical properties of the exploited material (extreme hardness and great resistance to deterioration and fragmentation) are very suitable materials for the

manufacture of track ballast for railway and highways (Hernandez-Enrile, 1981). The main lithologies found in the quarry are shown in Figure 2. According to the research (Segarra P. , et al., 2019), the dominant lithology in the blasts is orthomylonite, although there is a band of cataclasite in blasts B1, B2, B4 and B6.

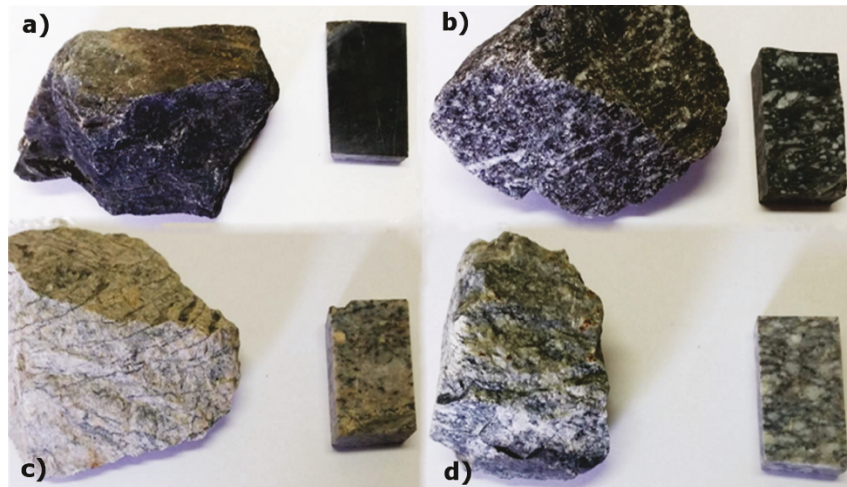


Figure 2: Ultramylonite (a), orthomylonite (b), prothomylonite (c) and cataclasite (d) from “El Aljibe” quarry. Source: (Fueyo & de la Cuadra, 2016)

The crushing and classification plant is designed to produce 700 t/h of final materials, of which the ballast represents 35 % of the production. The material that has come from this exploitation has played a very important role in the construction of the Spanish high-speed lines (AVE), in the sections Madrid-Seville, Madrid-Toledo and Madrid-Valencia.

In addition, the "El Aljibe" quarry carries out the following activities: rock characterisation pre- and post-blast and control of rock fragment size distribution, included in second work package.

2 Description of the blasts

2.1 Location of the blasts in the quarry

A total of twelve production blasts have been carried out in “El Aljibe” quarry from May 2017 to March 2019. The blasts were located one behind each other in the Southwest part of the pit in the block placed in the deepest level as Figure 3 shows.

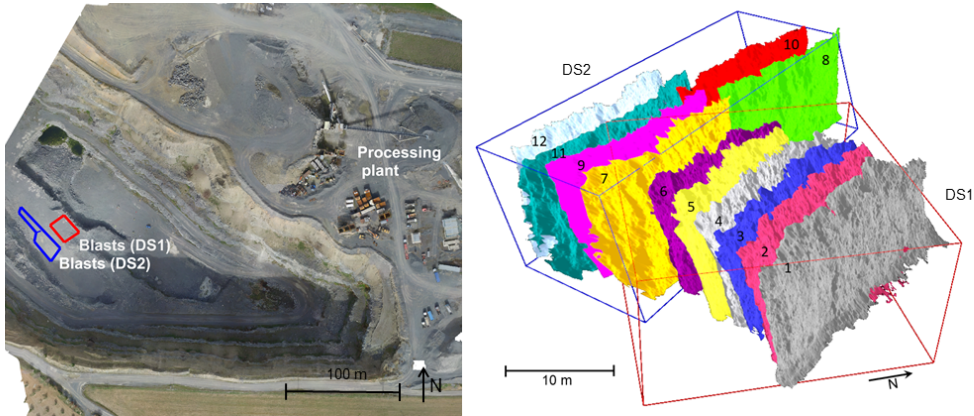


Figure 3: Orthophoto of the quarry showing the pit (left) and the processing plant; right: highwall faces of the twelve blasts; DS1 and DS2 refer to the first and second campaign, respectively (Bernardini, Paredes, Sanchidrian, Segarra, & Gomez)

The blasts consisted on one row with seven holes each. A Tamrock DX-800 with a Measuring-while-Drilling MWD system was used to drill the boreholes; these had a diameter of 89 mm and a nominal inclination of 15°. An emulsion sensitized with microspheres manufactured by MAXAM was used in all the tests. The blasts were fired from the westernmost blasthole (No. 7) towards the easternmost blasthole (No.1) using electronic detonators with 4 ms (blasts B1, B2, B5, B8, B10 and B11) and 23 ms (blasts B3, B4, B6, B7, B9 and B12) between holes.

2.2 Geometric measurements

According to the reports (Segarra P. , et al., 2018) and (Segarra P. , et al., 2019), geometric measurements were performed with a Quarryman ALS laser system (QLS) which has a typical accuracy in the distance of 10 cm and 0.02° in the vertical and horizontal angles. Hole deviation was monitored with a Pulsar Mk3 Microprobe (HDP) manufactured by geo-koncept. The probe has an outer diameter of 37 m and a length of 865 mm. It operates as an inertial measurement system from measurements made by an accelerometer, compass, and inclinometer in each of the three directions in space. The accuracy in azimuth is ±1° and ±0.25° in inclination. Geometric data are downloaded, processed, and analysed with Quarry X software (geo-koncept).

The main geometric characteristics of the blasts are given in Table 1 and Table 2. They show the mean and standard deviation (following the ± sign) of the parameters measured for each hole: where B is burden, Sp is spacing, H_b is bench height, h_{az} is hole azimuth, h_v is hole inclination, h_{eS} and h_{eB} are hole deviation, L is length and J is subdrill.

Table 1: Summary of geometrical data I (Segarra P. , et al., 2018) and (Segarra P. , et al., 2019)

Blast	B , m	S_p , m	H_b , m	L , m	J , m
B1	2.2±0.2	3.2±0.4	11.4±0.1	12.6±0.3	0.4±0.4
B2	2.6±0.2	3.2±0.3	11.1±0.5	12.0±1.0	0.0±0.9
B3	2.6±0.3	3.0±0.3	11.7±0.2	13.1±0.5	0.7±0.7
B4	2.6±0.4	3.1±0.2	11.6±0.2	13.7±0.2	1.4±0.3
B5	2.8±0.4	3.2±0.3	11.7±0.4	13.6±0.3	1.3±0.3
B6	2.6±0.4	3.1±0.6	11.5±0.2	13.0±0.3	0.8±0.2
B7	3.5±0.3	3.7±0.3	12.2±0.5	13.8±0.9	1.3±0.7
B8	4.1±0.4	3.7±0.3	13.1±0.4	15.3±0.3	2.1±0.4
B9	3.2±0.6	3.8±0.4	11.8±0.2	14.0±0.6	1.7±0.6
B10	3.4±0.3	3.7±0.4	12.8±1.0	14.6±1.8	1.4±1.8b
B11	3.3±0.4	4.2±0.8	11.9±0.4	13.7±0.6	1.7±0.6
B12	3.2±0.4	3.7±0.4	12.1±0.3	14.2±0.7	1.9±0.5

Table 2: Summary of geometrical data II (Segarra P. , et al., 2018) and (Segarra P. , et al., 2019)

Blast	h_{az} , °	h_v , °	h_{es} , m	h_{eb} , m
B1	49.2±7.5	19.3±2.1	0.49±0.31	0.76±0.42
B2	49.4±6.5	15.9±2.1	0.26±0.15	0.30±0.30
B3	55.4±5.4	18.2±1.8	0.78±0.43	0.54±0.32
B4	55.9±6.8	17.7±0.7	0.68±0.61	0.47±0.19
B5	54.9±9.7	17.1±1.5	0.64±0.54	0.41±0.29
B6	50.4±14	16.9±2.5	0.43±0.33	0.56±0.41
B7	56.3±6.9	16.3±1.1	1.1±0.6	0.2±0.2
B8	50.4±11.0	8.5±3.3	0.4±0.3	0.8±0.6
B9	49.2±11.8	16.8±2.7	0.7±0.3	0.6±0.3
B10	51.0±12.4	9.2±2.2	0.5±0.5	0.6±0.5
B11	46.8±17.6	15.4±4.0	1.0±0.5	0.7±0.4
B12	57.7±8.3	16.2±2.1	0.8±0.7	0.3±0.3

Specific consumption of each blast has also been calculated. This is the term that expresses the amount of explosive required to fragment 1 m³ or 1 t of rock. The specific

consumption (q) is calculated from the data shown in Table 4. As well, the mean burden (B_{mean}) of each blast is used, with the burdens already discarded, and the height of the bench (H_b).

Table 3: Data for calculation of specific consumption of each blast.

	B4	B6	B8	B10	B11	B12
Blasthole No.	5	6	7	7	7	7
Spacing (Sp), m	3	3	4.33	3.77	3.66	2.93
Stemming, m	1.8	1.8	2.5	1.5	2	1.5
Exp. mass, total, kg	86.3	79.8	99.7	102	96.4	87.8
Exp mass. AG, kg	74.1	71.2	81.9	88.1	85.4	71.1
In-row delay, ms	23	23	4	4	4	23
Hole diameter (\varnothing_{BH}), mm	89	89	89	89	89	89
Mean burden (B_{mean}), m	5.01	3.77	4.00	3.86	5.54	4.70
Bench height (H_b), m	11.6	11.5	13.1	12.8	11.9	12.1

Table 4: Specific consumption of borehole for each blast.

	B4	B6	B8	B10	B11	B12
Specific consumption, kg/m³	0.50	0.61	0.44	0.55	0.40	0.53

Specific consumption increases with hole diameter, rock strength and degree of fragmentation as well as with poor load distribution and generally poor geometric blasting design. In open pit blasting, the specific consumption can vary between 0.1 and 1.5 kg/m³ depending on the strength and turnover of the rock.

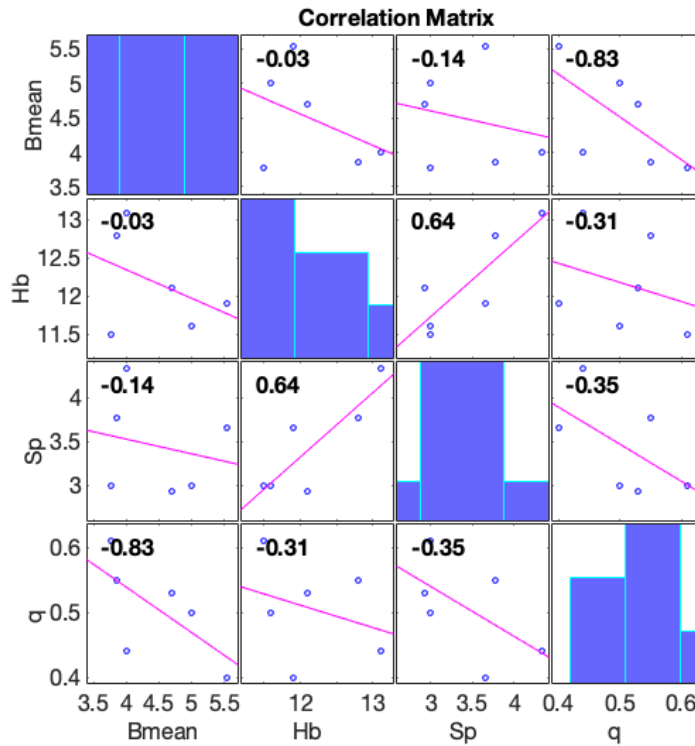


Figure 4: Correlation plot between specific consumption (q) and burden mean (B_{mean}), Spacing (S_p) and Bench height (H_b)

Figure 4 shows a Spearman correlation matrix between the following parameters: specific consumption (q), burden mean (B_{mean}), spacing (S_p) and bench height (H_b). The value of the linear relationship (Spearman's rho) of the correlation is indicated in the upper left corner of each graph, the correlation being significant (p -value ≤ 0.05) when highlighted in red.

The results show no significant correlation between the parameters. However, the high Spearman's rho value relating the specific consumption and burden indicates some dependence between parameters.

2.3 Set-up of the blasts and its high-speed video

The set-up described by (Chiappetta, Bauer, Dailey, & Burchell, 1983) for recording and analysing the rock movement has been adapted to the quarry conditions. In the boreholes used to measure rock movement (borehole no. 7), a detonator has been placed on the surface so that the moment of detonation can be observed without delay, see Figure 5.



Figure 5: Location of an external detonator (B4). Source: (Navarro, Segarra, & Castedo, 2018)

White bags (0.75 – 0.75 m approximately) have been placed as reference points in front of the explosive column so that they can be easily distinguished in the high-speed camera video. In addition, targets were marked in red to improve their visibility. They were marked at spacings of about 5 m from the toe to a distance about 35 m. Targets were placed in the crest and grade of the bench defining a perpendicular plane to the bench face from the selected borehole for each blast, see Figure 6, to reduce the movement of fragments over a surface. To define it, the QLS is set over the selected borehole. Then, the direction (or azimuth) of the two adjacent boreholes at each side is measured. The perpendicular orientation is obtained by pointing the QLS 90° from the resulting mean azimuth towards the bottom level. In “APPENDIX A: Position of reference targets used to film the blasts”, the coordinates of the targets are shown in Table A_1.

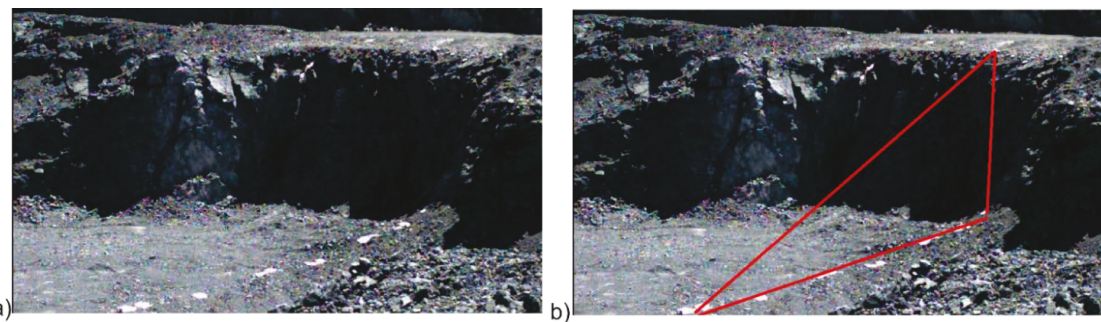


Figure 6: Reference targets. a) procedure to locate the reference targets in blast. b) plane formed by these targets in which rock motion is tracked.

(Navarro, Segarra, & Castedo, 2018) describes high speed video recording of rock movement in the blasts. All blasts were recorded with a High-Speed Camera (HSC) "FastCam Sa 3", model 120k C2, manufactured by Photron. The performance of the camera is based on the recording of images at a pre-set frame rate (frames per second, fps), which are saved in an internal memory. The camera allows to record from 50 fps to 120000 fps. Other setups to be considered are related with resolution of the images, shutter, shadows calibration, and type of trigger among others.



Figure 7: High-speed camera " FastCam Sa 3", model 120k C2, manufactured by Photron used for the recording of blasting (Photron Limited, 2014)

Figure 7 shows the device and Table 5 describes the setups of the High-Speed Camera (HSC) used to record blasts in both campaigns; as can be seen, the recording time ranges between 3.5 s and 5.8 s, hence there must be a high precision to trigger the recording. Blasts B3 and B7 could not be recorded with the High-Speed Camera due to a failure in triggering the camera.

Table 5: Setups of the camera for the twelve blasts (Segarra P. , et al., 2018) and (Segarra P. , et al., 2019)

Blast	Date (dd/mm/yyyy)	Frames rates (fps)	Resolution (px)	Recording time (s)	Shutter (1/fps)
B1	05/06/2017	2000	896 400	3.98	1/1
B2	20/06/2017	2000	896 400	3.98	1/1
B3	23/06/2017	-	-	-	-
B4	11/07/2017	2400	768 448	3.46	1/6000
B5	17/07/2017	2400	768 448	3.46	1/7500
B6	26/09/2017	2400	768 448	3.46	1/7500
B7	26/11/2018	-	-	-	-
B8	03/12/2018	1600	640 x 480	5.82	1/1600
B9	13/12/2018	1600	640 x 480	5.82	1/1600
B10	17/12/2018	2000	768 x 448	4.15	1/2000
B11	20/12/2018	2000	768 x 448	4.15	1/2000
B12	08/02/2019	2000	768 x 448	4.15	1/2000

The analysis is only accomplished for blasts B4, B6, B8, B10, B11 and B12 (these blasts are in bold in Table 5) due to various recording problems in the other blasts. In blasts B1 and B2, the setting was adjusted for sunny weather and became cloudy. In blast B5, due to the position of the camera, blasthole No. 5 was chosen, the initiation system failed in the borehole and was initiated from above, and blastholes No. 6 and No. 7 prevented visibility of any rock movement in blasthole No. 5. And during the filming of B9, the video was recorded with excessive zoom out and the rock fragments cannot be measured properly.

3 Transformation system and rock coordinates transformations

The high-speed camera provides a video of rock motion in two dimensions. To define this plane in the field a plane is marked in front of the borehole perpendicularly to the highwall face. As the axis camera separates from the direction of the highwall face, the probability of filming rock fragments outside this plane increases involving then large errors in the determination of the initial velocity and response time.

Ideally, the direction in which the camera is pointed should be parallel to the bench face. In the second campaign, the orientation and location of the bench face allowed the camera to be positioned almost parallel to the free face in all blasts, while this is not the case for blasts B1 to B6 made in the first campaign. If this does not occur deviations are created in the horizontal and vertical view of the 2D reference plane, with the coordinates and orientations followed in the 2D plane of the video being different from those in reality. Therefore, a transformation system is needed to match the trajectories of the rocks in the video with their real coordinates.

Reference targets, the white bags, were placed on the crest and at the toe of the bench to form a perpendicular plane to the free face of the bench. They were placed in front of the selected blastholes for each blast, which were triggered first, see Table 6. In this way, unobstructed detonation and rock movement could be observed.

Once the targets have been set, the direction of the plane that best fits the targets, when seen from above, has been calculated i.e. a line has been fitted to the planar coordinate of the targets (N, E). The slope of this line is used to calculate the azimuth of the reference plane, see Table 6. The calculations have been done with MATLAB see "Azimuth calculation" in the "APPENDIX E: MATLAB Code".

$$az = 90 - \tan^{-1} \left(\frac{\Delta Targ_y}{\Delta Targ_x} \right) \quad (1)$$

where az is the azimuth, $\Delta Targ_x$ and $\Delta Targ_y$ are the increments of the absolute coordinates of the targets for East and North components, respectively.

Table 6: Borehole selected for each blast and its length and its azimuth

	B4	B6	B8	B10	B11	B12
Borehole	No.5	No.6	No.7	No.7	No.7	No.7
Length, m	13.25	12.69	15.35	14.46	13.08	13.72
Azimuth, °	40.08	55.00	49.82	38.06	47.52	44.76

The methodology from (Navarro, Segarra, & Castedo, 2018) is applied to transform the coordinates of the tracked fragments in the video to the field in the reference plane ZY. Figure 8 shows a schematic of the transformation system; the vertical plane ZY perpendicular to the bench face, formed by the bags (reference targets) placed on the crest and the toe of the bench, and its perpendicular (X axis, parallel to the bench face)

define the trajectory of the rock in the field; in the camera reference system, the trajectory of the rock is followed in the Z"Y" system. As can be seen, the optical X' and Z' axes, from the location of the high-speed camera, are rotated an angle ω and θ with respect to the X and Z axes, respectively; the Y and Y' axes overlap.

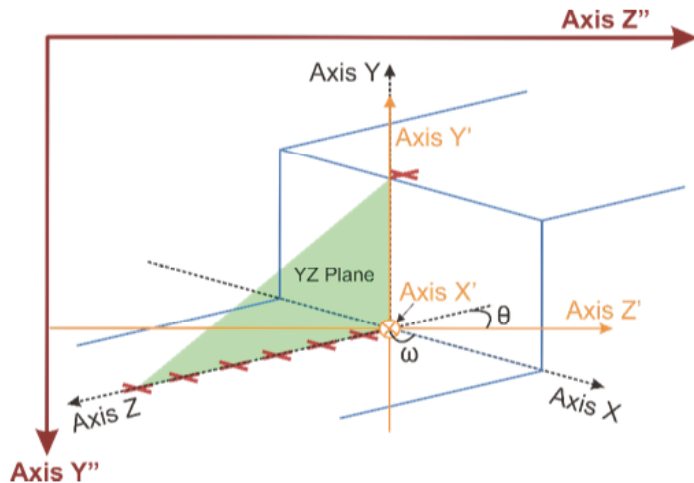


Figure 8: Transformation system between coordinates in the field and coordinates in the video. Red crosses indicate the position of the targets. Source: (Navarro, Segarra, & Castedo, 2018)

Assuming that the fragments tracked in the video move in reality within the plane defined by the reference targets, the local coordinates in this plane are considered. For this purpose, the coordinates in the field are transformed to a local system within the YZ plane, taking as (0,0) the closest target to the camera. From the distances to this target in the ZY plane, the local coordinates of the other targets are calculated. These data are shown in Table A_2. Considering that \mathbf{U}_C and \mathbf{U}_R are local position vectors in the video (camera) and in the field, respectively, on the reference plane defined by targets in the crest and toe of the bench:

$$\mathbf{U}_C = \mathbf{A} + \mathbf{B} \cdot \mathbf{U}_R \quad (2)$$

where, \mathbf{A} is the translation matrix of the reference axes and \mathbf{B} is the transformation matrix defined as the product of three matrixes, $\mathbf{R} \ E \ Sk$, that considers:

- The rotation matrix (\mathbf{R}) of the reference plane of the Z-Z' axes with respect to the Y-Y' axes by an angle θ :

$$\mathbf{R} = \begin{bmatrix} \cos \theta & -\sin \theta \\ \sin \theta & \cos \theta \end{bmatrix} \quad (3)$$

- The scaling factor matrix (\mathbf{E}) of the image, i.e., scaling factor between the reference plane in the video and reality, according to the Z and Y directions:

$$\mathbf{E} = \begin{bmatrix} V_z & 0 \\ 0 & V_y \end{bmatrix} \quad (4)$$

- The skewing matrix (\mathbf{Sk}) over Y axis, so that any point along the Y'' axis remain still, whereas other points are moved parallel to Y' a distance proportional to a perpendicular distance to the Y'' axis (Figure 9)

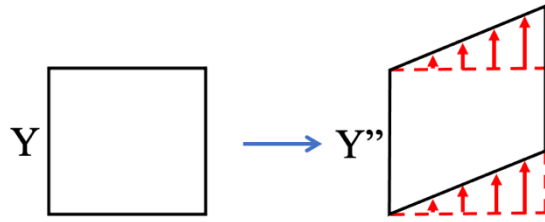


Figure 9: Skewing over Y axis. Source: (Navarro, Segarra, & Castedo, 2018)

It is necessary to calculate coordinates in the reality from those measured in the screen, thus Eq. (2) is transformed in:

$$\mathbf{U}_R = \mathbf{C} + \mathbf{B}^{-1} \cdot \mathbf{U}_c \text{ where } \mathbf{C} = \mathbf{AB}^{-1} \quad (5)$$

where, \mathbf{B}^{-1} is the inverse matrix of \mathbf{B} .

$$\mathbf{C} = \begin{bmatrix} c_1^* \\ c_2^* \end{bmatrix} \text{ and } \mathbf{B}^{-1} = \begin{bmatrix} b_{1,1}^* & b_{1,2}^* \\ b_{2,1}^* & b_{2,2}^* \end{bmatrix} \quad (6)$$

The software Photron FASTCAM Viewer 3.0 software (2006) has been used to calculate the coordinates of the targets in the video (U_{Cz}, U_{Cy}). Considering these coordinates and coordinates of the targets in the local plane (U_{Rz}, U_{Ry}) (see Table A_2 in “APPENDIX A: Position of reference targets used to film the blasts”), the model parameters $c_1^*, c_2^*, b_{1,1}^*, b_{1,2}^*, b_{2,1}^*, b_{2,2}^*$ in Eq. 6 are obtained minimizing the expression obtained operating in Eq. 5:

$$\sum_{P=1}^n \left[(U_{Rz,P} - a_1^* - b_{11}^* \cdot U_{Cz,P} - b_{12}^* \cdot U_{Cy,P})^2 + (U_{Ry,P} - a_2^* - b_{21}^* \cdot U_{Cz,P} - b_{22}^* \cdot U_{Cy,P})^2 \right] \quad (7)$$

where, n is the number of reference targets measured.

The root mean square error (RMSE) is calculated as follows to quantify the quality of the transformation:

$$RMSE = \sqrt{\frac{\sum_{P=1}^n [(U_{Rz,P} - \hat{U}_{Rz,P})^2 + (U_{Ry,P} - \hat{U}_{Ry,P})^2]}{n}} \quad (8)$$

where, $\hat{U}_{RZ,P}$ and $\hat{U}_{Ry,P}$ are the targets coordinates in the local plane YZ calculated from Eq. 5 using the model parameters.

Table 7: Model coefficients c_1^* , c_2^* , $b_{1,1}^*$, $b_{1,2}^*$, $b_{2,1}^*$, $b_{2,2}^*$

Blast	C		B⁻¹			
	c_1^*	c_2^*	$b_{1,1}^*$	$b_{1,2}^*$	$b_{2,1}^*$	$b_{2,2}^*$
B4	-2.570	21.824	0.059	-0.019	-0.013	-0.045
B6	-2.780	23.548	0.058	-0.018	-0.013	-0.052
B8	-5.260	32.298	0.076	-0.002	-0.003	-0.075
B10	-8.773	26.037	0.064	-0.003	-0.002	-0.065
B11	-3.807	24.730	0.060	-0.004	-0.001	-0.062
B12	-8.116	22.491	0.059	0.001	0.002	-0.060

The model coefficients are shown in Table 7 for B4, B6, B8, B10, B11 and B12 and the resulting $\hat{U}_{RZ,P}$ and $\hat{U}_{Ry,P}$ coordinates are in Table A_2. The RMSE is ranged from 0.14 to 0.84 m with mean and standard deviation of 0.54 and 0.30, m, respectively. It measures the amount of error between the measured and calculated target positions. RMSE quantifies how different the set of values is. The smaller an RMSE value is, the closer the predicted and observed values are. This means that in blasts B4 and B6, with an RMSE of 0.77 and 0.84 respectively, the fit is worse. The fit differs by more than half a metre. In contrast, in blasts B8 and B12, with an RMSE of 0.17 and 0.14 respectively, the fit is good. The fit has an error of just over 10 cm between measured and calculated targets. Although the difference is small, the second campaign is better measured and calculated than the first campaign.

3.1 Rock coordinate transformation

For assessing the movement of the rock in front of each borehole under study the software Photron FASTCAM Viewer 3.0 is used. For each video record, the trajectory of 6 to 8 rock fragments at different heights are measured at equal sample time, until they hit the ground, or until they disappear within the cloud of broken rock and dust. Care has been taken that they are within the reference plane; but it is difficult to ensure this when the axis camera forms an angle with the highwall face. Each rock position tracked is associated to a time from the video images. “APPENDIX B: Trajectory of the rocks measured from the video” shows coordinates in the video reference system and the

associated time with respect to the moment in which the camera was triggered. Figure 10 is an example of how the video coordinates are measured with the software, is a sequence of four images. The first image (a) is fixed when the detonation flash is observed. This will be the initial time for our blasting. And the initial co-ordinate of the rock from which the movement is to be tracked (yellow lines) is set. Images (b), (c) and (d) show the video sequence in different frames. The same time interval is used throughout the blasting to follow the movement of the rock. The yellow line is still fixed at the initial coordinates and the green line shows the coordinates of the rock in the different frames.

For each blast, time t is composed of a time increment that depends on each blast (see "APPENDIX B: Trajectory of the rocks measured from the video") and an approximate initial time, which is the time from the initiation of the explosive in the borehole to the first evidence of movement of the rock in front of it, see Table 8:

Table 8: Approximated time when the rock starts to move.

Blast	Approximated time [s]							
	Rock 1	Rock 2	Rock 3	Rock 4	Rock 5	Rock 6	Rock 7	Rock 8
B4	0.679	0.680	0.654	0.680	0.680	0.680	-	-
B6	0.644	0.644	0.644	0.644	0.644	0.644	-	-
B8	1.018	1.017	1.015	1.015	1.013	1.013	1.011	1.000
B10	0.916	0.915	0.912	0.910	0.909	0.908	0.908	0.907
B11	0.938	0.935	0.933	0.931	0.929	0.929	0.928	-
B12	1.163	1.162	1.161	1.160	1.158	1.156	1.155	1.154

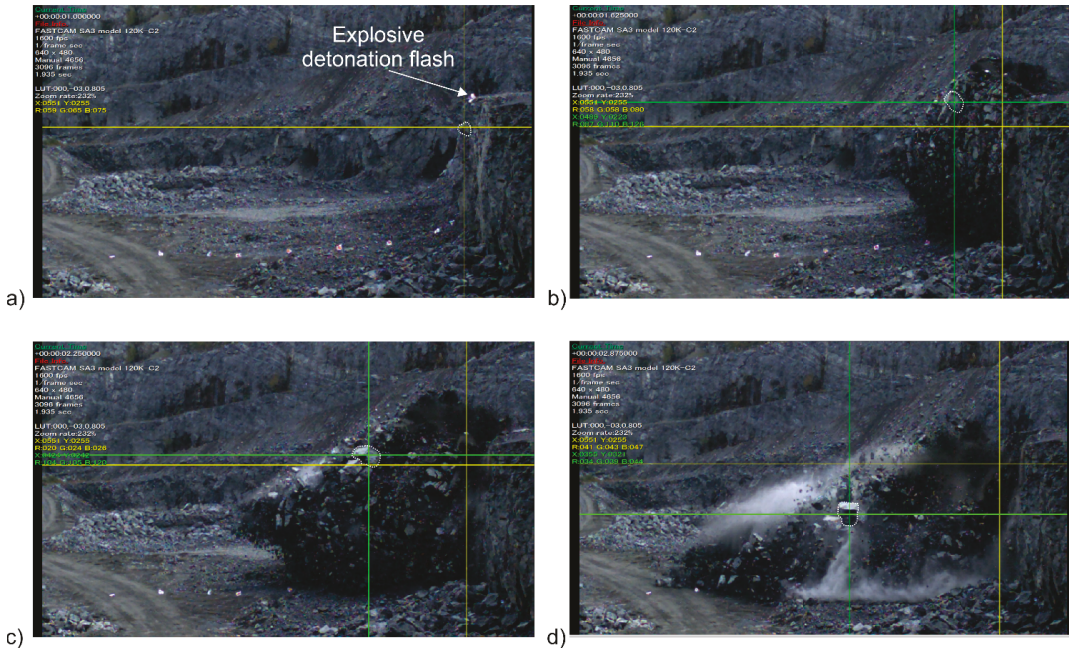


Figure 10: Analysis of rock trajectory in blast B8 with Photron Fastcam Viewer software. Source: (Segarra P., et al., 2019)

Eq. 5 with the parameters in Table 7 is used to transform the coordinates in the reference system of the video to coordinates in the local plane ZY (See “APPENDIX C: Trajectory of the rocks from the transformation system”). For the analysis of the rock trajectory, the fragments are assumed to be spheres with a mean diameter calculated from measuring the coordinates of the rock diagonals in the video. These coordinates are introduced in Eq. 5, to assess the actual coordinates from which the distance is obtained. The resulting diameters are shown in Table 9; they were longer (up to 1.3 m) for blasts B4 and B6 made with a high powder factor, than in the rest of the blasts. The calculations have been done with MATLAB see "Main code" in the "APPENDIX E: MATLAB Code".

Table 9: Mean diameter for each rock measured in the video

Blast	\varnothing, Mean Diameter [m]							
	Rock 1	Rock 2	Rock 3	Rock 4	Rock 5	Rock 6	Rock 7	Rock 8
B4	1.07	0.74	1.3	1.05	0.63	0.83	-	-
B6	1.03	1.01	0.84	0.69	0.47	0.55	-	-
B8	0.58	0.56	0.5	0.43	0.46	0.44	0.45	0.41
B10	0.51	0.59	0.45	0.38	0.39	0.38	0.36	0.35
B11	0.32	0.41	0.51	0.35	0.36	0.35	0.36	-
B12	0.45	0.44	0.4	0.34	0.35	0.36	0.35	0.32

4 Determination of the position of each fragment in relation to the plane YZ

As explained at “Objective and scope”, one of the aims of this work is to model the movement of the blast face. To achieve this, it is necessary to transform the data measured in the field and from the high-speed camera into data that can be used to build the model. This is done to place each rock tracked on the projection of the YZ plane and subsequently on the 3D model. For this, it is necessary to determine the relative height of the rock and its burden.

4.1 Burden matrix and borehole coordinates

The coordinates of the selected borehole for each blast and the coordinates of the burden matrix (BM) are required for this project. BM represents the minimum distances from the borehole to the face of the bench at different depths and at different distances from the plane through the borehole, calculated with the azimuth, shown in Table 6. BM is obtained using Quarry X software. For the different depths, an interval of 0.5 m was used, using the borehole collar coordinates as the reference point. The final depth depends on the depth of each borehole, shown in Table 6. For the different distances between the bench and the plane passing through the borehole, the interval [-4, 4] has been used, with intermediate distances of 0.5 m each, considering 0 the plane passing through the borehole. The data obtained, depth and distances, can be found in “APPENDIX D: Burden matrix and profiles for each blast obtained from software Quarry X”.

The idea is to determine a plane on which one can determine a point of the BM located at a distance equal to the burden from any position of the borehole. For this purpose, a "Pchip" (piecewise cubic Hermite interpolation polynomial) interpolation of the borehole coordinates is performed in order to define a position vector for the borehole path, \mathbf{d}_i . An interval of 0.5 m between points has been set. Then the first and second derivatives are computed at each depth of the BM. With those derivatives, one may obtain the Frenet frame (tangent vector \mathbf{T} , normal vector \mathbf{N} and binormal vector \mathbf{B}) at every depth through which one may built a plane where points of the BM are located. These three vectors are unitary and perpendicular to each other and are calculated as follows:

$$\mathbf{T} = \left(\frac{\mathbf{d}'_i(t)}{\|\mathbf{d}'_i(t)\|} \right) \quad (9)$$

where, $\mathbf{d}'_i(t)$ is the first derivative for the interpolation data.

$$\mathbf{N} = \left(\frac{\mathbf{d}_i' \times \mathbf{d}_i''(t)}{\|\mathbf{d}_i' \times \mathbf{d}_i''(t)\|} \right) \quad (10)$$

where, $\mathbf{d}_i''(t)$ is the second derivative for the interpolation data.

$$\mathbf{B} = \mathbf{T} \times \mathbf{N} \quad (11)$$

where \times denotes cross product.

A plane (Π_1) formed by the normal vector and the binormal vector is then assumed, see Figure 11. The coefficients of the general equation of the plane formed by the vectors \mathbf{B} and \mathbf{N} and the normal vector of this plane (\mathbf{P}_1) are obtained:

$$\Pi_1: A_1x + B_1y + C_1z + D_1 = 0 \quad (12)$$

Where A , B , C and D are the coefficients of the general equation of the plane. They have been calculated as follows:

$$A_1 = B_y \cdot N_z - B_z \cdot N_y \quad (13)$$

$$B_1 = -(B_x \cdot N_z - B_z \cdot N_x) \quad (14)$$

$$C_1 = B_x \cdot N_y - B_y \cdot N_x \quad (15)$$

$$D_1 = A_1 \cdot d_x - B_1 \cdot d_y - C_1 \cdot d_z \quad (16)$$

where, d_x , d_y and d_z are the components of vector \mathbf{d}_i .

The normal vector to this plane (\mathbf{P}_1) is also calculated:

$$\mathbf{P}_1 = (A_1 \quad B_1 \quad C_1) \quad (17)$$

A vertical plane (Π_2) that is parallel to the plane passing through the targets is also calculated, as well as its normal vector (\mathbf{P}_2):

$$A_2 = -sl ; B_2 = 1 ; C_2 = 0 \quad (18)$$

where, sl is the slope of the line fitted to the coordinates of the target plane (N, E).

$$sl = \tan(90 - az) \quad (19)$$

where, az is the azimuth for each blast. See Table 6.

The independent term (D_2) in the equation of the vertical plane (Π_2) will be different for each distance of the BM. This leads to a set of parallel planes. Depending on the distance from the borehole to the rock to be calculated, it will be between -4 and 4 in steps of 0.5 m.

Having obtained both planes, the BM point at a distance equal to the burden must be calculated. Figure 11 represents the planes Π_1 and Π_2 and their intersection (yellow line) which represent each point in the BM. A vector s also appears, this represents the distance between the borehole and the corresponding point on the BM at the intersection of the Π_1 and Π_2 planes.

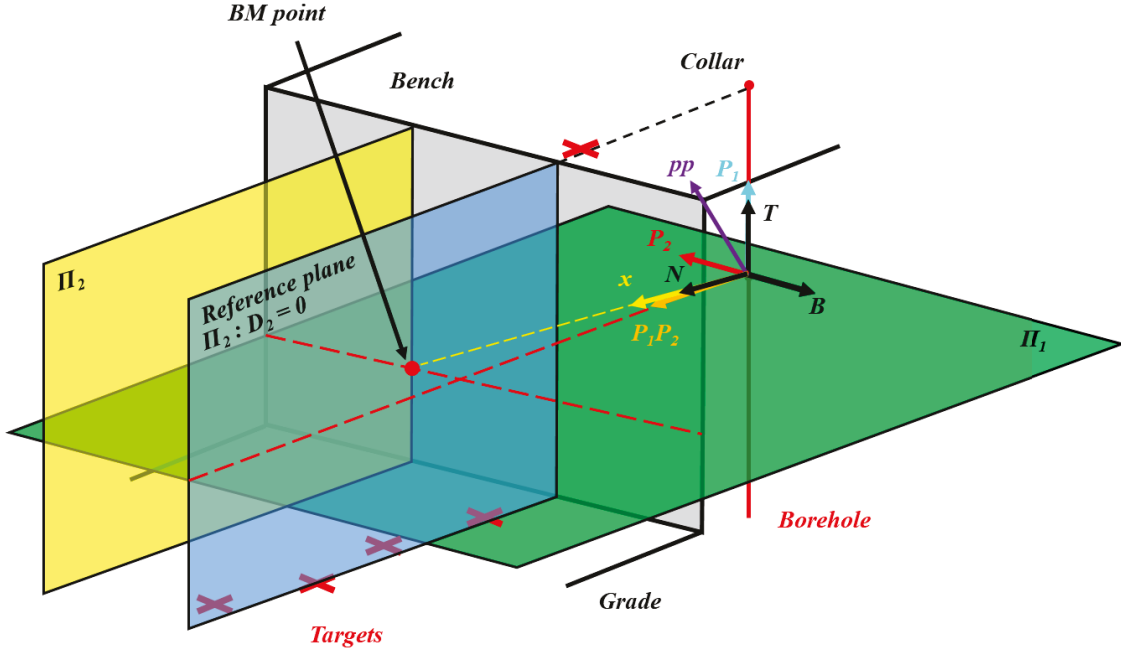


Figure 11: Burden matrix transformation scheme with respect to borehole coordinates for an idealized vertical hole.

To, it is necessary to calculate the dot products (n_i) of the normal vectors and the cross vector ($\mathbf{P}_1 \mathbf{P}_2$):

$$n_1 = 1 ; n_2 = 1 ; n_{12} = \mathbf{P}_1 \cdot \mathbf{P}_2 \quad (20)$$

$$\mathbf{P}_1 \mathbf{P}_2 = -\mathbf{P}_1 \times \mathbf{P}_2 = -\begin{pmatrix} \vec{i} & \vec{j} & \vec{k} \\ A_1 & B_1 & C_1 \\ A_2 & B_2 & C_2 \end{pmatrix} \quad (21)$$

With these calculations, the vector pp is obtained, which is a linear combination of the normal vectors \mathbf{P}_1 and \mathbf{P}_2 . This is used to calculate the burden between the borehole and the corresponding plane Π_2 :

$$pp = \left(\frac{-D_1 \cdot n_2 + D_2 \cdot n_{12}}{n_1 \cdot n_2 - (n_{12})^2} \right) \cdot \mathbf{P}_1 + \left(\frac{-D_2 \cdot n_1 + D_1 \cdot n_{12}}{n_1 \cdot n_2 - (n_{12})^2} \right) \cdot \mathbf{P}_2 \quad (22)$$

The cartesian coordinates for each point in the BM are finally obtained as follows:

$$CoordBM = \left(\frac{d_x + x_1 \cdot BM_{ij}}{\sqrt{x_1^2 + x_2^2 + x_3^2}}, \frac{d_y + x_2 \cdot BM_{ij}}{\sqrt{x_1^2 + x_2^2 + x_3^2}}, \frac{d_z + x_3 \cdot BM_{ij}}{\sqrt{x_1^2 + x_2^2 + x_3^2}} \right) \quad (23)$$

where, d_x , d_y and d_z are the components of vector \mathbf{d}_i ; BM_{ij} are the data obtained from Quarry X software for the burden matrix (see “APPENDIX D: Burden matrix and profiles for each blast obtained from software Quarry X”) where i and j denote depth and distance, respectively, for each position in the matrix; and x_1 , x_2 and x_3 are the components of a vector \mathbf{x} , which is calculated through vectors pp and $PIP2$ using the MATLAB function myfun.m (see APPENDIX E: MATLAB Code).

Once the coordinates associated with that point on the burden matrix have been calculated, the 3D plot including the borehole, the burden matrix and targets are drawn. The 3D result for each blast can be seen in Figure 12. Green circles are the representation of the BM; the red circles are the targets; and the blue and red dots are the representation of the borehole coordinates and the interpolation of the borehole coordinates with an interval of 0.5 m (\mathbf{d}_i), respectively.

The calculations have been done with MATLAB see "Main code" in the "APPENDIX E: MATLAB Code".

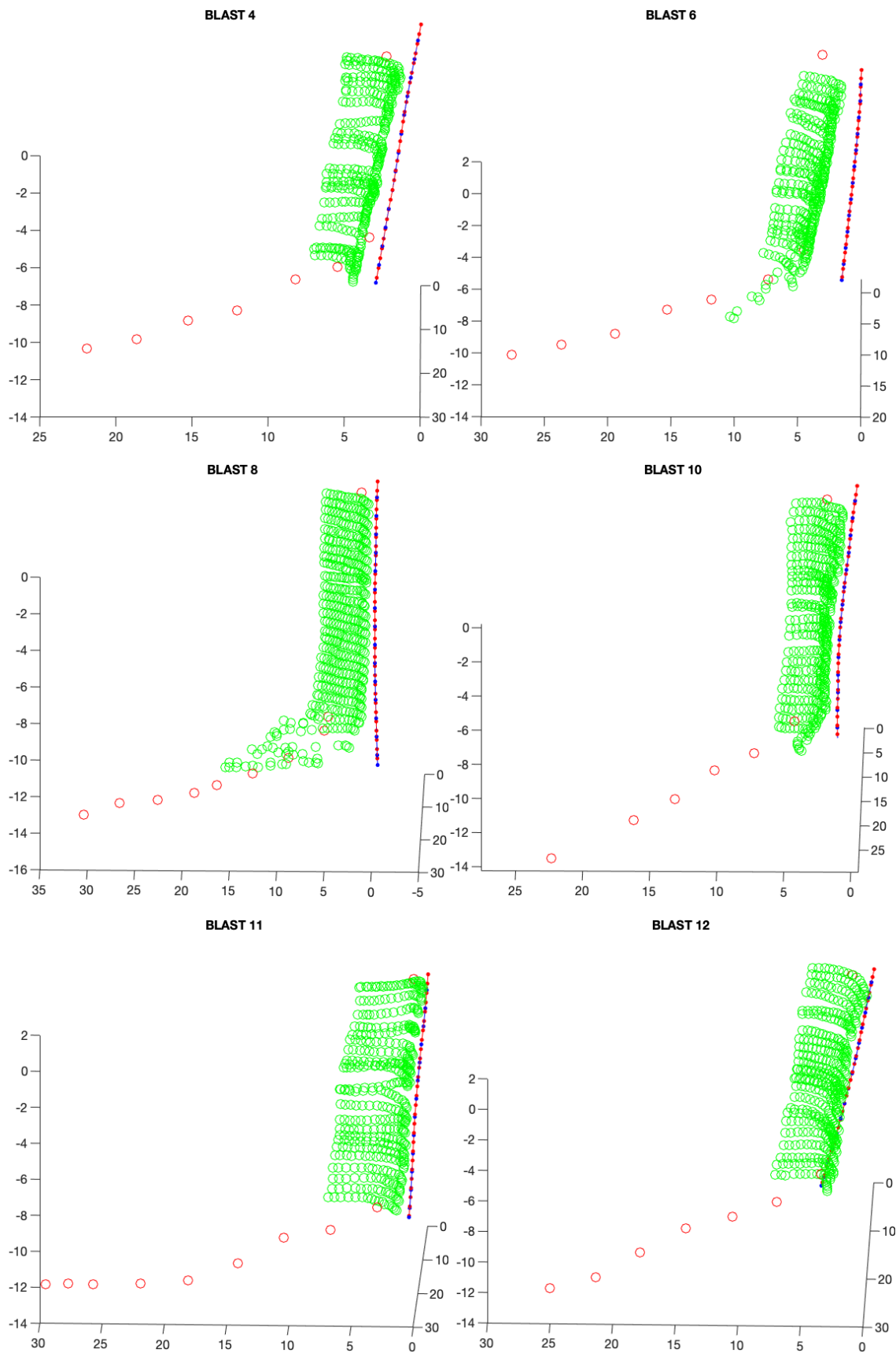


Figure 12: 3D plot of BM and borehole selected for each blast.

4.2 Projection of 3D points of the BM and targets onto the YZ reference plane.

It is also possible to obtain the 2D projection of the burden matrix and the targets on the reference plane ($D_2 = 0$). This is useful to know whether a fragment is too far away from the local plane YZ and therefore can be utilized as a criterion to exclude or not the measurements.

For getting this projection, the tangent vector to the reference plane (\mathbf{v}_T), its normal vector (\mathbf{v}_N) and the cross vector of both (\mathbf{v}_{TN}) are considered as the change of base matrix \mathbf{M} for the transformation from 3D to 2D.

$$\mathbf{v}_T = [-\cos(\tan^{-1}(sl)) \quad -\sin(\tan^{-1}(sl)) \quad 0] \quad (24)$$

$$\mathbf{v}_N = \left[\frac{sl}{\sqrt{sl^2+1}} \quad \frac{-1}{\sqrt{sl^2+1}} \quad 0 \right] \quad (25)$$

$$\mathbf{v}_{TN} = \mathbf{v}_T \times \mathbf{v}_N \quad (26)$$

$$\mathbf{M} = (\mathbf{v}_T^T \quad \mathbf{v}_N^T \quad \mathbf{v}_{TN}^T) = \begin{pmatrix} -\cos(\tan^{-1}(sl)) & \frac{sl}{\sqrt{sl^2+1}} & 0 \\ -\sin(\tan^{-1}(sl)) & \frac{-1}{\sqrt{sl^2+1}} & 0 \\ 0 & 0 & 1 \end{pmatrix} \quad (27)$$

where, sl is the slope of the line fitted to the coordinates of the reference plane (N, E).

Matrix \mathbf{M} , obtained from Eq. 27, is used to change the base from 3D to 2D. See Figure 13.

The burden profile is also obtained for the plane perpendicular to the borehole ($D_2=0$). It is calculated from the central CoordBM and the transformation matrix \mathbf{M} . See Figure 14.

The calculations have been done with MATLAB see "Main code" in the "APPENDIX E: MATLAB Code".

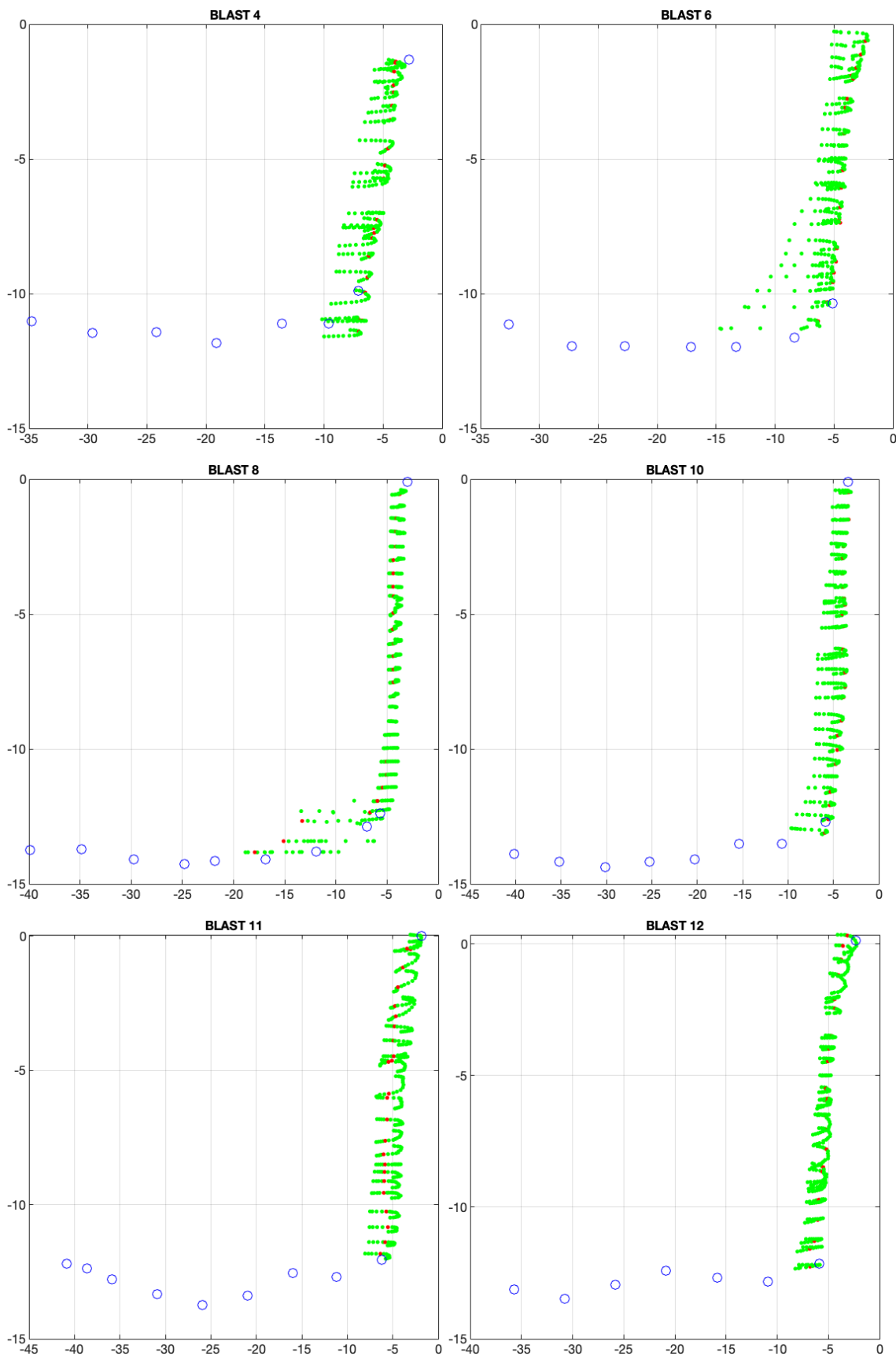


Figure 13: Projection on the plane of the targets for each blast.

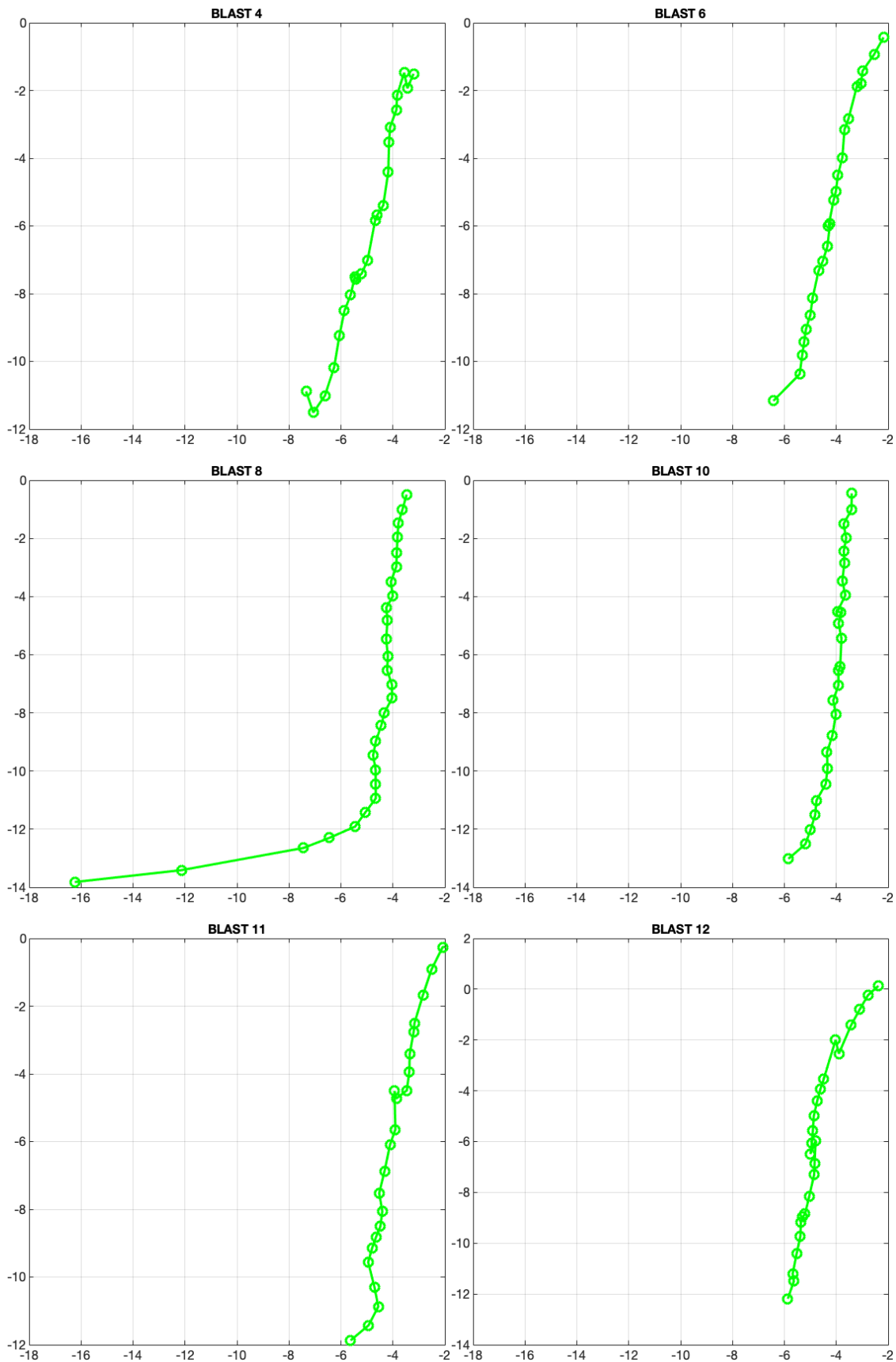


Figure 14: Profile of the burden for each blast ($D_2=0$).

5 Trajectory determination for each fragment

Once the reference plane has been defined, it is necessary to calculate the trajectories of the fragments.

5.1 Adjusting trajectories

The following system of forces acting on the centre of gravity of the rock, see Figure 15, is used to minimise the trajectory of the rocks. The forces acting on the gravity centre of the target, are the following: V is the magnitude of the velocity vector of a target at time t ; \dot{z} and \dot{y} are respectively the components of the vector velocity in the Y and Z axis; θ is the pitch angle (not to be confused with the rotation angle in section 5.2); F_D is the aerodynamic drag (in the opposite direction to *the* velocity vector); m is the mass of the target and g is the acceleration of gravity. The following geometrical relations apply:

$$\cos \theta = \frac{\dot{z}}{V} = \frac{\dot{z}}{\sqrt{\dot{z}^2 + \dot{y}^2}} ; \sin \theta = \frac{\dot{y}}{V} = \frac{\dot{y}}{\sqrt{\dot{z}^2 + \dot{y}^2}} \quad (28)$$

Aerodynamic drag is opposite to the movement of the rock and is given by:

$$F_D = \frac{1}{2} \cdot \rho \cdot V^2 \cdot C_D \cdot S \quad (29)$$

For this purpose, time relative to the initiation of the explosive (t) and local coordinates obtained in Section 3.1 are given in “APPENDIX B: Trajectory of the rocks measured from the video”.

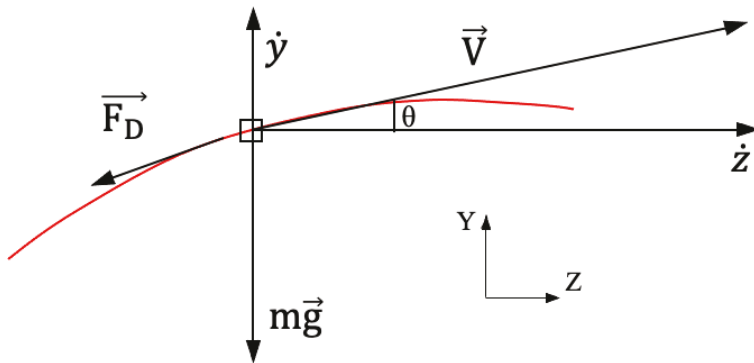


Figure 15: Forces acting on the gravity centre of the rock. Source: (Segarra P., et al., 2003)

In order to obtain the position of each fragment one must solve the following equations iteratively in the order in which they appear:

$$\left\{ \begin{array}{l} \dot{z}_i = \dot{z}_{i-1} + \ddot{z}_{i-1} \cdot (t_i - t_{i-1}) \\ \dot{y}_i = \dot{y}_{i-1} + \ddot{y}_{i-1} \cdot (t_i - t_{i-1}) \\ \ddot{z}_i = -\frac{1}{2} \cdot \frac{\rho_a \cdot C_D \cdot S}{m} \cdot \dot{z}_i \cdot \sqrt{\dot{z}_i^2 + \dot{y}_i^2} \\ \ddot{y}_i = -g - \frac{1}{2} \cdot \frac{\rho_a \cdot C_D \cdot S}{m} \cdot \dot{y}_i \cdot \sqrt{\dot{z}_i^2 + \dot{y}_i^2} \\ z_i = z_{i-1} + \dot{z}_i \cdot (t_i - t_{i-1}) \\ y_i = y_{i-1} + \dot{y}_i \cdot (t_i - t_{i-1}) \end{array} \right. \quad (30)$$

where, i ranges from the first ($i=1$) to the last measured position, m is the mass of a fragment (kg), g is gravity (9.81 m/s^2), ρ_a is air density (1.1614 kg/m^3), S is the surface of the cross section of the fragment (m^2), C_D is drag coefficient, which depends on Reynolds number (Re), \dot{y} and \dot{z} are velocities (m/s) in axis y and z respectively, \ddot{y} and \ddot{z} are accelerations (m/s^2) in axis y and z respectively, and y and z are the position (in m) in the reference system YZ calculated from the coordinates measured in the video.

$$m = \frac{4\pi}{3} \cdot \rho_R \cdot \left(\frac{\phi}{2}\right)^3 \quad (31)$$

$$S = \pi \cdot \left(\frac{\phi}{2}\right)^2 \quad (32)$$

$$C_D = \frac{24}{\text{Re}} + \frac{2.6 \cdot \left(\frac{\text{Re}}{5}\right)}{1 + \left(\frac{\text{Re}}{5}\right)^{1.52}} + \frac{0.411 \cdot \left(\frac{\text{Re}}{263000}\right)^{-7.94}}{1 + \left(\frac{\text{Re}}{263000}\right)^{-8}} + \left(\frac{\text{Re}^{0.8}}{461000}\right) \quad (33)$$

$$\text{Re} = \frac{\rho_a \cdot \sqrt{\dot{y}^2 + \dot{z}^2} \cdot \phi}{\mu} \quad (34)$$

where, ρ_R is density of the rock (2721 kg/m^3), μ is dynamic air viscosity ($18.46 \cdot 10^{-6} \text{ kg} \cdot \text{m}^{-1} \cdot \text{s}^{-1}$) and ϕ is rock diameter (m), assuming it has a spherical shape, see Table 9.

In this work, a sort of total least squares regression analysis is used to fit the trajectories of the fragments. “A sort” means that the residuals of the fitting do not represent the shortest distance between the data point and the fitted curve (this is what standard total least squares do). The parameter to be minimized is the sum of “distances” between data and the fitted trajectory varying initial velocities (\dot{z}_0, \dot{y}_0). Initial position of the fragments is fixed in all cases. Calculations have been done with MATLAB see “Function: funveloc2” and “Function: funtrayect2” in the “APPENDIX E: MATLAB Code”.

The initial velocity (v_0) is calculated with the following equation:

$$v_0 = \sqrt{\dot{z}_0 + \dot{y}_0} \quad (35)$$

And the ejection angle (α) is calculated as follows:

$$\alpha = \tan^{-1} \left(\frac{\dot{y}_0}{\dot{z}_0} \right) \quad (36)$$

Table 10 shows the ejection angle in degrees and initial velocities of the different rocks for each blast measured in metres per second.

Table 10: Ejection angle formed by the initial velocity components (°) and initial velocity for rocks of each blast (m/s)

		Blast 4	Blast 6	Blast 8	Blast 10	Blast 11	Blast 12
Rock 1	$\alpha, {}^\circ$	53.27	50.06	47.23	48.62	51.14	42.53
	$v_0, \text{ m/s}$	20.48	15.12	10.48	7.13	12	7.02
Rock 2	$\alpha, {}^\circ$	47.18	39.23	39.77	32.36	39.51	35.46
	$v_0, \text{ m/s}$	24.49	19.64	11.21	9.3	12.6	6.95
Rock 3	$\alpha, {}^\circ$	32.83	29.18	33.8	24.12	27.03	39.15
	$v_0, \text{ m/s}$	27.04	18.12	12.42	11.09	13.67	7.12
Rock 4	$\alpha, {}^\circ$	31.22	24.36	23.99	21.35	19.13	37.23
	$v_0, \text{ m/s}$	26.91	17.05	11.83	13.19	13.94	8.1
Rock 5	$\alpha, {}^\circ$	26.65	19.56	16.19	15.93	10.61	26.12
	$v_0, \text{ m/s}$	26.27	16.4	11.49	14.21	12.79	8.03
Rock 6	$\alpha, {}^\circ$	26.96	2.26	8.15	14.38	9.72	17.8
	$v_0, \text{ m/s}$	16.94	14.19	8.66	15.4	10.45	6.06
Rock 7	$\alpha, {}^\circ$	-	-	2.08	12.22	5.32	11.83
	$v_0, \text{ m/s}$	-	-	6.03	14.13	6.13	5.21
Rock 8	$\alpha, {}^\circ$	-	-	2.2	8.87	-	9.33
	$v_0, \text{ m/s}$	-	-	5.87	10.76	-	3.55

The initial velocities obtained show that both at the crest and at the toe of the bench is where there is the lowest initial velocity, being slightly higher at the crest; and that it is in the central part of the bench where there is the highest initial velocity.

On the other hand, the ejection angles are greater at the crest and smaller the closer the rock fragment is ejected to the foot of the bench. At the crest, the rocks are more ejected.

The measured and fitted trajectories are, shown in Figure 16. As can be seen in the graphs, the trajectories do not fit completely well. This may be due to the error of transformation of the local coordinates of the rocks.

Table 11 shows minimum error of the trajectory adjustment for rock of each blast in meters. It can be seen that the orientation of the camera relative to the face of the bench influences the quality of the calculation, as the fit will be better when the axis of the camera is parallel to the crest of the bench. For example, blasts B8 and B12, with errors between (0.07 m - 0.22 m) and (0.08 m - 0.19 m) respectively, have a good fit. In contrast, blasts B4 and B6, whose chamber orientation was worse, have larger errors, between (0.27 m - 1.12 m) and (0.14 m - 0.62 m) respectively.

Table 11: minimum error of the trajectory adjustment for rocks of each blast (m)

	Blast 4	Blast 6	Blast 8	Blast 10	Blast 11	Blast 12
Rock 1	0.29	0.60	0.13	0.25	0.16	0.19
Rock 2	0.27	0.62	0.14	0.20	0.29	0.08
Rock 3	1.12	0.43	0.22	0.24	0.26	0.17
Rock 4	0.65	0.24	0.11	0.12	0.16	0.15
Rock 5	0.62	0.27	0.08	0.15	0.19	0.17
Rock 6	0.38	0.14	0.15	0.15	0.07	0.14
Rock 7	-	-	0.14	0.18	0.07	0.09
Rock 8	-	-	0.07	0.17		0.09

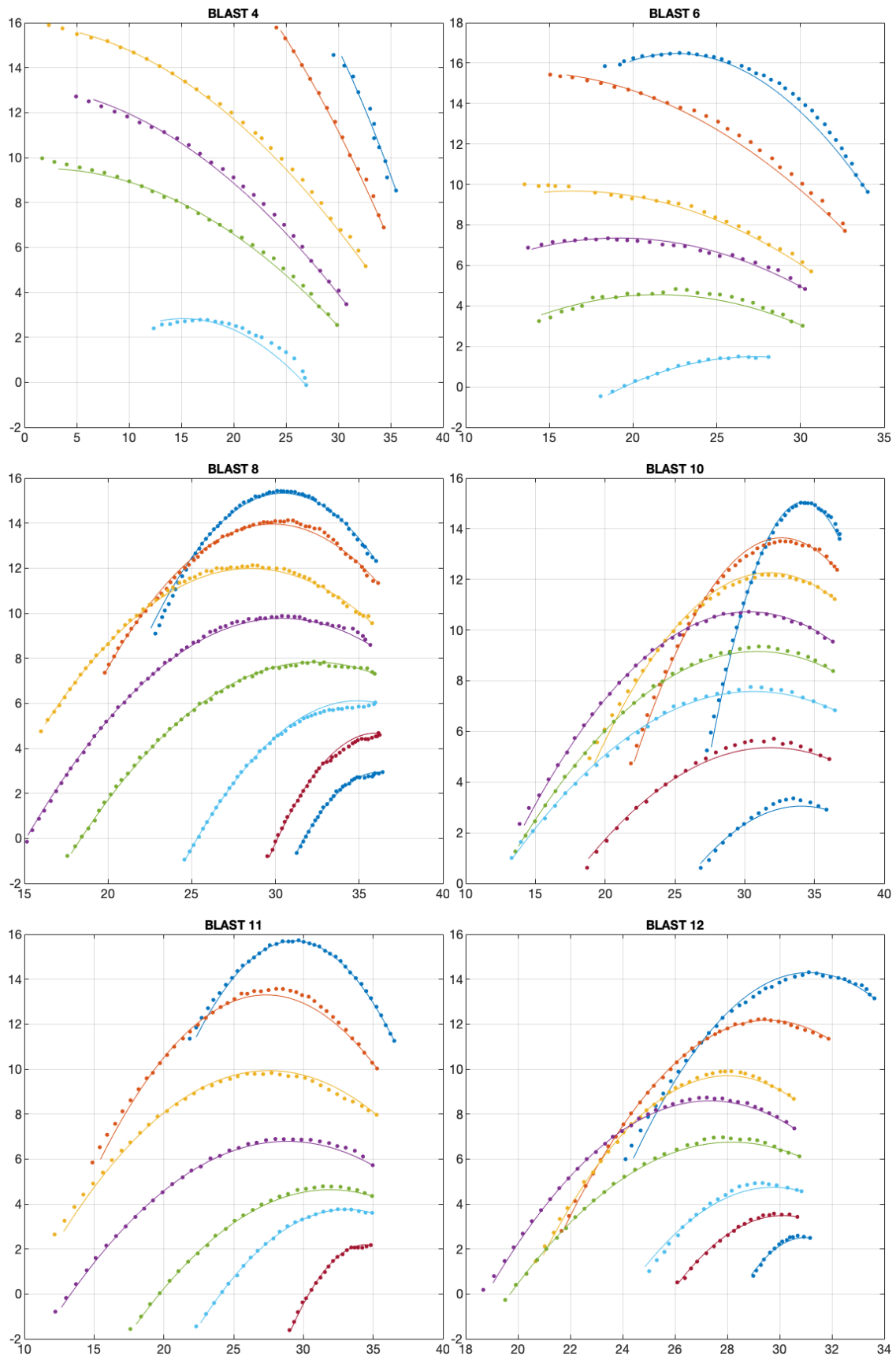


Figure 16: Trajectories of fragment rock measured for each blast.

5.2 3D Model

The aim of this section is to try to build a 3D model of each blast. What is intended is to show the trajectory of the rocks as if they would move along their original paths. In this regard, the data need to be transformed. The calculation performed is based on the assumption that the fragments move in a specific direction defined by the straight line between the fragment and the borehole. In this regard, the BM point closest to the initial position of the fragments in 2D is used to define this direction. It is called *NPoints* (see section 7). This is also a way to determine the burden and the height above grade of a fragment. The angle between the reference plane and the direction (γ) is used to rotate the ZY plane. This angle must be corrected because of the reference system applied in this way:

$$\tau = \gamma - (90 - az) \quad (37)$$

The rotation matrix along the vertical axis is defined as:

$$R = \begin{bmatrix} \cos \tau & -\sin \tau & 0 \\ \sin \tau & \cos \tau & 0 \\ 0 & 0 & 1 \end{bmatrix}$$

$$U_R^{3D} = [-U_{R_z}^{2D} \cdot \cos(90 - az) \quad -U_{R_z}^{2D} \cdot \sin(90 - az) \quad U_{R_y}^{2D}] \cdot R$$

where, U_R^{2D} are local coordinates in reality transformed to the reference plane. The negative sign is due to the code considers the rotation to be counter-clockwise when viewed by an observer looking along the z-axis towards the origin if the rotation angle is positive.

Once the necessary transformations have been performed to have all the data in 3D, the models are drawn. See Figure 17.

It is observed that the rocks belonging to blasts 4 and 6 are not properly ejected from the BM. This is due to the fact that the measured data have a very high initial error, as the videos were not recorded with the camera axis parallel to the crest of the bench. It can also be seen that in the graph, some rocks stand out above the bench, but it must be taken into account that when calculating the BM, the highest part of the bench has been disregarded due to lack of data. See “APPENDIX D: Burden matrix and profiles for each blast obtained from software Quarry X”.

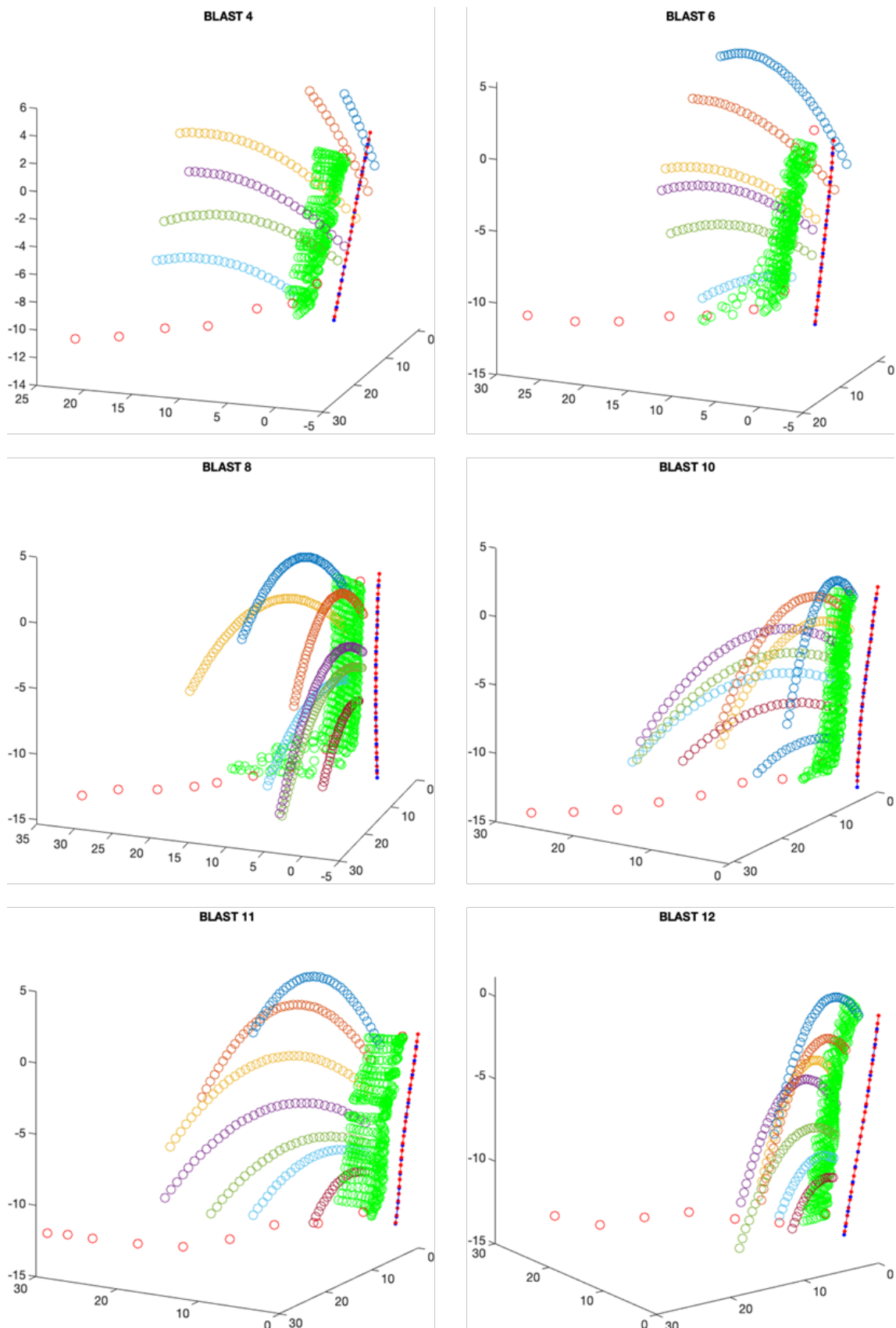


Figure 17: 3D plot of each blast.

5.3 Burden and height of each rock

To calculate the burden and the height corresponding to the position of each fragment, one must select the point of the BM closest to the first point of each trajectory. Table 12 shows the burdens and heights for each fragment in all the blasts considered.

Table 12: Burden and height for rocks of each blast^{*}.

		Blast 4	Blast 6	Blast 8	Blast 10	Blast 11	Blast 12
Rock 1	$B_f, \text{ m}$	3.17	2.11	3.90	3.37	4.15	2.25
	$H_f, \text{ m}$	11.71	12.09	13.90	14.03	11.87	13.74
Rock 2	$B_f, \text{ m}$	3.41	2.86	3.74	3.61	5.22	3.81
	$H_f, \text{ m}$	11.26	11.02	12.86	12.95	10.41	11.92
Rock 3	$B_f, \text{ m}$	4.37	4.02	4.16	3.79	5.53	5.25
	$H_f, \text{ m}$	7.86	7.70	11.01	11.63	8.60	9.23
Rock 4	$B_f, \text{ m}$	4.97	4.08	4.14	3.80	6.00	5.26
	$H_f, \text{ m}$	6.25	6.66	10.06	10.03	6.25	7.83
Rock 5	$B_f, \text{ m}$	5.63	4.48	4.04	3.88	5.83	5.01
	$H_f, \text{ m}$	5.21	5.32	8.87	9.00	5.45	6.69
Rock 6	$B_f, \text{ m}$	7.87	5.05	3.93	3.69	5.86	5.20
	$H_f, \text{ m}$	2.25	3.16	7.87	7.29	4.57	4.97
Rock 7	$B_f, \text{ m}$	-	-	4.09	4.10	6.19	5.32
	$H_f, \text{ m}$	-	-	6.37	5.51	2.82	4.01
Rock 8	$B_f, \text{ m}$	-	-	3.95	4.63	-	5.53
	$H_f, \text{ m}$	-	-	4.90	3.44	-	3.30

*The height is measured from the bottom.

6 Response time

The response time (t_{resp}) is the time a fragment takes to start moving after the explosive detonates. With the high-speed camera video, it is virtually impossible to determine that moment visually, since the phenomenon happens in milliseconds and movement cannot be clearly distinguished.

The response time is calculated utilizing the cumulative distance the fragment travels ($dist_i$) and the time the fragment takes to travel such distance. Assuming that the initial position of the fragment is known ($dist_0 = 0$), the objective is to fit the trajectory the fragment follows and, from it, calculate the cumulative distance travelled by the fragment. In this case, initial velocities and response time are free parameters. They are determined through a least squares regression analysis for each fragment. Thus, distance travelled at i^{th} position may be calculated by:

$$dist_i = \sum_{j=1}^i \sqrt{(y_j - y_{j-1})^2 + (z_j - z_{j-1})^2} \quad i \in \{1, \dots, n-1\} \quad (38)$$

where, (y_i, z_i) are coordinates of each point.

The sum of squared residuals between actual cumulative distances ($dist_i$) and the predicted ones ($dist'_i$) is minimized:

$$err = \sum w \cdot (dist_i - dist'_i)^2 \quad (39)$$

where, w are weights that have been used to emphasize points near the initial time.

Two types of weighting functions have been tested, $w = \frac{1}{t}$ and $w = \frac{1}{t^2}$, the latter giving the best results. *Dist* has been obtained once time is obtained, the response time is calculated as follows:

$$t_{resp} = t^1 - t^0 \quad (40)$$

where, t^0 is the time when the explosive detonates, the moment at which a flash is observed in the video, and t^1 is the time when rocks start moving.

Table 13 shows the response times of the different rocks for each blast in milliseconds. Also, **¡Error! No se encuentra el origen de la referencia.** and **¡Error! No se encuentra el origen de la referencia.** show the graphs relating the accumulated distance to time and a zoom around the initial time.

Table 13: Response time for rocks of each blast, with $w = \frac{1}{t^2}$.

[ms]	Blast 4	Blast 6	Blast 8	Blast 10	Blast 11	Blast 12
Rock 1	3.134	20.833	16.250	21.500	16.000	19.500
Rock 2	3.117	17.668	15.633	26.500	17.500	21.000
Rock 3	-	17.733	15.250	28.500	11.000	21.000
Rock 4	3.117	17.733	15.673	21.500	8.000	22.000
Rock 5	3.122	17.733	14.125	20.500	9.500	17.000
Rock 6	3.117	17.733	14.500	9.000	9.000	17.000
Rock 7	-	-	13.000	21.500	7.500	11.500
Rock 8	-	-	-	20.500	-	11.500

In the table, there are two rocks for which the regression analysis fails. This is the case for rock 3 from blast 4 and rock 8 from blast 8.

It is also noted that response times, in some cases, do not go in ascending order from the base of the bench to the crest, when it should be in this way, since the detonation

starts at the bottom of the borehole and moves up the drillhole. Therefore, some rocks have been discarded for analysis with certain models.

7 Correlation between parameters

Once the models have been obtained, the correlation between the parameters defining the blasting operations is studied. Results obtained from previous sections are summarized in Table 14.

For the analysis of the results, the burden and height of each rock have been calculated for the corresponding borehole of each blast. The calculations have been done with MATLAB, see "Main code" in the "APPENDIX E: MATLAB Code".

Table 14: Initial parameters of each rock

Blast	Rocks	B_f (m)	H (m)	H_f (m)	t_{resp} (ms)	v_{0x} (m/s)	α ($^{\circ}$)
4	1	3.17	13.25	11.71	3.13	20.45	52.76
	2	3.41	13.25	11.26	3.12	24.45	46.73
	3	4.37	13.25	7.86	3.12	27.00	32.54
	4	4.97	13.25	6.25	3.12	26.86	30.94
	5	5.63	13.25	5.21	3.12	26.23	26.41
	6	7.87	13.25	2.25	3.12	16.91	26.73
6	1	2.11	12.69	12.09	20.83	15.12	50.10
	2	2.86	12.69	11.02	17.67	19.64	39.26
	3	4.02	12.69	7.70	17.73	18.12	29.20
	4	4.08	12.69	6.66	17.73	17.05	24.37
	5	4.48	12.69	5.32	17.73	16.40	19.58
	6	5.05	12.69	3.16	17.73	14.19	2.27
8	1	3.90	15.36	13.90	16.25	10.47	47.23
	2	3.74	15.36	12.86	15.63	11.21	39.78
	3	4.16	15.36	11.01	15.25	12.41	33.80
	4	4.14	15.36	10.06	15.67	11.83	23.99
	5	4.04	15.36	8.87	14.12	11.49	16.19
	6	3.93	15.36	7.87	14.50	8.66	8.15
	7	4.09	15.36	6.37	13.00	6.04	2.08
	8	3.95	15.36	4.90	-	5.87	2.19
10	1	3.37	14.46	14.03	21.50	7.13	48.62
	2	3.61	14.46	12.95	26.50	9.30	32.35
	3	3.79	14.46	11.63	28.50	11.09	24.11
	4	3.80	14.46	10.03	21.50	13.19	21.34
	5	3.88	14.46	9.00	20.50	14.21	15.92
	6	3.69	14.46	7.29	9.00	15.39	14.37
	7	4.10	14.46	5.51	21.50	14.12	12.21
	8	4.63	14.46	3.44	20.50	10.76	8.86
11	1	4.15	13.08	11.87	16.00	12.00	51.23

	2	5.22	13.08	10.41	17.50	12.60	39.56
	3	5.53	13.08	8.60	11.00	13.67	27.07
	4	6.00	13.08	6.25	8.00	13.94	19.15
	5	5.83	13.08	5.45	9.50	12.79	10.62
	6	5.86	13.08	4.57	9.00	10.45	9.71
	7	6.19	13.08	2.82	7.50	6.13	5.29
12	1	2.25	13.72	13.74	19.50	7.02	42.53
	2	3.81	13.72	11.92	21.00	6.95	35.45
	3	5.25	13.72	9.23	21.00	7.12	39.16
	4	5.26	13.72	7.83	22.00	8.11	37.25
	5	5.01	13.72	6.69	17.00	8.03	26.12
	6	5.20	13.72	4.97	17.00	6.06	17.80
	7	5.32	13.72	4.01	11.50	5.21	11.81
	8	5.53	13.72	3.30	11.50	3.55	9.28

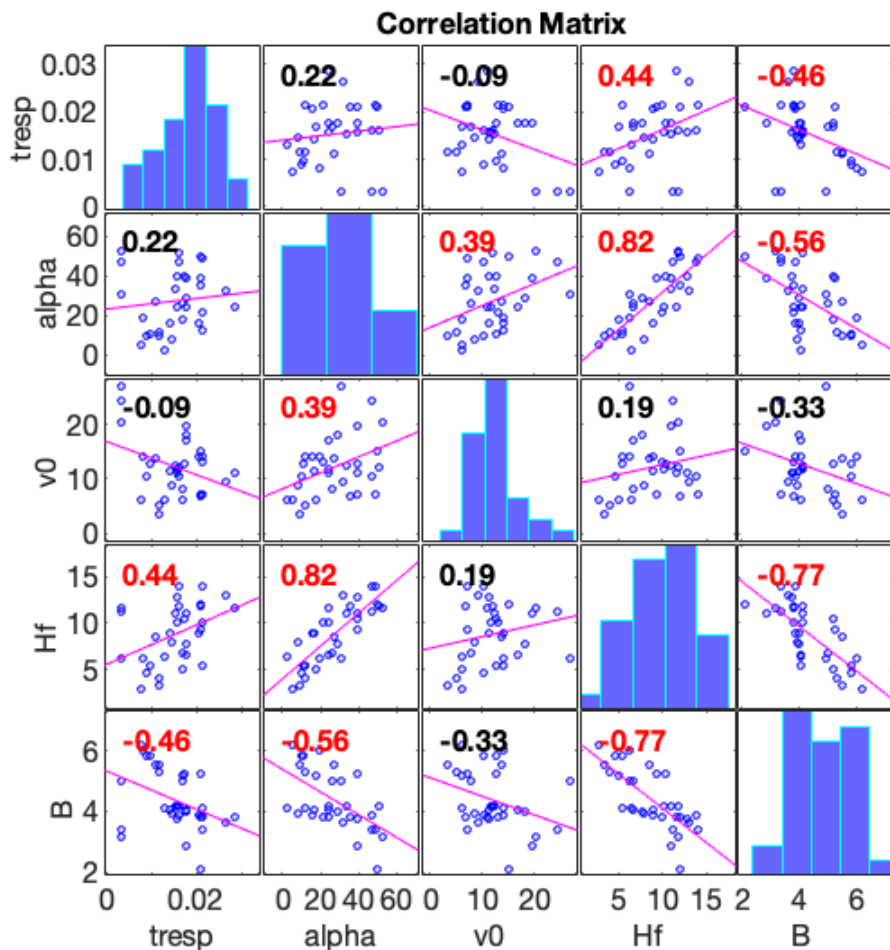


Figure 18: Correlation plot for parameters from Table 14

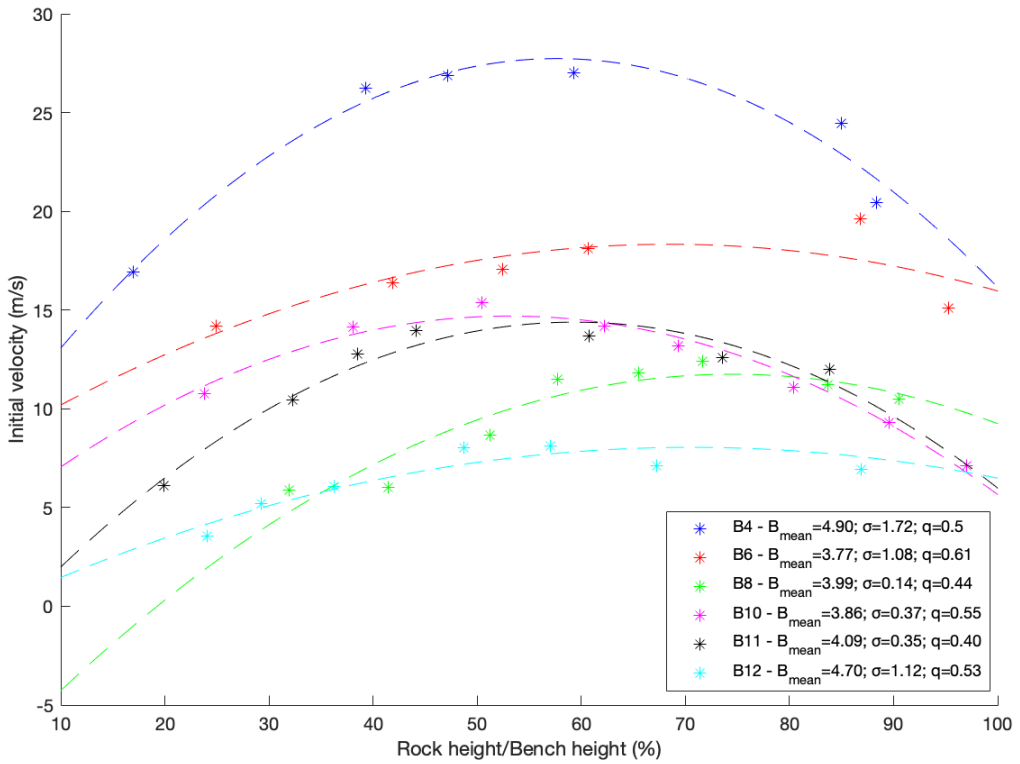


Figure 19: Initial velocity vs. rock height to bench height ratio (0 and 100 % corresponds to the toe and crest, respectively).

Figure 18 shows a Spearman correlation matrix between the follows parameters: burden (B_f), height (H_f), initial velocity (v_0), ejection angle (α), and response time (t_{resp}). The value of the linear relationship (R-value) of the correlation is indicated in the upper left corner of each graph, the correlation being significant (p-value ≤ 0.05) when highlighted in red. Calculations have been done with MATLAB, see "Correlations" in the "APPENDIX E: MATLAB Code".

Figure 19 shows the initial velocity vs. rock height to bench height ratio (0 and 100 % corresponds to the toe and crest, respectively). The legend shows the average burden of each blast, the standard deviation, and its specific consumption. It is observed that the maximum initial velocity is found when the ratio between the height and the load is between the middle of the bench (50%) and its approach to the crest (75%). Calculations have been done with MATLAB, see "Initial velocity as a quadratic function" in the "APPENDIX E: MATLAB Code".

The results show a significant direct linear correlation between the following parameters: $H_f - t_{resp}$, $H_f - \alpha$, and $\alpha - v_0$; and a significant indirect linear correlation between: $B - t_{resp}$, $B - \alpha$ and $B - H_f$. The results show a positive and significant linear

relationship between the initial velocity (v_0) and the ejection angle: the larger the angle, the higher the initial velocity. No other significant correlations are obtained between the initial velocity and rest of parameters; note that for there is a quadratic relation with the height of the fragments, that involves a low correlation coefficient. Figure 19 shows the initial velocity as a quadratic function of the ratio of rock height to bench height. The analysis is performed: the resulting adjustment coefficient of the determination ranges from 0.37 (B6) to 0.96 (B10). This suggests that the largest displacement and highest velocity occur near the centre of the explosive column, and for the same instant the face velocity decreases as the distance to the crest and to the toe decreases. It appears that the velocity at the toe is generally lower than in the crest.

There is also a positive and significant linear relationship between fragment height (H_f) and response time (t_{resp}), which is due to time needed by the detonation to reach the height of the fragment. t_{resp} is negative correlated with the angle beta. There is also a positive correlation between the ejection angle relative to the horizontal (α) and angle with the line defined by the targets (β); the smaller the launch angle and the smaller the deviation from the y-axis.

The results show a negative and significant linear relationship between burden (B) and response time (t_{resp}). This may occur in the case that burden does not have so much weight with respect to response time, since common sense indicates that they should be positively correlative.

8 Response time and initial velocity analysis

The aim of this section is to compile a series of analyses of the results obtained for initial speed and response times. Before analysing the response time, it is necessary to discard some rocks to make the results as coherent and consistent as possible. The following rocks have been discarded for the analysis of the response time:

- For blast 4, the response times of rocks 5 and 6 have been discarded. This is because these rocks are at the foot of the bench and the burden is much larger than in the rest of the bench. As well, response time of rock 4 has been discarded due to the value is negative and it cannot be possible, this would mean that the rock is ejected before the explosive detonates.

- For blast 6, the response times of rocks 5 and 6 have been discarded. This is because these rocks are at the foot of the bench and the burden is much larger than in the rest of the bench.
- For blast 10, the response times of rocks 6 and 8 have been discarded. The first is discarded because the response time obtained is very discordant with the rest of the times of this blasting. The second, because it is at the foot of the bench.
- For blast 12, the response times of rocks 1 and 3 have been discarded. This is because both times are not consistent with the other times of this blast. As they are found at the top of the bench, the response time should be increasing as the height. However, for those rocks, the time does not follow that logic.

8.1 Analysis of response time

To analyse response time results, some formulas found in the research of (Sanchidrian, Segarra, & Lopez, 2005) have been used. The calculations have been done with MATLAB see "Analysis of response time, initial velocity" in the "APPENDIX E: MATLAB Code".

8.1.1 Model 1: $t_{resp} = B^\alpha + H_f^\kappa$

For the first analysis of response time, model $t_{resp} = B^\alpha + H_f^\kappa$ has been evaluated. It is fitted for each blast individually, for the two campaigns independently and leaving blast 4 out of the analysis due to the small number of rocks taken into account. This is discarded because when analysing them individually, it leads to a poor fit. Table 15 shows the coefficients (α, κ) and the correlation coefficient (R^2) obtained. Significant coefficients are shown in bold.

Table 15: Results from analysis of model 1 for response time

	α	κ	R^2
B4, B6, B8, B10, B11, B12	-0.381	0.517	0.111
1st campaign (B4-B6)	0.733	0.965	-0.111
2nd campaign (B8-B12)	-0.394	0.513	0.277
B6, B8, B10, B11, B12	1.031	1.122	0.238
B4	0.319	0.209	-2.412
B6	1.523	1.118	0.063
B8	1.555	0.794	0.777
B10	1.961	0.976	0.395
B11	0.665	1.061	0.818
B12	1.282	1.124	0.229

The coefficients (α, κ) should be positive, since with increasing burden and height, the response time should be longer. Therefore, the overall analysis of all blasts and the second campaign does not give a significant result. No reasonable model is obtained by pooling all the data since campaigns 1 and 2 are very different from each other.

Looking also at the correlation coefficient, R^2 for B4 is negative, as it was said above, so it is not significant either. In the first campaign as well due to there are only two blasts from this campaign: B4 and B6.

In the rest of the analyses, the results obtained are significant since the coefficients are positive and the R^2 is also positive. Although the analysis is better for the individual blasts, especially for B8 ($R^2=0.777$) and B11 ($R^2=0.818$), as the closer the correlation coefficient is to 1, the better the result. For all the blasts combined the results are not good. This is due to the quality of the data in blasts B4 and B6.

8.1.2 Model 2: $tresp = (B/C_p)^\alpha + (H_f/D)^\kappa$

For the second analysis of response time, $tresp = (B/C_p)^\alpha + (H_f/D)^\kappa$ has been evaluated. It is extracted from the research of (Sanchidrian, Segarra, & Lopez, 2005).

P-wave propagation velocity (C_p) and detonation velocity (D) are required to fitting the models. Detonation velocity is the speed at which the shock wave front travels through a detonating explosive for each borehole of each blast. P-wave propagation velocity is the velocity of the longitudinal waves (primary waves). These waves cause the ground to compress and expand alternately in the direction of propagation. Both data are obtained from the report (Gomez, Bermejo, & Navarro, 2019) and are shown in Table 16.

Table 16: Other parameters for each blast.

	Blast 4	Blast 6	Blast 8	Blast 10	Blast 11	Blast 12
C_p [m/s]	5714	5550	5764	6453	4686	5083
D [m/s]	5159	5148	5907	5971	5959	5963

The same number of analyses and blast combinations (all blasts, all except B4, first campaign, second campaign and each blast individually) have been carried out. Table 17 shows the coefficients (α, κ) and the correlation coefficient (R^2) obtained.

Table 17: Results from analysis of model 2 for response time

	α	κ	R^2
B4, B6, B8, B10, B11, B12	-0.381	0.517	0.167
1st campaign (B4-B6)	5.136	-0.388	-0.031
2nd campaign (B8-B12)	-0.394	0.513	0.397
B6, B8, B10, B11, B12	-0.393	0.483	0.408
B4	-0.078	-0.048	0.758
B6	4.511	-0.455	-4.276
B8	-0.368	0.168	0.116
B10	-0.420	0.118	0.013
B11	-0.358	0.276	0.215
B12	-0.404	0.225	0.229

In this case, the coefficients (α, κ) should also be positive, as in the first model. It is observed that this is not true in any analysis. Also, the R^2 is quite low for all the analyses except for blast 4 ($R^2=0.758$). It is not a significant model for the response times obtained in this research.

8.2 Analysis of initial velocity

For the initial velocity adjustment, points mentioned at the beginning of the section 8 have been eliminated. The calculations have been done with MATLAB see "Analysis of response time, initial velocity" in the "APPENDIX E: MATLAB Code".

$$8.2.1 \text{ Model 1: } V_0 = \left(a \left(\frac{H_f}{H} \right)^2 + b \left(\frac{H_f}{H} \right) + c \right) \cdot B^d$$

$$\text{For the first analysis of initial velocity, model } V_0 = \left(a \left(\frac{H_f}{H} \right)^2 + b \left(\frac{H_f}{H} \right) + c \right) \cdot B^d$$

has been evaluated. The model has been analysed for each blast individually, for the two campaigns independently, leaving blast 4 out of the analysis due to the small number of rocks taken into account. This discarding is because when analysing them individually for response time a negative correlation coefficient is obtained, as it has been explained above. Table 18 shows the coefficients (a,b,c,d) and the correlation coefficient (R^2) obtained. The coefficients a,b,c indicate how is the parabola made by the rocks as a function of height, they can be either positive or negative. The coefficient d should be negative since it would be inversely proportional to the velocity. The higher the burden, the lower the initial velocity.

Table 18: Results from analysis of model 1 for initial velocity

	a	b	c	d	R²
B4, B6, B8, B10, B11, B12	-48.876	87.997	-16.876	-0.765	-0.088
1st campaign (B4-B6)	13.384	-14.909	4.738	1.857	0.885
2nd campaign (B8-B12)	0.594	0.357	-0.080	1.661	0.024
B6, B8, B10, B11, B12	-42.175	75.745	-14.696	-0.764	0.057
B4	0.539	1.548	-0.397	2.133	1.000
B6	4.550	3.043	-0.350	0.737	1.000
B8	-0.631	1.920	-0.699	2.022	0.985
B10	-78.829	124.752	1.089	-1.798	0.981
B11	2.100	-1.775	0.548	2.008	1.000
B12	0.512	0.920	-0.173	1.361	-0.204

This analysis shows that the correlation coefficient is close to 1 in almost all cases. Although it is somewhat lower when the results of several blasts are combined. For blast B4 R² is equal to 1 because few rocks are considered, and the problem is reduced to estimate almost a straight line.

8.2.2 Model 2: $V_0 = aH_f^2 + bH_f + c$

The following analysis takes as a reference the very significant R² that have emerged in the previous analysis. Thus, the model $V_0 = aH_f^2 + bH_f + c$ has been evaluated. In this way, the aim is to evaluate the quadratic relationship between speed and height.

The same number of analyses and blast combinations (all blasts, all except B4, first campaign, second campaign and each blast individually) have been carried out. Table 19 shows the coefficients (a,b,c) and the correlation coefficient (R²) obtained.

Table 19: Results from analysis of model 2 for initial velocity

	a	b	c	R²
B4, B6, B8, B10, B11, B12	-4.742	18.128	-3.353	0.393
1st campaign (B4-B6)	5.890	1.368	8.157	0.245
2nd campaign (B8-B12)	-7.616	17.696	-3.363	0.657
B6, B8, B10, B11, B12	-5.097	16.670	-3.183	0.568
B4	-136.338	190.722	-45.763	1.000
B6	-46.395	79.991	-22.331	0.988
B8	-20.381	43.638	-14.925	0.959
B10	-2.160	6.761	0.731	0.921
B11	-0.541	14.816	-2.621	0.982
B12	-17.021	24.829	-4.628	0.988

It is observed that for the individual blast analyses the R² is quite high. For blast B4 R² is equal to 1 because few rocks are considered, and the problem is reduced to estimate almost a straight line. However, for the combination of blasts, the results worsen, especially in the first campaign. This means that the initial velocity at which a rock exits has a strong dependence on the height at which it is located.

8.2.3 Results

According to the correlation coefficients shown in the previous parts, it can be determined that initial velocity can be approximated with the model $V_0 = a \left(\frac{H_f}{H} \right)^2 + b \left(\frac{H_f}{H} \right) + c$.

Nevertheless, model $V_0 = \left(a \left(\frac{H_f}{H} \right)^2 + b \left(\frac{H_f}{H} \right) + c \right) \cdot B^d$ will be used as in addition to the height it considers the burden and can provide a better fit to the blast.

8.3 Analysis of ejection angle (α)

For the ejection angle relative to the horizontal (°), points mentioned at the beginning of the section 8 have been eliminated. The calculations have been done with MATLAB, see "Analysis of response time, initial velocity and ejection angle (α)" in the "APPENDIX E: MATLAB Code".

As demonstrated in the initial velocity analysis, the rock trajectory defines a parabolic curve as a function of height and burden. Therefore, for the analysis of the

ejection angle, the trigonometric relationship of a parabolic throw between ejection angle and velocity is used.

$$8.3.1 \text{ Model 1: } \sin \alpha = \frac{v_0 y}{\left(a \left(\frac{H_f}{H} \right)^2 + b \left(\frac{H_f}{H} \right) + c \right) \cdot B^d}$$

For the first analysis of the launch angle, an adjustment is made as a function of the vertical component of the velocity and the initial velocity.

Model $\sin \alpha = \frac{v_0 y}{\left(a \left(\frac{H_f}{H} \right)^2 + b \left(\frac{H_f}{H} \right) + c \right) \cdot B^d}$ has been evaluated. The model has been

analysed for each blast individually, for the two campaigns independently, leaving blast 4 out of the analysis due to the small number of rocks taken into account. This discarding is because when analysing them individually for response time a negative correlation coefficient is obtained, as it has been explained above. Table 20 shows the coefficients (a,b,c,d) and the correlation coefficient (R^2) obtained. The coefficients a,b,c indicate how is the parabola made by the rocks as a function of height, they can be either positive or negative. The coefficient d should be positive since it would be inversely proportional to the velocity. The higher the burden, the lower the ejection angle.

Table 20: Results from analysis of model 1 for ejection angle

	a	b	c	d	R^2
B4, B6, B8, B10, B11, B12	-745.609	691.030	84.208	-1.671	0.530
1st campaign (B4-B6)	17.057	-19.007	7.557	1.488	0.923
2nd campaign (B8-B12)	-44.830	56.356	-4.542	-0.030	0.838
B6, B8, B10, B11, B12	-313.052	352.605	-16.250	-1.166	0.785
B4	-0.624	1.773	-0.513	3.110	1.000
B6	13.124	-12.974	4.948	1.619	1.000
B8	-27.741	40.711	-8.738	0.488	0.999
B10	-78.256	72.497	19.055	-0.650	0.999
B11	-333.829	354.387	-11.474	-1.020	0.997
B12	-523.253	584.558	-52.124	-1.620	0.999

It is observed that for every blast analyses the R^2 is quite high. For blasts B4 and B6 R^2 is equal to 1 because few rocks are considered, and the problem is reduced to estimate almost a straight line. In this analysis, combinations of blasts have high quality results. That means that ejection angle has a strong dependence of height and burden rock, as well as initial velocity and its vertical component.

$$8.3.2 \text{ Model 2: } \cos \alpha = \frac{v_{0z}}{\left(a\left(\frac{H_f}{H}\right)^2 + b\left(\frac{H_f}{H}\right) + c \right) \cdot B^d}$$

For the second analysis of the launch angle, an adjustment is made as a function of the horizontal component of the velocity and the initial velocity.

Model $\cos \alpha = \frac{v_{0z}}{\left(a\left(\frac{H_f}{H}\right)^2 + b\left(\frac{H_f}{H}\right) + c \right) \cdot B^d}$ has been evaluated. The same number of

analyses and blast combinations (all blasts, all except B4, first campaign, second campaign and each blast individually) have been carried out. Table 21 shows the coefficients (a,b,c,d) and the correlation coefficient (R^2) obtained. The coefficients a,b,c indicate how is the parabola made by the rocks as a function of height, they can be either positive or negative. The coefficient d should be positive since it would be inversely proportional to the velocity. The higher the burden, the lower the ejection angle.

Table 21: Results from analysis of model 2 for ejection angle

	a	b	c	d	R^2
B4, B6, B8, B10, B11, B12	-103.812	129.170	-9.629	-0.443	-5.418
1st campaign (B4-B6)	-804.864	893.413	-86.345	-1.097	0.984
2nd campaign (B8-B12)	-30.257	38.030	-2.676	0.209	-3.238
B6, B8, B10, B11, B12	-88.305	107.805	-4.788	-0.485	-3.907
B4	-0.774	2.000	-0.577	3.075	1.000
B6	13.143	-12.989	4.955	1.617	1.000
B8	-22.154	32.768	-7.614	0.724	0.924
B10	-113.546	101.739	30.461	-0.934	0.994
B11	-173.712	193.816	-13.634	-0.592	0.918
B12	-614.016	682.805	-61.648	-1.705	0.881

It is observed that for every blast analyses the R^2 is quite high. For blasts B4 and B6 R^2 is equal to 1 because few rocks are considered, and the problem is reduced to estimate almost a straight line. However, for the combination of blasts, the results worsen. This means that the ejection angle at which a rock exits has a strong dependence on the height at which it is located, as seen with the initial velocity.

8.3.3 Results

According to the correlation coefficients shown in the previous parts, it can be determined that the ejection angle has a strong dependence on height and burden, as well as on the initial velocity. However, thanks to the analysis of the $\sin \alpha =$

$\frac{v_{0y}}{\left(a\left(\frac{H_f}{H}\right)^2 + b\left(\frac{H_f}{H}\right) + c\right) \cdot B^d}$ and $\cos \alpha = \frac{v_{0z}}{\left(a\left(\frac{H_f}{H}\right)^2 + b\left(\frac{H_f}{H}\right) + c\right) \cdot B^d}$ models, it can be determined that it

has a greater dependence on the vertical component of the initial velocity than on the horizontal component.

9 Conclusions

This work provided a 3D model of the fragment projection for each of the 6 blasts studied. Due to the poor quality of the video recording with the high-speed camera, errors have been obtained in reproducing the model more accurately. However, the fact that the fragments follow the real trajectories supports the approach followed.

In addition, the performance of the response time, initial velocity and ejection angle has been evaluated using models created specifically for the data obtained and models obtained from (Sanchidrian, Segarra, & Lopez, 2005) research. The models that best fit the results are $t_{resp} = \left(B/C_p\right)^\alpha + \left(H_f/D\right)^\kappa$ for response time, $V_0 = \left(a\left(\frac{H_f}{H}\right)^2 + b\left(\frac{H_f}{H}\right) + c\right) \cdot B^d$ for initial velocity, which directly affects the calculation of the ejection angle. It has also been shown that the ejection angle depends more on the vertical component of the velocity than on the horizontal component.

Future work focuses on obtaining better response times that do not modify the initial velocities and thus can better fit the measured trajectories.

Also, as seen with the second campaign compared to the first, it is recommended to record future videos by placing the high-speed camera as perpendicular as possible to the projection plane, as this considerably reduces the error in obtaining the trajectories of the rock fragments and, consequently, the 3D model of the blast.

Regarding the specific consumption, for future similar blasting, one could try to improve the design to improve the quality of the blasting and obtain more material.

Nevertheless, thanks to this research, a first approximation of how any given blast will detonate can be obtained. An approximation of the trajectories, response time and initial velocity can be determined, which will be used to construct a safety distance and possible rock fragmentation.

10 References and Bibliography

- Benito Arnó e Hijos. (2016). *Corporative information. "El Aljibe" quarry.* Retrieved from <http://www.arno.es/es/>
- Bernardini, M., Paredes, C., Sanchidrian, J., Segarra, P., & Gomez, S. (n.d.). *The influence of sampling scale on the in-situ block size distribution. (submitted).*
- Blair, B. (1960). *Use of High-speed camera in blasting studies.* United States Department of the Interior.
- Chiappetta, R. (1998). Blast Monitoring Instrumentation and Analysis Techniques, with an Emphasis on Field Applications. *International Journal on Rock Fragmentation by Blasting-Fragblast*, 2(1), 101-102.
- Chiappetta, R., & Mammele, M. (1987). Analytical High-Speed Photography to Evaluate Air Decks, Stemming Retention and Gas Confinement in Presplitting, Reclamation and Gross Motion Applications. *Proc. 2nd International Symposium on Rock Fragmentation by Blasting*, (pp. 257-301). Keystone, Colorado; Society for Experimental Mechanics, Bethel, CT.
- Chiappetta, R., Bauer, A., Dailey, P., & Burchell, S. (1983). The use of high speed motion picture photography in blast evaluation and design. *Proc. 9th Conference on Explosives and Blasting Technique*, (pp. 258-309). Dallas, Texas, U.S.A: International Society of Explosives Engineers.
- Chiappetta, R., Vanderberg, B., & Schrag, D. (2001). Blast Desings and Diagnosticts Using Portable, Solid State, High Speed Videography Systems. *Proc. 10th High Tech Seminar on the State of the Art, Blasting Technology, Instrumentation and Explosive Applications*, (pp. VII-1 to VII27). 22-26 July, Nashville, Blasting Analysis International, Allentown PA.
- Franco Garcia, M., & Segarra, P. (2019). *"Determinación de la fragmentación por voladura mediante cribado y análisis digital de imágenes terrestres y aéreas en la cantera El Aljibe" Final Thesis.*
- Fueyo, L., & de la Cuadra, C. (2016). *Actualización del informe de obtención del distintivo de calidad ADIF para el suministro de balasto. Estudio geológico, geotécnico y petrográfico.* Fueyo Consultores y Benito Arnó e Hijos SAU.

- Gaudin, D., Taddeucci, J., Houghton, B., Orr, T., Andronico, D., Del Bello, E., . . . Scarlato, P. (2016). *3-D high-speed imaging of volcanic bomb trajectory in basaltic explosive eruptions*.
- Gomez, S., Bermejo, M., & Navarro, J. (2019). *Near-Field Seismic Model for Rock Damage. SLIM Deliverable Report D3.1*. Madrid: Research and Innovation Program, Gran Agreement No. 730294.
- Hernandez-Enrile, J. (1981). Evolución microestructural de rocas cuarzo-feldespáticas como resultado del aumento de la deformación en la milonita de Toledo. *Cuadernos Geología Ibérica*, 7, 547-566.
- Mishra, A., & Gupta, R. (1990). Design of blasting using high resolution camera. *7th International Symposium on Rock Fragmentation by Blasting*, (pp. 378-389). 11-15 August, Beijing, Metallurgical Industry Press, Beijing.
- Navarro, J., Segarra, P., & Castedo, R. (2018). *High speed video recording to determine rock movement*.
- Oñederra, I., & Esen, S. (2003). Selection of inter-hole and inter-row timing for surface blasting-an approach based on burden relief analysis. *2nd World Conference on Explosives and Blasting*, (pp. 269-275). 10-12 September, Prague, Balkema, Netherlands.
- Photron Limited. (2014). *FASTCAM SA 3 - Hardware Manual*.
- Sanchidrian, J., Segarra, P., & Lopez, L. (2005). *On the relation of rock face response time and initial velocity with blasting parameters*. Universidad Politécnica de Madrid - ETSI Minas y Energía.
- Segarra Catasus, P. (2004). Chapter 4: Measurement and analysis of the bench face movement. In *Análisis experimental de la fragmentación, vibraciones y movimiento de la roca en voladuras a cielo abierto* (pp. 24-47).
- Segarra, P., Sanchidrian, J. A., Lopez, L. M., Pascual, J., Ortiz, R., Gomez, A., & Smoech, B. (2003). *Analysis of bench face movement in quarry blasting*.
- Segarra, P., Sanchidrian, J., Castedo, R., Perez Fortes, A., Iglesias, L., Fernandez, A., . . . Nyberg, U. (2018). *Controlling rock fragment size distribution: Large and small-scale testing (1)*.

- Segarra, P., Sanchidrian, J., Perez Fortes, P., Iglesias, L., Navarro, J., Gomez, S., . . . Johansson, D. (2019). *Controlling rock fragment size distribution: Large and small-scale testing (2)*.
- SLIM. (2021). "Sustainable Low Impact Mining solution for exploitation of small mineral deposits based on advanced rock blasting and environmental technologies". Retrieved from <https://www.slim-project.eu>
- The MathWorks, Inc. (2021). *Matlab*. Retrieved from MathWorks: <https://www.mathworks.com/products/matlab.html>

**VIDEO ANALYSIS OF THE BLAST FACE AT THE EL
ALJIBE QUARRY**

DOCUMENT 02: ABBREVIATIONS

ABBREVIATIONS

List of measured parameters

Acronym	Definition
\vec{n}_1	Normal vector to the plane Π_1
\vec{n}_2	Normal vector to the plane Π_2
U_R^{2D}	Local coordinates in reality transformed to the reference plane parallel to the borehole.
U_R^{3D}	Local coordinates in reality in 3D
\vec{v}_{targ}	Normal vector to the plane passing through the targets (Π_2)
$\vec{v}_{T targ}$	Cross vector of $\vec{v}_{T targ}$ and \vec{v}_{targ}
$\vec{v}_{T targ}$	Tangent vector to the plane passing through the targets (Π_2)
Π_1	Plane perpendicular to the borehole
Π_2	Plane parallel to the plane formed by the targets
ρ_a	Air density (1.1614 kg/m3)
ρ_R	Density of the rock (2721 kg/m3)
az	Angle formed by the targets measured from North to East
B	Burden. Minimum distance between the fragment and the borehole (m)
BM	Symmetric matrix whose x and y axes represent the distance from the borehole to both sides and the depth, respectively. The matrix data represents the bench burden, i.e., the distance from the borehole to the free face of the bench at a certain depth
C_D	Drag coefficient
$CoordBM$	Coordinates x, y and z corresponding to the BM
Cp	p-wave propagation velocity (m/s)
dd_i	Interpolation of 0.05 m interval relative to the collar of the borehole
d_i	Interpolation of 0.5 m interval relative to the collar of the borehole
$dist$	Cumulative distance between positions of fragments (m)
$dist'$	Cumulative distance between positions of fragments (m) from the equations
E	Scaling factor matrix
g	Gravity (9.81 m/s ²)
H	Height of the bench (m)
h_{az}	blasthole azimuth (°)

h_{eS}, h_{eB}	Blasthole deviation ($^{\circ}$). Difference at the bottom of the blasthole between the intended and the actual position in the burden and spacing direction.
H_f	Initial position of the fragment in relation to the height of the bench (m) from the bottom of the borehole
h_v	blasthole inclination ($^{\circ}$)
J	Subdrill length (m)
L	Blasthole length (m)
L_c	Loaded length of the borehole (m)
M	Change of basis matrix.
$NPoints$	Absolute coordinates of the minimum distances for each rock
\varnothing	Size of fragment diameter whose trajectory has been measured (m)
$ProjCoordBM$	Projection of BM from 3D to 2D
$ProjCoordTarg$	Projection of targets from 3D to 2D
q	Specific consumption (kg/m^3)
R	Rotation matrix
R^2	Coefficient of correlation [0-1]
R_C	Coordinates for some rocks obtained from the video
Re	Number of Reynolds
RR	Coordinates for some rocks in the reality
S	Surface of the cross section (m^2),
Sk	Skewing matrix over Y axis
sl	Slope of the regression line formed by the plane passing through the targets.
Sp	Spacing between boreholes for each blast (m)
t	time (s or ms)
$t0$	Initial time (s or ms)
$Targ$	Absolute coordinates of targets
$TransfBM$	Transformation of the projections of BM with respect to the plane YZ.
$TransfTarg$	Transformation of the projections of BM with respect to the plane YZ.
$tresp$	Response time. Fragment ejection time from the time of detonation of the borehole (s)
U_C	Local coordinates from the video of the reference plane defined by targets in the crest and bottom floor of the bench
U_R	Local coordinates in the reality of the reference plane defined by targets in the crest and bottom floor of the bench
V_0	Initial velocity at which the fragment is ejected in the blast (m/s)

V_c	Loaded volume of the borehole (m^3)
$V_{removed}$	Volume of rock extracted in the borehole (m^3)
α	Ejection angle relative to the horizontal ($^\circ$)
β	Angle with the line defined by the targets ($^\circ$)
μ	Dynamic air viscosity ($18.46 \text{ kg}\cdot\text{m}^{-1}\cdot\text{s}^{-1}$)

**VIDEO ANALYSIS OF THE BLAST FACE AT THE EL
ALJIBE QUARRY**

**DOCUMENT 03: APPENDIX A. Position of reference targets
used to film the blasts**

APPENDIX A: Position of reference targets used to film the blasts

Table A_1: Absolute coordinates of the targets for each blast

Blast	Targets	Coordinates (m)		
		East	North	Height
4	Crest	428155.76	4400173.76	653.17
	T1	428156.88	4400178.45	644.58
	T2	428159.00	4400179.96	643.36
	T3	428161.76	4400182.82	643.36
	T4	428165.55	4400186.86	642.65
	T5	428168.78	4400190.81	643.04
	T6	428172.17	4400195.03	643.02
	T7	428175.43	4400199.04	643.46
6	Crest	428150.25	4400169.52	654.63
	T1	428151.69	4400174.11	644.16
	T2	428154.55	4400175.62	642.89
	T3	428158.98	4400177.94	642.54
	T4	428162.51	4400179.62	642.55
	T5	428166.60	4400183.54	642.58
	T6	428170.84	4400185.34	642.57
	T7	428174.76	4400189.01	643.37
8	Crest	428124.05	4400192.52	654.96
	T1	428127.67	4400192.40	642.67
	T2	428139.10	4400203.81	640.90
	T3	428135.43	4400200.51	640.98
	T4	428131.67	4400197.24	641.26
	T5	428128.02	4400193.98	642.17
	T6	428141.43	4400205.67	640.79
	T7	428145.22	4400208.91	640.98
	T8	428149.25	4400212.02	641.34
	T9	428152.90	4400215.49	641.32
10	Crest	428123.00	4400187.48	655.09
	T1	428125.41	4400188.79	642.49
	T2	428128.35	4400192.64	641.69
	T3	428131.26	4400196.27	641.697
	T4	428134.14	4400200.23	641.121
	T5	428137.12	4400204.23	641.014
	T6	428140.08	4400208.11	640.813
	T7	428143.15	4400212.17	641.017
	T8	428146.19	4400216.12	641.297

Blast	Targets	Coordinates (m)		
		East	North	Height
11	Crest	428135.74	4400167.08	655.519
	T1	428138.53	4400170.57	643.475
	T2	428142.20	4400173.86	642.839
	T3	428145.80	4400177.10	642.958
	T4	428149.38	4400180.50	642.137
	T5	428153.21	4400183.75	641.781
	T6	428156.90	4400187.05	642.179
	T7	428160.60	4400190.40	642.737
	T8	428162.53	4400192.31	643.16
12	Crest	428135.14	4400163.03	655.483
	T1	428137.59	4400165.59	643.21
	T2	428140.99	4400169.30	642.55
	T3	428144.41	4400172.85	642.668
	T4	428148.03	4400176.36	642.936
	T5	428151.58	4400179.79	642.432
	T6	428155.07	4400183.31	641.883
	T7	428158.62	4400186.77	642.24

Table A_2: Local coordinates obtained from the video (U_C) versus field coordinates measured in YZ local plane (U_R) versus local coordinates obtained from the transformation system (\hat{U}_R)

Blast	Target	Video coordinates (U_C)		Field coordinates in YZ local plane, m (U_R)		Field coordinates in YZ local plane calculated, m (\hat{U}_R)		RMSE
		Z	Y	Z	Y	Z	Y	
4	Crest	610	64	32.03	10.85	32.17	10.87	0.77
	T1	596	296	27.71	1.12	27.09	0.61	
	T2	556	316	25.18	-0.1	24.36	0.25	
	T3	513	335	21.21	-0.1	21.47	-0.03	
	T4	436	371	15.68	-0.81	16.25	-0.63	
	T5	365	386	10.58	-0.42	11.78	-0.36	
	T6	270	419	5.16	-0.44	5.56	-0.57	
	T7	163	439	0	0	-1.13	-0.05	
6	Crest	620	78	31.31	11.26	31.54	11.24	0.84
	T1	492	346	19.28	-0.83	19.25	-0.97	
	T2	594	287	27.46	0.79	26.2	0.72	
	T3	573	308	24.24	-0.48	24.61	-0.09	
	T4	437	359	15.43	-0.82	15.85	-0.91	
	T5	364	383	9.82	-0.79	11.21	-1.18	
	T6	248	400	5.37	-0.8	4.22	-0.5	
	T7	178	408	0	0	0.05	0.02	
8	Crest	560	219	36.88	14.06	36.77	14.02	0.68
	T1	536	380	34.21	1.77	34.54	2.05	
	T2	516	392	32.89	1.26	32.99	1.22	
	T3	453	408	27.99	0.36	28.17	0.24	
	T4	387	413	23.02	0.07	23.15	0.09	
	T5	322	418	18.08	0	18.2	-0.06	
	T6	256	423	15.1	-0.11	13.18	-0.21	
	T7	218	422	10.12	0.08	10.3	0	
	T8	154	421	5.03	0.44	5.44	0.29	
	T9	90	424	0	0	0.58	0.29	

Blast	Target	Video coordinates (U_C)		Field coordinates in YZ local plane, m (U_R)		Calculated local coordinates, m (\hat{U}_R)		RMSE
		Z	Y	Z	Y	Z	Y	
10	Crest	716	172	36.85	13.79	36.86	13.79	0.17
	T1	680	371	34.33	1.2	34.04	1.02	
	T2	612	379	29.49	0.39	29.63	0.61	
	T3	538	384	24.84	0.4	24.84	0.4	
	T4	464	395	19.94	-0.18	20.04	-0.19	
	T5	388	399	14.95	-0.28	15.12	-0.33	
	T6	311	403	10.07	-0.48	10.14	-0.46	
	T7	231	402	4.99	-0.28	4.98	-0.27	
	T8	151	400	0	0	-0.18	-0.02	
11	Crest	690	188	36.8	12.4	36.96	12.37	0.6
	T1	623	379	32.4	0.3	32.05	0.53	
	T2	543	393	27.5	-0.3	27.17	-0.27	
	T3	466	397	22.6	-0.2	22.51	-0.45	
	T4	389	409	17.7	-1	17.81	-1.13	
	T5	311	413	12.7	-1.4	13.09	-1.3	
	T6	230	409	7.7	-1	8.23	-0.98	
	T7	152	403	2.7	-0.4	3.56	-0.53	
	T8	71	393	0	0	-1.28	0.16	
12	Crest	694	182	33.4	13.2	33.39	13.19	0.14
	T1	628	382	29.9	1	29.74	1.13	
	T2	545	393	24.8	0.3	24.82	0.29	
	T3	464	389	19.9	0.4	20	0.35	
	T4	381	381	14.9	0.7	15.05	0.64	
	T5	296	388	9.9	0.2	10.01	0.04	
	T6	209	392	5	-0.4	4.84	-0.39	
	T7	127	380	0	0	-0.05	0.14	

VIDEO ANALYSIS OF THE BLAST FACE AT THE EL
ALJIBE QUARRY

DOCUMENT 03: APPENDIX B. Trajectory of the rocks
measured from the video.

APPENDIX B: Trajectory of the rocks measured from the video

For all blasts, the rock order is descending from the crest to the toe of the bench, with rock 1 being closest to the crest and rock 8 (or the last in each case, rock 6 for blasts B4 and B6, and rock 7 for B11) being closest to the toe of the bench.

Table B_1: Trajectory of rocks from the video of blast 4

Time (s)	Rock 1 (px)		Rock 2 (px)		Rock 3 (px)		Rock 4 (px)		Rock 5 (px)		Rock 6 (px)	
	Z'	Y'	Z'	Y'	Z'	Y'	Z'	Y'	Z'	Y'	Z'	Y'
0.679583	677	96	669	135	653	178	635	221	627	244	598	312
0.7215	660	88	658	126	638	167	620	212	611	238	594	306
0.763417	653	74	645	111	622	158	603	208	595	235	589	301
0.805334	640	64	630	99	606	156	587	202	580	227	573	293
0.847251	630	58	615	93	588	150	571	197	566	223	559	291
0.889168	626	45	599	84	570	140	554	188	549	219	548	290
0.931085	616	33	583	71	553	134	538	182	532	216	535	289
0.973002	594	23	568	60	536	127	521	176	515	211	519	288
1.014919	582	11	552	51	518	122	504	171	498	210	510	289
1.056836	566	5	536	41	499	117	485	166	480	208	499	289
1.098753	547	0	519	32	480	112	468	162	462	206	488	288
1.14067			503	23	464	107	450	159	444	205	478	289
1.182587			487	14	453	105	433	155	426	204	467	290
1.224504			471	6	432	101	415	152	409	204	456	292
1.266421			455	0	412	97	396	151	391	203	446	294
1.308338					393	94	377	148	373	202	434	296
1.350255					374	93	358	145	355	201	423	299
1.392172					354	91	339	144	336	203	412	303
1.434089					335	89	318	144	317	203	401	307
1.476006					314	87	298	145	300	203	390	311
1.517923					293	86	279	146	280	204	380	316
1.55984					272	85	259	146	261	205	368	320
1.601757					251	85	239	147	241	207	357	327
1.643674					230	86	218	148	222	210		
1.685591					209	86	198	149	203	213		
1.727508					184	90	178	150	183	216		
1.769425					162	93			164	219		
1.811342					139	94			145	221		
1.853259					118	97						

Table B_2: Trajectory of rocks from the video of blast 6

Table B_3: Trajectory of rocks from the video of blast 8

Time (s)	Rock 1		Rock 2		Rock 3		Rock 4		Rock 5		Rock 6		Rock 7		Rock 8	
	(px) Z'	(px) Y'														
1	551	242	553	255	549	279	548	292	552	309	553	326	556	344	560	367
1.03125	548	240	549	254	546	275	544	289	550	308	552	327	557	345	557	368
1.0625	544	238	544	251	542	275	542	287	546	306	548	328	555	346	554	368
1.09375	542	234	542	248	539	274	538	285	541	306	544	329	554	346	553	369
1.125	540	233	540	246	536	273	534	283	536	306	540	329	551	347	552	370
1.15625	536	230	535	243	529	270	527	283	531	306	535	330	548	348	549	370
1.1875	533	227	531	241	526	268	523	282	526	306	531	330	546	348	546	371
1.21875	529	224	527	239	522	265	518	282	521	306	527	331	543	348	542	371
1.25	527	221	523	236	518	264	514	281	516	306	524	331	540	349	540	371
1.28125	523	219	520	233	514	262	509	281	512	304	520	332	538	350	538	372
1.3125	520	217	517	231	510	259	505	280	509	305	517	332	536	351	536	373
1.34375	517	216	513	229	506	259	500	280	504	304	513	333	533	353	534	375
1.375	514	214	510	227	503	257	496	279	499	305	510	334	529	355	531	376
1.40625	512	213	506	225	499	255	492	278	495	305	506	335	526	357	529	377
1.4375	509	211	502	225	495	254	488	278	490	307	503	336	523	359	527	379
1.46875	505	210	498	224	491	253	483	278	486	307	500	337	520	360	524	380
1.5	502	208	495	224	487	252	478	278	482	308	497	338	519	362	522	383
1.53125	500	207	491	223	483	251	474	279	477	309	494	340	516	363	520	385
1.5625	497	206	488	222	479	250	470	279	472	309	490	342	513	364	517	388
1.59375	494	206	485	221	473	250	465	280	467	310	487	343	510	367	514	390
1.625	492	205	481	221	467	250	461	280	463	312	483	346	508	369	512	393
1.65625	489	205	478	222	462	250	458	281	459	313	480	348	506	372	510	396
1.6875	486	204	475	222	458	249	452	281	456	315	477	349	503	375	508	398
1.71875	483	204	471	222	454	249	448	283	450	316	474	351	501	378	506	401
1.75	480	204	468	223	450	250	443	283	446	318	471	354	498	381	503	405
1.78125	477	204	465	223	446	250	439	284	441	321	467	357	496	384	501	408
1.8125	475	204	462	223	442	251	434	286	437	322	463	359	494	387	499	411
1.84375	472	204	459	224	437	251	430	287	432	325	460	363	491	390	497	414
1.875	469	205	454	225	434	252	426	289	428	326	457	365	489	393	494	418
1.90625	466	205	451	226	430	252	422	290	424	330	453	368	486	397	-	-
1.9375	464	206	447	227	426	252	417	293	420	332	449	372	484	400	-	-
1.96875	461	207	445	228	422	254	413	296	415	333	446	375	482	404	-	-
2	458	208	441	229	418	254	409	297	411	337	443	379	479	408	-	-
2.03125	455	208	437	231	413	256	404	300	406	340	440	382	477	412	-	-
2.0625	452	210	434	232	409	258	400	302	401	343	437	386	475	417	-	-
2.09375	450	211	430	233	405	259	396	305	397	346	433	390	471	421	-	-
2.125	446	212	426	236	401	261	391	308	392	349	430	394	-	-	-	-
2.15625	443	214	424	237	397	262	387	310	388	353	427	398	-	-	-	-
2.1875	440	216	420	239	392	265	382	314	383	356	423	403	-	-	-	-
2.21875	437	218	417	241	388	267	378	317	379	360	420	407	-	-	-	-
2.25	435	220	414	243	384	270	374	320	374	364	417	412	-	-	-	-
2.28125	432	222	411	246	379	273	369	323	369	367	413	417	-	-	-	-

Table B_4: Trajectory of rocks from the video of blast 10

Table B_5: Trajectory of rocks from the video of blast 11

Table B_6: Trajectory of rocks from the video of blast 12

**VIDEO ANALYSIS OF THE BLAST FACE AT THE EL
ALJIBE QUARRY**

**DOCUMENT 03: APPENDIX C. Trajectory of the rocks from
the transformation system**

APPENDIX C: Trajectory of the rocks from the transformation system

For all blasts, the rock order is descending from the crest to the toe of the bench, with rock 1 being closest to the crest and rock 8 (or the last in each case, rock 6 for blasts B4 and B6, and rock 7 for B11) being closest to the toe of the bench.

Table C_1: Trajectory of rocks from the transformation system of blast 4

Time (s)	Rock 1 (m)		Rock 2 (m)		Rock 3 (m)		Rock 4 (m)		Rock 5 (m)		Rock 6 (m)	
	Z'	Y'	Z'	Y'	Z'	Y'	Z'	Y'	Z'	Y'	Z'	Y'
0.679583	35.52	8.53	34.34	6.89	32.62	5.17	30.77	3.47	29.88	2.55	26.94	-0.12
0.7215	34.66	9.11	33.85	7.44	31.93	5.86	30.05	4.08	29.04	3.03	26.81	0.20
0.763417	34.50	9.84	33.35	8.28	31.14	6.48	29.11	4.48	28.15	3.38	26.60	0.49
0.805334	33.91	10.46	32.68	9.02	30.23	6.78	28.27	4.96	27.40	3.93	25.80	1.06
0.847251	33.42	10.86	31.90	9.49	29.27	7.29	27.41	5.40	26.65	4.30	25.00	1.34
0.889168	33.42	11.50	31.11	10.10	28.38	7.97	26.57	6.03	25.71	4.70	24.37	1.53
0.931085	33.04	12.17	30.40	10.90	27.48	8.47	25.73	6.51	24.76	5.06	23.62	1.75
0.973002	31.92	12.91	29.71	11.59	26.60	9.01	24.83	7.01	23.84	5.51	22.68	2.00
1.014919	31.42	13.61	28.92	12.21	25.62	9.47	23.91	7.46	22.85	5.78	22.13	2.08
1.056836	30.58	14.09	28.15	12.87	24.59	9.95	22.87	7.93	21.82	6.11	21.48	2.22
1.098753	29.55	14.56	27.31	13.50	23.55	10.42	21.93	8.34	20.78	6.44	20.85	2.41
1.14067	-	-	26.52	14.11	22.69	10.86	20.92	8.71	19.73	6.72	20.23	2.50
1.182587	-	-	25.73	14.73	22.07	11.09	19.99	9.11	18.69	7.01	19.56	2.60
1.224504	-	-	24.93	15.30	20.90	11.55	18.97	9.49	17.68	7.23	18.88	2.66
1.266421	-	-	24.09	15.78	19.79	12.00	17.86	9.78	16.63	7.52	18.25	2.70
1.308338	-	-	-	-	18.71	12.38	16.79	10.17	15.58	7.80	17.50	2.77
1.350255	-	-	-	-	17.61	12.68	15.72	10.56	14.53	8.08	16.79	2.78
1.392172	-	-	-	-	16.46	13.03	14.61	10.85	13.37	8.24	16.07	2.75
1.434089	-	-	-	-	15.36	13.38	13.36	11.13	12.24	8.50	15.34	2.71
1.476006	-	-	-	-	14.16	13.74	12.16	11.35	11.23	8.72	14.62	2.68
1.517923	-	-	-	-	12.93	14.07	11.01	11.56	10.03	8.94	13.94	2.59
1.55984	-	-	-	-	11.70	14.39	9.83	11.82	8.88	9.15	13.15	2.57
1.601757	-	-	-	-	10.45	14.67	8.62	12.04	7.66	9.32	12.37	2.40
1.643674	-	-	-	-	9.19	14.90	7.36	12.28	6.48	9.44	-	-
1.685591	-	-	-	-	7.95	15.18	6.16	12.50	5.30	9.56	-	-
1.727508	-	-	-	-	6.39	15.33	4.95	12.72	4.06	9.69	-	-
1.769425	-	-	-	-	5.03	15.49	-	-	2.88	9.80	-	-
1.811342	-	-	-	-	3.65	15.75	-	-	1.71	9.97	-	-
1.853259	-	-	-	-	2.35	15.89	-	-	-	-	-	-

Table C_2: Trajectory of rocks from the transformation system of blast 6

Table C_3: Trajectory of rocks from the transformation system of blast 8

Time (s)	Rock 1		Rock 2		Rock 3		Rock 4		Rock 5		Rock 6		Rock 7		Rock 8	
	(m)		(m)		(m)		(m)		(m)		(m)		(m)		(m)	
	Z'	Y'	Z'	Y'	Z'	Y'	Z'	Y'	Z'	Y'	Z'	Y'	Z'	Y'	Z'	Y'
1	36.01	12.32	36.13	11.34	35.77	9.56	35.66	8.59	35.93	7.31	35.96	6.03	36.15	4.68	36.40	2.94
1.03125	35.79	12.48	35.83	11.43	35.55	9.87	35.37	8.83	35.78	7.39	35.88	5.96	36.22	4.60	36.17	2.88
1.0625	35.49	12.64	35.46	11.67	35.25	9.88	35.22	8.99	35.48	7.55	35.58	5.90	36.07	4.53	35.94	2.89
1.09375	35.35	12.95	35.31	11.90	35.02	9.97	34.92	9.15	35.10	7.57	35.27	5.84	35.99	4.53	35.86	2.82
1.125	35.20	13.03	35.16	12.06	34.80	10.05	34.62	9.31	34.72	7.59	34.97	5.85	35.76	4.47	35.78	2.75
1.15625	34.90	13.27	34.79	12.30	34.27	10.30	34.09	9.34	34.34	7.60	34.59	5.80	35.53	4.40	35.55	2.76
1.1875	34.68	13.50	34.49	12.46	34.05	10.46	33.79	9.43	33.96	7.62	34.28	5.81	35.38	4.41	35.32	2.69
1.21875	34.38	13.74	34.19	12.63	33.75	10.70	33.41	9.44	33.58	7.64	33.98	5.75	35.15	4.42	35.02	2.71
1.25	34.24	13.97	33.90	12.87	33.45	10.79	33.11	9.53	33.20	7.65	33.75	5.76	34.92	4.36	34.87	2.71
1.28125	33.94	14.14	33.68	13.10	33.15	10.95	32.73	9.55	32.90	7.82	33.44	5.70	34.77	4.29	34.71	2.64
1.3125	33.71	14.30	33.45	13.26	32.86	11.19	32.43	9.64	32.67	7.75	33.21	5.71	34.61	4.22	34.56	2.58
1.34375	33.49	14.38	33.15	13.42	32.55	11.20	32.05	9.65	32.29	7.85	32.91	5.65	34.38	4.08	34.40	2.43
1.375	33.27	14.54	32.93	13.58	32.33	11.36	31.75	9.74	31.91	7.79	32.68	5.58	34.07	3.95	34.17	2.37
1.40625	33.12	14.62	32.63	13.75	32.03	11.53	31.44	9.83	31.61	7.80	32.37	5.52	33.84	3.81	34.02	2.30
1.4375	32.89	14.78	32.33	13.76	31.73	11.61	31.14	9.84	31.22	7.67	32.14	5.46	33.61	3.67	33.86	2.16
1.46875	32.59	14.87	32.03	13.85	31.43	11.70	30.76	9.86	30.92	7.68	31.91	5.39	33.38	3.60	33.63	2.09
1.5	32.37	15.03	31.80	13.86	31.13	11.79	30.38	9.88	30.61	7.62	31.68	5.33	33.30	3.46	33.47	1.88
1.53125	32.22	15.11	31.50	13.95	30.82	11.88	30.07	9.82	30.23	7.56	31.45	5.19	33.07	3.39	33.32	1.73
1.5625	31.99	15.20	31.27	14.03	30.52	11.97	29.77	9.83	29.85	7.58	31.14	5.05	32.84	3.33	33.08	1.52
1.59375	31.77	15.21	31.05	14.12	30.07	11.99	29.39	9.77	29.47	7.52	30.91	4.99	32.60	3.11	32.85	1.38
1.625	31.62	15.29	30.74	14.13	29.61	12.01	29.09	9.79	29.16	7.39	30.60	4.78	32.44	2.97	32.69	1.16
1.65625	31.39	15.30	30.51	14.07	29.23	12.03	28.85	9.72	28.86	7.33	30.37	4.64	32.28	2.75	32.53	0.95
1.6875	31.16	15.38	30.29	14.08	28.93	12.11	28.40	9.74	28.62	7.19	30.14	4.57	32.05	2.54	32.38	0.80
1.71875	30.94	15.39	29.98	14.09	28.63	12.13	28.09	9.61	28.16	7.13	29.90	4.43	31.89	2.32	32.22	0.58
1.75	30.71	15.40	29.75	14.02	28.32	12.07	27.71	9.62	27.86	7.00	29.67	4.22	31.66	2.11	31.98	0.30
1.78125	30.48	15.41	29.52	14.04	28.02	12.08	27.41	9.56	27.47	6.79	29.36	4.01	31.50	1.89	31.82	0.08
1.8125	30.33	15.42	29.30	14.05	27.71	12.02	27.02	9.43	27.16	6.73	29.05	3.87	31.34	1.67	31.66	-0.14
1.84375	30.10	15.43	29.07	13.98	27.33	12.04	26.71	9.37	26.78	6.52	28.81	3.58	31.10	1.46	31.50	-0.36
1.875	29.87	15.37	28.68	13.92	27.10	11.97	26.41	9.23	26.47	6.46	28.58	3.44	30.94	1.24	31.26	-0.65
1.90625	29.64	15.38	28.45	13.86	26.80	11.99	26.10	9.17	26.16	6.17	28.27	3.23	30.71	0.95	-	-
1.9375	29.49	15.31	28.15	13.80	26.49	12.00	25.71	8.96	25.85	6.04	27.96	2.95	30.55	0.73	-	-
1.96875	29.26	15.25	27.99	13.73	26.19	11.86	25.40	8.75	25.47	5.98	27.72	2.73	30.39	0.44	-	-
2	29.03	15.18	27.69	13.67	25.88	11.88	25.10	8.69	25.15	5.69	27.48	2.44	30.15	0.15	-	-
2.03125	28.80	15.19	27.38	13.53	25.50	11.74	24.71	8.49	24.77	5.49	27.25	2.23	29.99	-0.14	-	-
2.0625	28.57	15.05	27.15	13.47	25.19	11.61	24.40	8.35	24.38	5.28	27.01	1.94	29.82	-0.51	-	-
2.09375	28.41	14.98	26.84	13.41	24.88	11.55	24.09	8.14	24.07	5.07	26.70	1.66	29.51	-0.79	-	-
2.125	28.11	14.92	26.53	13.20	24.57	11.41	23.70	7.93	23.68	4.86	26.46	1.37	-	-	-	-
2.15625	27.87	14.78	26.38	13.13	24.27	11.35	23.39	7.80	23.37	4.58	26.22	1.08	-	-	-	-
2.1875	27.64	14.64	26.07	12.99	23.88	11.14	23.01	7.51	22.98	4.37	25.91	0.72	-	-	-	-
2.21875	27.41	14.50	25.84	12.85	23.57	11.01	22.69	7.30	22.67	4.08	25.67	0.43	-	-	-	-
2.25	27.25	14.36	25.60	12.71	23.26	10.80	22.38	7.09	22.28	3.80	25.43	0.07	-	-	-	-
2.28125	27.02	14.22	25.37	12.50	22.87	10.59	22.00	6.89	21.89	3.59	25.12	-0.29	-	-	-	-

Table C_4: Trajectory of rocks from the transformation system of blast 10

Table C_5: Trajectory of rocks from the transformation system of blast 11

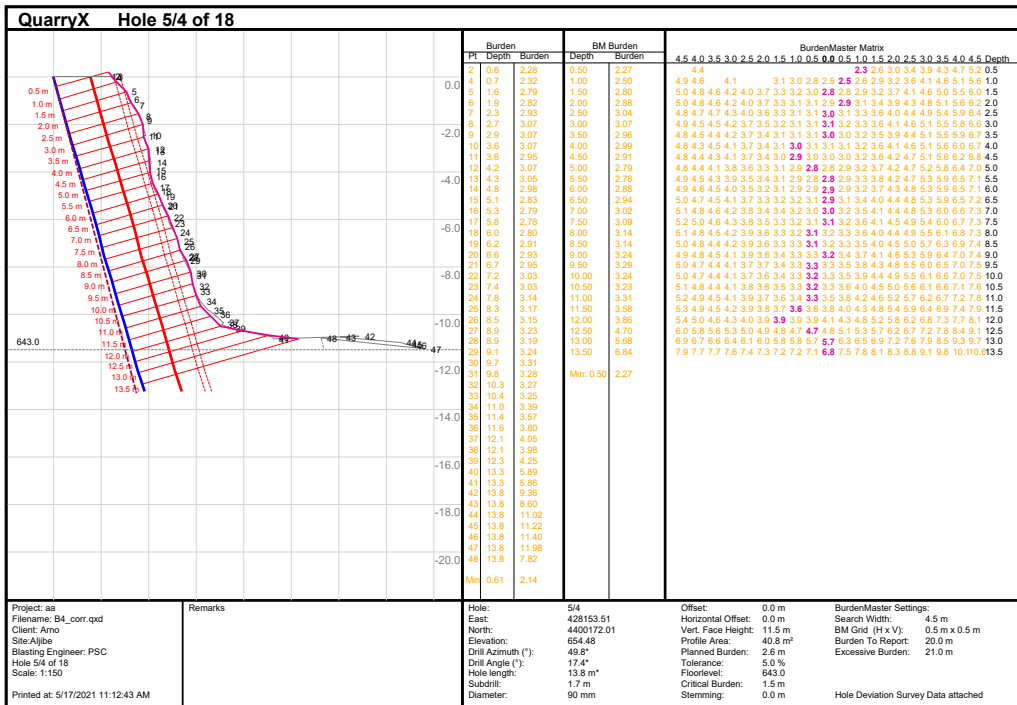
Table C_6: Trajectory of rocks from the transformation system of blast 12

**VIDEO ANALYSIS OF THE BLAST FACE AT THE EL
ALJIBE QUARRY**

**DOCUMENT 03: APPENDIX D. Burden matrix and profiles for
each blast from software Quarry X**

APPENDIX D: Burden matrix and profiles for each blast obtained from software Quarry X

1 Burden matrix



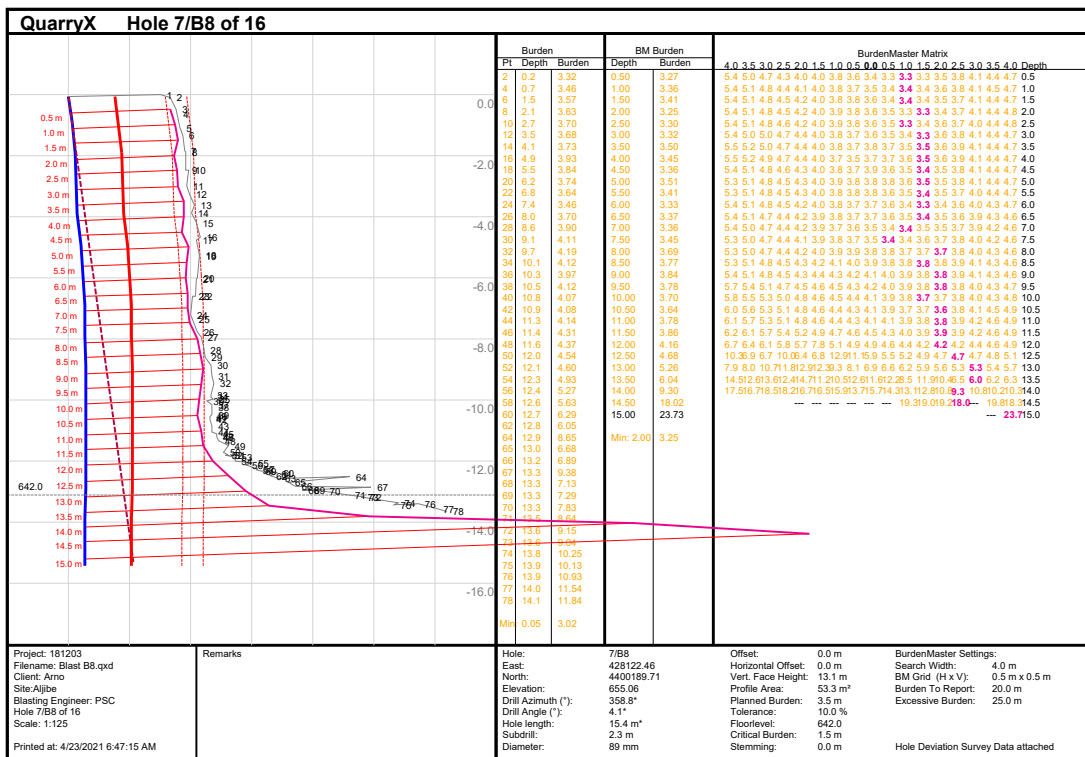
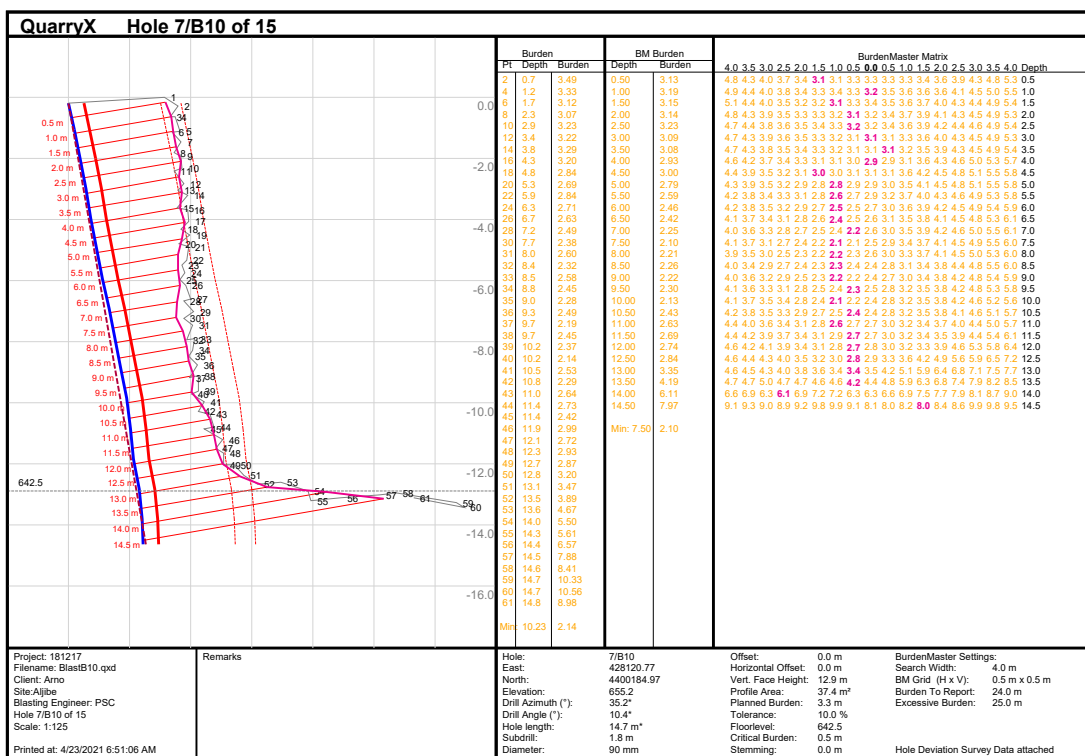


Figure D_3: Burden matrix of blast 8



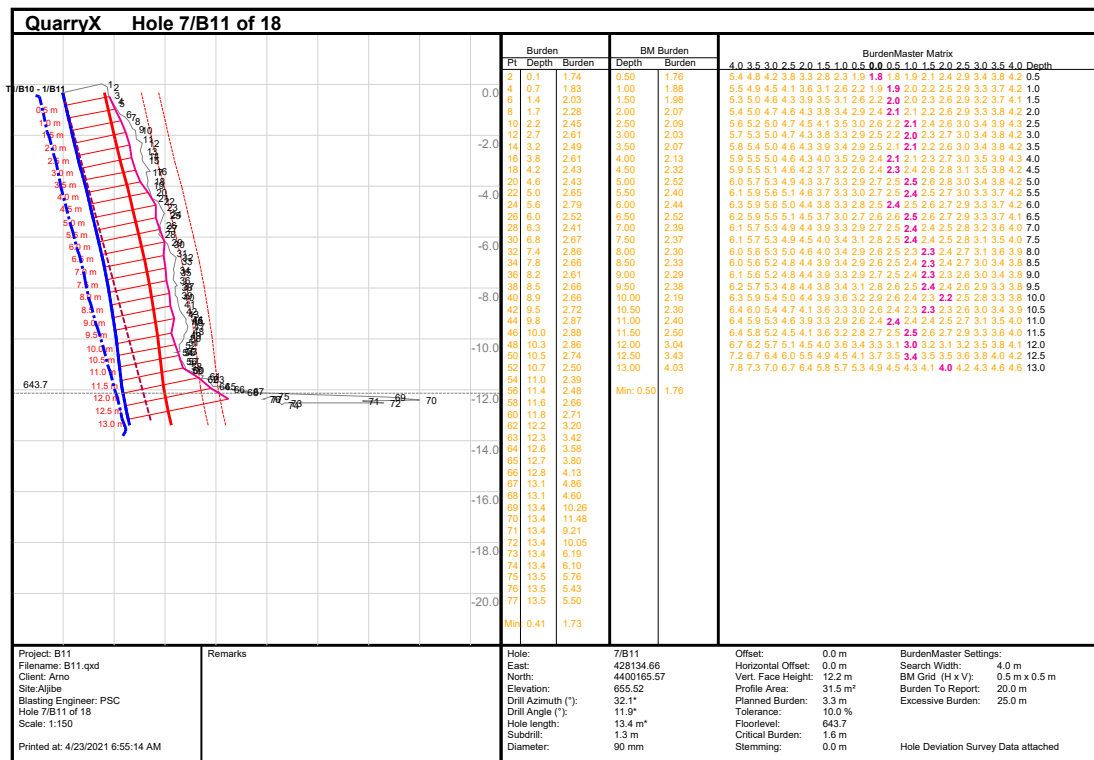


Figure D_5: Burden matrix of blast 11

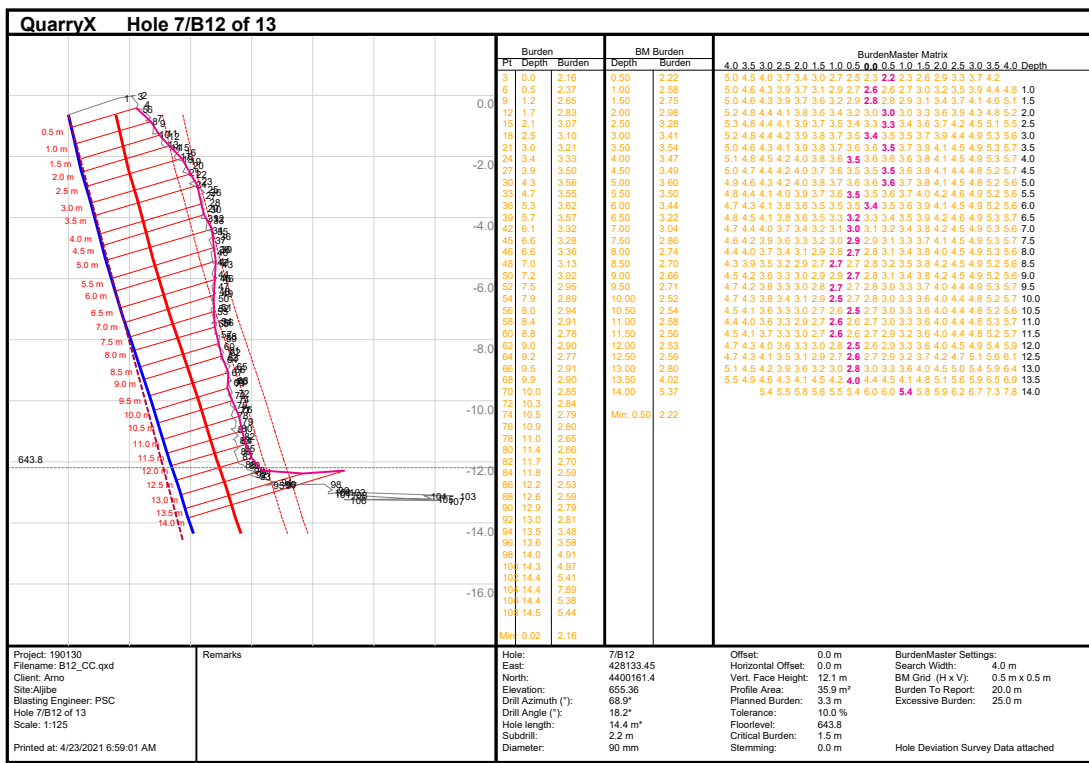


Figure D_6: Burden matrix of blast 12

2 Profiles

QuarryX

Blasting Engineer: PSC
 Client: Arno
 Site: Aljibe
 Hole 5/4 of 18

Project: aa
 Filename: B4_corr.qxd
 Printed at: 5/17/2021 11:13:32 AM
 Scale: 1:125

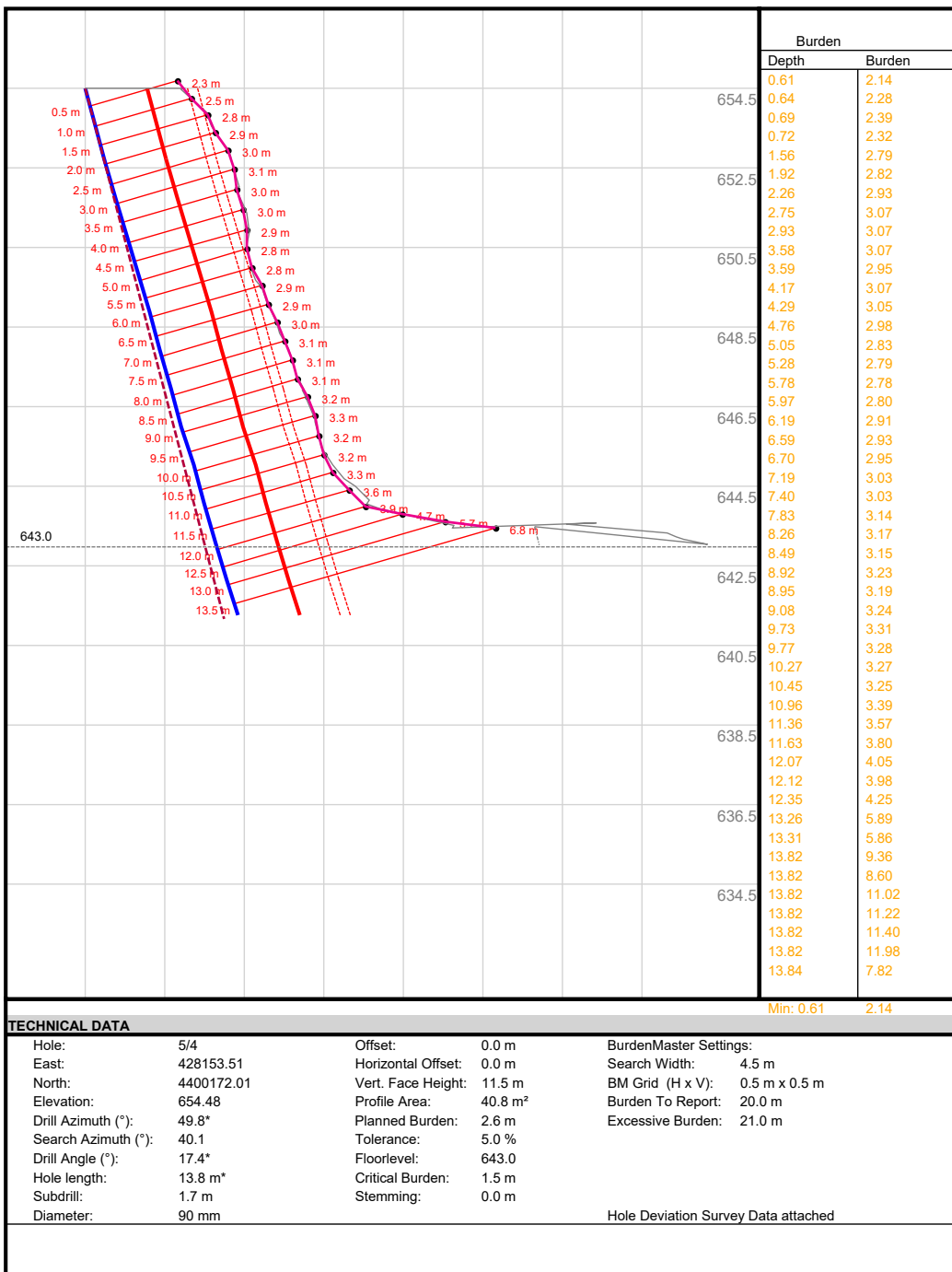


Figure D_7: Profile of blast 4

QuarryX

Blasting Engineer: PSC
 Client: Arno
 Site: Aljibe
 Hole 6/1 of 9

Project: B6
 Filename: B6_corr.qxd
 Printed at: 5/17/2021 12:52:36 PM
 Scale: 1:75

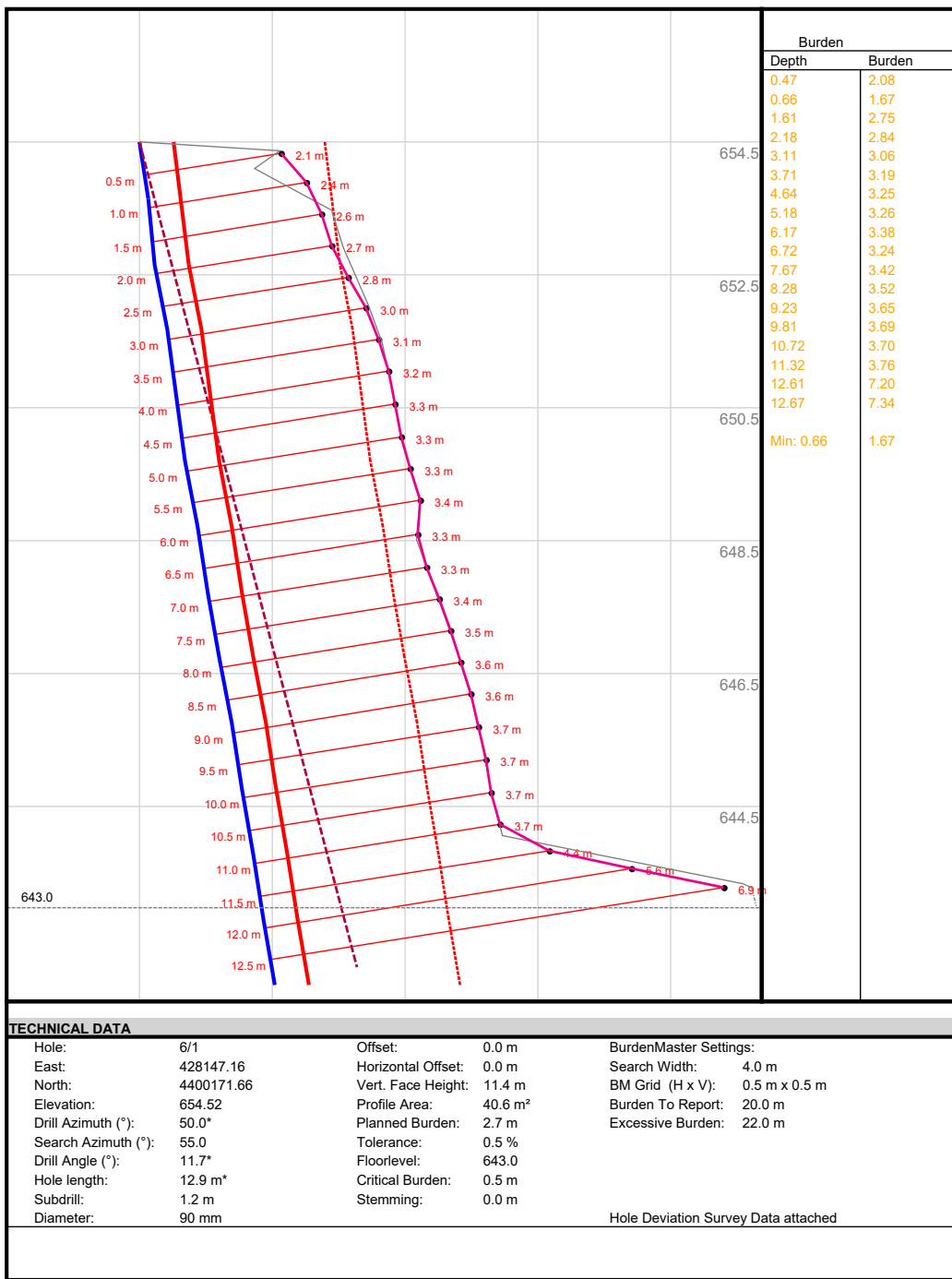


Figure D_8: Profile of blast 6

QuarryX

Blasting Engineer: PSC
 Client: Arno
 Site: Aljibe
 Hole 7/B8 of 16

Project: 181203
 Filename: Blast B8.qxd
 Printed at: 4/23/2021 7:01:07 AM
 Scale: 1:100

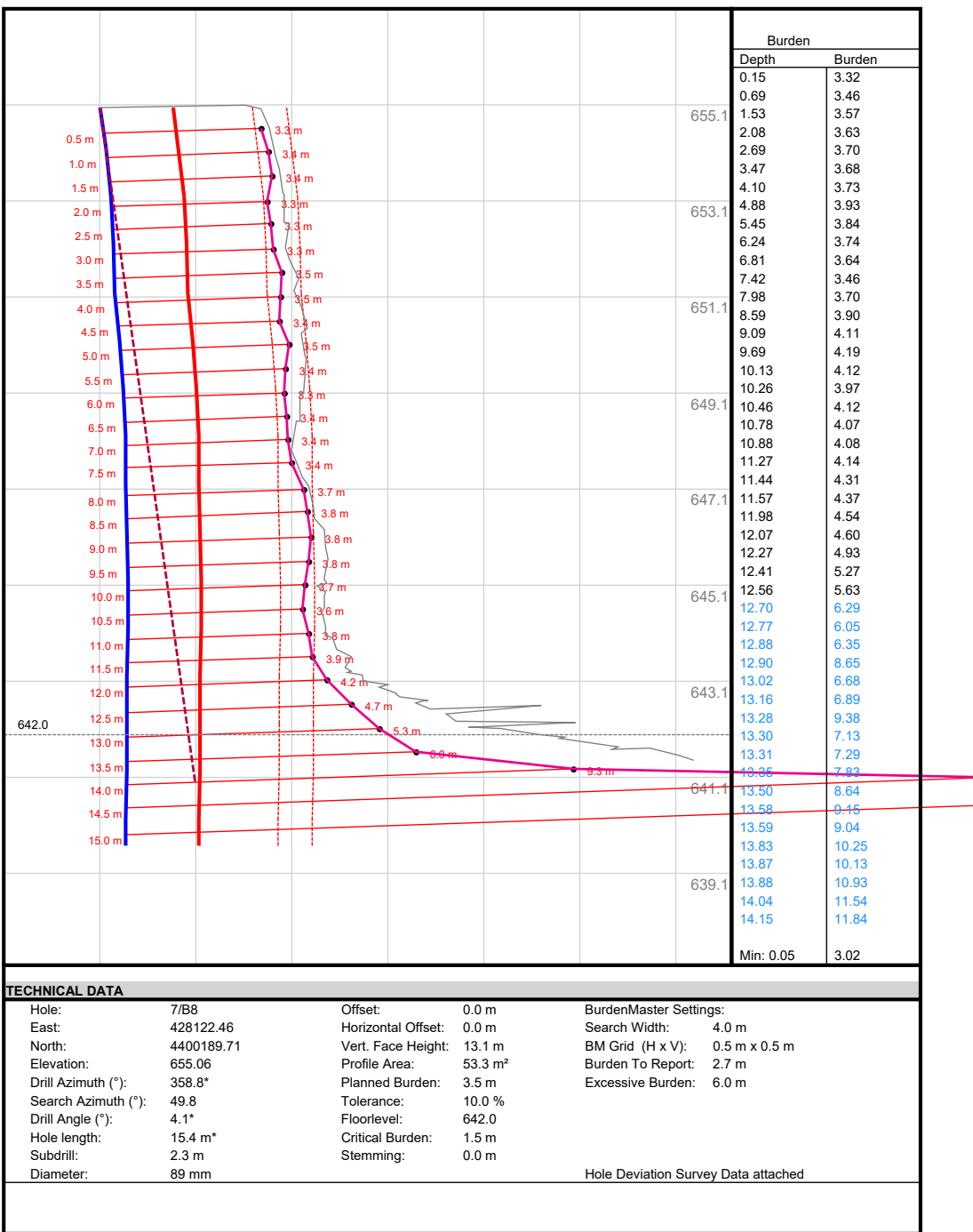


Figure D_9: Profile of blast 8

QuarryX

Blasting Engineer: PSC
 Client: Arno
 Site: Aljibe
 Hole 7/B10 of 15

Project: 181217
 Filename: BlastB10.qxd
 Printed at: 4/23/2021 6:52:37 AM
 Scale: 1:100

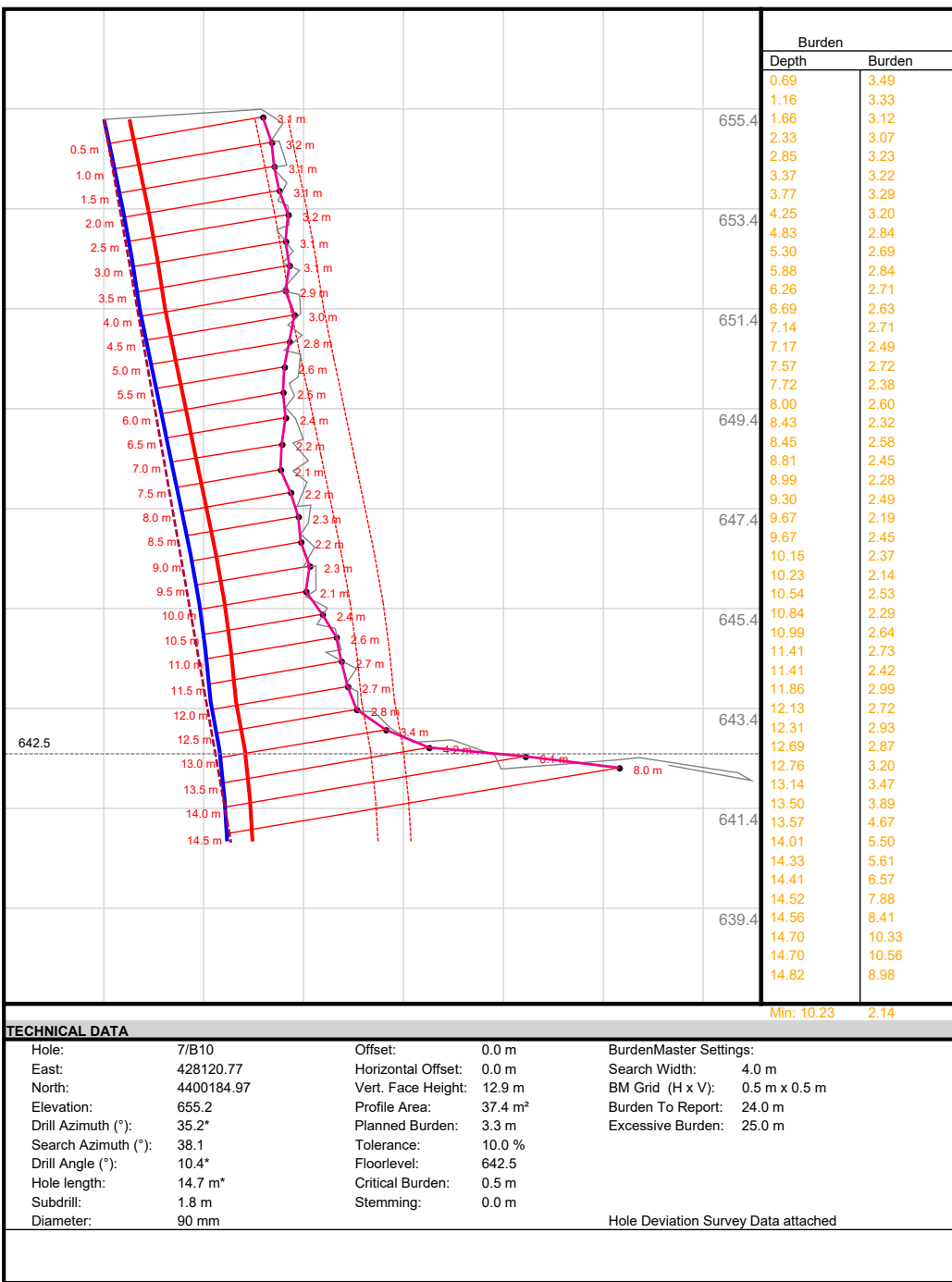


Figure D_10: Profile of blast 10

QuarryX

Blasting Engineer: PSC
 Client: Arno
 Site: Aljibe
 Hole 7/B11 of 18

Project: B11
 Filename: B11.qxd
 Printed at: 4/23/2021 6:55:54 AM
 Scale: 1:125



Figure D_11: Profile of blast 11

QuarryX

Blasting Engineer: PSC
 Client: Arno
 Site: Aljibe
 Hole 7/B12 of 13

Project: 190130
 Filename: B12_CC.qxd
 Printed at: 4/23/2021 7:00:13 AM
 Scale: 1:100

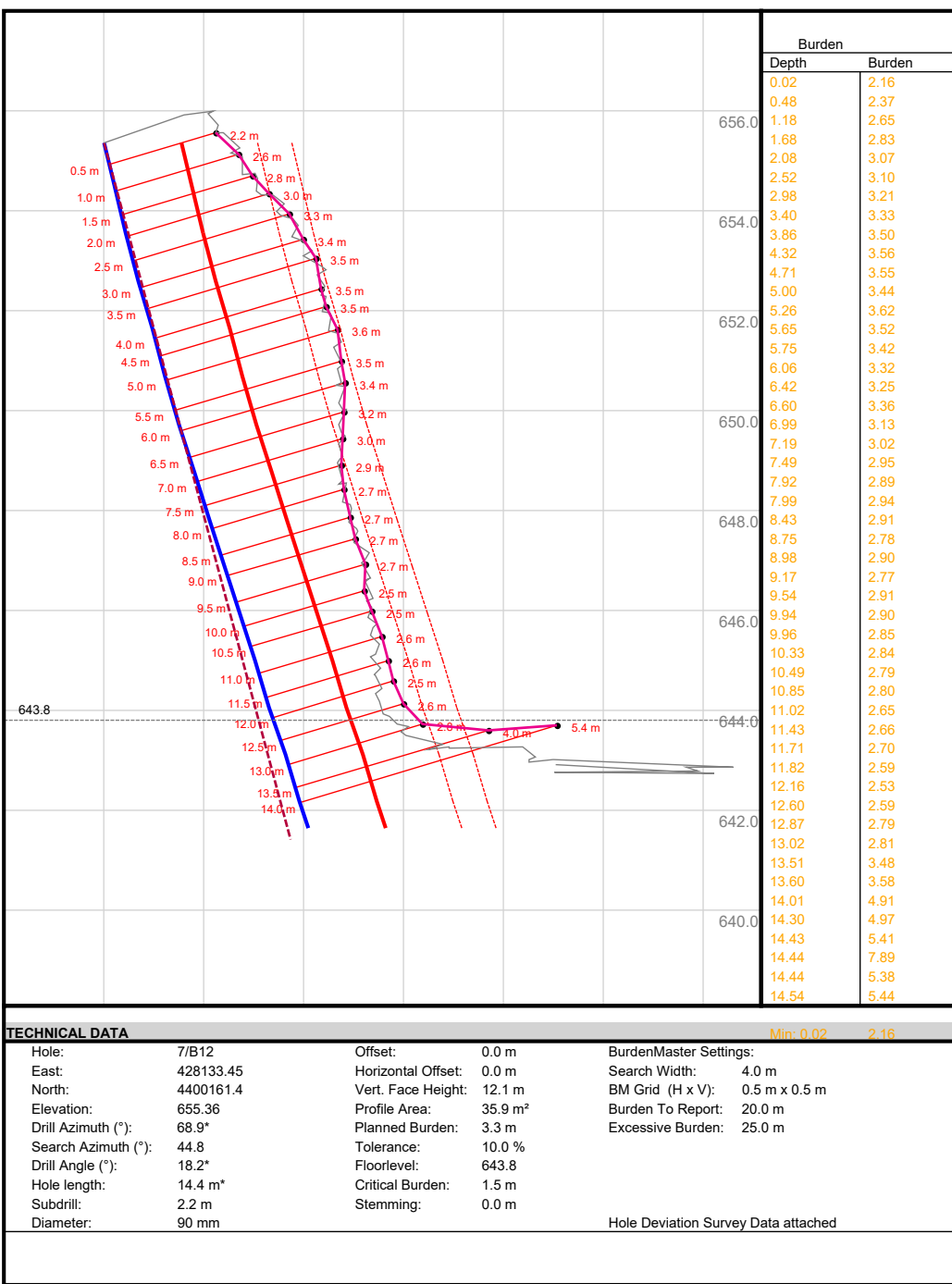


Figure D_12: Profile of blast 12

VIDEO ANALYSIS OF THE BLAST FACE AT THE EL
ALJIBE QUARRY

DOCUMENT 03: APPENDIX E. MATLAB Code

APPENDIX E: MATLAB Code

The codes that have been programmed with the MATLAB software for each blast are shown below. The code used for blast 8 has been chosen, but it can be extrapolated to the rest of the blasts. Except for the analysis of response time, velocity, and its components. In this case, the analysis is shown for the set of all blasts.

1 Main code

```

clear
clc
%% =====
%% == Adjustment code for the transformation matrix of the
CAV ==
%% =====
%% Calculation of the transformation matrix for blasting
blast=8; %Blast to be analysed
str1="B";
str2=string(blast);
str3=".xlsx";
str=strcat(str1,str2,str3); %Name of excel file to open
Ur=xlsread(str,1,'D3:E22').'; %Real coordinates of the
targets (m)
Uc=xlsread(str,1,'B3:C22').'; % Coordinates in the image
(px)
n=size(Ur,2); %Number of targets
x0rangos=[-4 -4 -4 -4 -4 -4;
4 4 4 4 4]; %Range of initial values of the
transformation matrix.
numpar=size(x0rangos,2); %Number of parameters
it=2000; %Number of iterations

aleat=sobolset(numpar,'Skip',1000,'Leap',100);
aleat=scramble(aleat,'MatousekAffineOwen');
x0base=net(aleat,it);
RMSEopt=1e10;
```

```

options = optimset('Display','off');
for jj=1:it
val=[];
x0=[];
RMSE=[];
x0=x0rangos(1,:)+x0base(jj,:).* (x0rangos(2,:)-x0rangos(1,:));
[adj,val,exitflag]=fminsearch(@(x)minf(x,Ur,Uc),x0,options);
;
if exitflag==1
RMSE=sqrt(val/n);
if RMSE<RMSEopt
RMSEopt=RMSE;
disp(['Iteration',num2str(jj),', RMSE =',num2str(RMSEopt)]);
A=[adj(1);adj(2)];
B=[adj(3),adj(4);adj(5),adj(6)];
end
end
end

Urnew=zeros(2,n);
for ii=1:n
Urnew(:,ii)=A+B*Uc(:,ii);
end

err=(Urnew-Ur).^2;

%%Transformation of rock coordinates
t=xlsread(str,2,'A3:A64');
profile=xlsread(str,3,'A3:B36').';
profile(1,:)=36+0.9-profile(1,:);
RockC=xlsread(str,2,'B3:Q64').';
RockR=zeros(size(RockC,1),size(RockC,2));

```

```

for jj=1:size(RockC,1)/2
    for ii=1:size(RockC,2)
        RockR(2*jj-1:2*jj,ii)=A+B*RockC(2*jj-1:2*jj,ii);
    end
end

%% Burdenmatrix (profile) .
load('B8BH7.mat');
ref=B8BH7(1,1:3);
B8BH7(:,1:3)=B8BH7(:,1:3)-B8BH7(1,1:3);
CS=-B8BH7(:,3);
dd = interp1(CS, B8BH7(:,1:3), 0:0.5:CS(end), 'pchip');
ddaux = interp1(CS, B8BH7(:,1:3), 0:0.05:CS(end), 'pchip');

figure
plot3(B8BH7(:,1),B8BH7(:,2),B8BH7(:,3),'.b-');
hold on
plot3(dd(:,1),dd(:,2),dd(:,3),'.r-');
dx=gradient(dd(:,1));
ddx=gradient(dx);
dy=gradient(dd(:,2));
ddy=gradient(dy);
dz=gradient(dd(:,3));
ddz=gradient(dz);
N=[ddx ddy ddz]./vecnorm([ddx ddy ddz],2,2);
T=[dx dy dz]./vecnorm([dx dy dz],2,2);
B=cross(T,N,2)./vecnorm(cross(T,N,2),2,2);
daspect([1 1 1]);

AA1=B(:,2).*N(:,3)-B(:,3).*N(:,2);
BB1=-(B(:,1).*N(:,3)-B(:,3).*N(:,1));
CC1=B(:,1).*N(:,2)-B(:,2).*N(:,1);
DD1=-AA1.*dd(:,1)-BB1.*dd(:,2)-CC1.*dd(:,3);

```

```

P1=[AA1 BB1 CC1];

m=tan(deg2rad(90-49.8));

AA2=-m*ones(size(AA1,1),1);
BB2=ones(size(AA1,1),1);
CC2=zeros(size(AA1,1),1);

P2=[AA2 BB2 CC2];
P1P2=-cross(P1,P2,2);
n1n1=dot(P1,P1,2);
n1n2=dot(P1,P2,2);
n2n2=dot(P2,P2,2);

BM=xlsread('B8.xlsx',3,'E3:U30');

AuxD2=4:-0.5:-4;
Depth=0.5:0.5:14;
CoordBM=cell(numel(Depth),numel(AuxD2));

for kk=1:size(BM,2)
    DD2=zeros(size(AA1,1),1)+AuxD2(kk);
    pp=(((-DD1.*n2n2+DD2.*n1n2)./(n1n1.*n2n2-
    n1n2.^2)).*P1+((-DD2.*n1n1+DD1.*n1n2)./(n1n1.*n2n2-
    n1n2.^2)).*P2;

    for jj=2:size(AA1,1)-2 %From 2 to AA1-2 because the 1st
coord of BM is -0.5 and AA1-2 is the number of depths.
        x0=dd(jj,1); y0=dd(jj,2); z0=dd(jj,3);
        [x,fval] =
fsolve(@(x)myfun(x,pp(jj,:)),dd(jj,:),BM(jj-
1,kk),P1P2(jj,:)),[1 1 1]);
        plot3(x0+x(1)*BM(jj-
1,kk)/sqrt(x(1)^2+x(2)^2+x(3)^2),y0+x(2)*BM(jj-

```

```

1, kk) /sqrt(x(1)^2+x(2)^2+x(3)^2), z0+x(3)*BM(jj-
1, 5) /sqrt(x(1)^2+x(2)^2+x(3)^2), 'og');

CoordBM{jj-1, kk}=[x0+x(1)*BM(jj-
1, kk) /sqrt(x(1)^2+x(2)^2+x(3)^2), y0+x(2)*BM(jj-
1, kk) /sqrt(x(1)^2+x(2)^2+x(3)^2), z0+x(3)*BM(jj-
1, 5) /sqrt(x(1)^2+x(2)^2+x(3)^2)];

hold on
end
end

%Target coordinates (absolute).
World=[124.0499 192.517 654.96;
127.6661 192.397 642.67;
139.1009 203.805 640.9;
135.4279 200.506 640.98;
131.6736 197.242 641.26;
128.02 193.984 642.17;
141.4331 205.666 640.79;
145.2161 208.911 640.98;
149.2511 212.021 641.34;
152.8976 215.492 641.32];

World=World-ref;
plot3(World(:,1),World(:,2),World(:,3),'or');
view(-49.8-90,0);
BMmin=xlsread('B8.xlsx',3,'W3:W30');
Depth=0.5:0.5:14;
Disp=-4:0.5:4;
figure
for ii=1:length(Disp)
    plot(BM(:,ii),Depth);
    hold on
end
hold off
set(gca, 'YDir', 'reverse')

```

```

%%Projection on the plane.

ur=[-cos(atan(m)) -sin(atan(m)) 0]; %tangent vector
n=[m/sqrt(m^2+1) -1/sqrt(m^2+1) 0]; %normal vector
uz=cross(ur,n);
matrix=[ur.' n.' uz.']; %base matrix
wproj=cell(size(AA1,1)-1,size(BM,2));
transf=cell(size(AA1,1)-1,size(BM,2));
for kk=1:size(BM,2)
    for jj=2:size(AA1,1)-2
        wproj{jj-1,kk}=CoordBM{jj-1,kk}-dot(CoordBM{jj-1,kk},n,2).*n;
        Aux=(matrix\wproj{jj-1,kk}).';
        transf{jj-1,kk}=[Aux(1) Aux(3)];
        if kk==5
            plot(Aux(1),Aux(3),'r.')
        else
            plot(Aux(1),Aux(3),'g.')
        end
        hold on
    end
end
clear Aux

for ii=1:size(World,1)
    Worldp(ii,:)=World(ii,:)-dot(World(ii,:),n,2).*n;
    Aux=(matrix\Worldp(ii,:)).';
    Worldt(ii,:)=Aux;
    plot(Aux(1),Aux(3),'bo')
end
ref=Worldt(end,[1 3]);
clear Aux
grid on
hold off

```

```

%% PROFILE
perfil=cell2mat(CoordBM(:, 9));
XX=perfil(:, 1);
YY=perfil(:, 2);
F=fit(XX, YY, 'poly1'); %y=p1*x+p2
p1=F.p1;

figure
vtang=[-cos(atan(p1)) -sin(atan(p1)) 0];
vnorm=[p1/sqrt(p1^2+1) -1/sqrt(p1^2+1) 0];
vbin=cross(vtang,vnorm);
cbase=[vtang.' vnorm.' vbin.']; % Matrix change of base,
tangent and normal vector
PRF=(cbase\perfil.')';
plot(PRF(:,1),PRF(:,3),'-og','LineWidth',1.5)
grid on

%%TRAJECTORIES
t_video=[1.0175 1.016875 1.015 1.01475 1.013125 1.0125
1.010625 1];
D=[0.58 0.56 0.5 0.43 0.46 0.44 0.45 0.41]; %fragment size
col=colormap(lines);
figure
for jj=1:(size(RockR,1)/2)
    Aux=RockR(2*jj-1:2*jj,:);
    TF=isnan(Aux);
    H=any(TF, 'all');
    if H==1
        [~,idx]=find(TF==1,1, 'first');
        Aux(:,idx:end)=[];
        taux=t(1:idx-1);
    else
        taux=t(1:end);
    end
end

```

```

taux(1)=t_video(jj);
k=[taux(:,1)'; Aux(1,:); Aux(2,:)];
[vinic,fval(jj),exitflag(jj)]=fminsearch(@(x)
funveloc2(x,k,D(jj)),[-10 10]); %obtains the initial
velocities to minimise error

v0(jj,:)=vinic;
vv0(jj,:)=sqrt((v0(jj,1))^2+(v0(jj,2))^2);
angv0(jj,:)=-rad2deg(atan(v0(jj,2)/v0(jj,1)));
XX=funtrayec2(vinic,k,D(jj));
solM{1,jj}=[XX(:,1)+ref(1) XX(:,2)+ref(2)];
plot(XX(:,1),XX(:,2),'-','Color',col(jj,:))
hold on
plot(Aux(1,:),Aux(2,:),'.','Color',col(jj,:))

end
grid on
hold off

%%RESPONSE TIME
d1=zeros(size(RockR,1)/2,size(RockR,2)); %distance 1
d2=zeros(size(RockR,1)/2,size(RockR,2)); %distance 2

for jj=1:(size(RockR,1)/2)-1
    Aux=RockR(2*jj-1:2*jj,:); %Coordinates
    taux=[t_video(jj) t(2:end)']; %times
    weights=1./(taux-t(1)).^2; %weights (-tflash)
    x0=Aux(1,1);
    y0=Aux(2,1);
    d1(jj,:)=[0 cumsum(vecnorm(diff(Aux,1,2),2,1))]; %cumulative distance
    d2(jj,:)=vecnorm(Aux-Aux(:,1),2,1); %distance from each point to the starting point
    % Remove NaN values
    idnan=isnan(d2(jj,:));
    TT=taux(~idnan);

```

```

Dist=d1(jj,~idnan);
W=weights(~idnan);

%Index

id=[1 3:numel(TT)-19];

%tiempo de respuesta
[betat0(jj,:),fval(jj),exitflag(jj)]=fmincon(@(x)
fundist4(x,TT(id),x0,y0,D(jj),Dist(id),W(id)),
[-5 5 1.01],[],[],[],[-20 -20 t(1)], [20 20 t(2)]);
t0(jj)=betat0(jj,3);

tresp(jj)=t0(jj)-t(1); %tinitial-tflash
plot(TT(id),Dist(id),'o','Color',col(jj,:))
hold on
grid on
plot(betat0(jj,3):0.01:TT(id(end)),%
fundist3(betat0(jj,:),betat0(jj,3):0.01:TT(id(end)),x0,y0,
D(jj)),'-','Color',col(jj,:))
title('BLAST 8')
xlabel('Time')
ylabel('Distance')
end
hold off

figure
for jj=1:(size(RockR,1)/2)-1
Aux=RockR(2*jj-1:2*jj,:); %Coordinates
taux=[t_video(jj) t(2:end)']; %Times
weights=1./ (taux-1).^2; %Weights (-tflash)
k=[taux(1,:); Aux(1,:); Aux(2,:)];
YY=funtrayec2(betat0(jj,1:2),k,D(jj));
plot(YY(:,1),YY(:,2),'-', 'Color',col(jj,:))
grid on

```

```

hold on
plot(Aux(1,:),Aux(2,:),'.' , 'Color', col(jj,:))
end
hold off

%%PARAMETERS FOR FRAGMENTS

%Minimum distance from the first point of each trajectory to
those of the BM and its position in the table
for jj=1:size(RockR,1)/2
solR(2*jj-1:2*jj,:)=[RockR(2*jj-1,:)+ref(1);
RockR(2*jj,:)+ref(2)]; %Transform RockR into system ref BM-
2D
end
Mind=reshape(solR(:,1),2,size(solR,1)/2);
for ii=1:size(Mind,2)
Dist=zeros(size(CoordBM,1),size(CoordBM,2));
for jj=1:size(CoordBM,1)
for kk=1:size(CoordBM,2)
Dist(jj,kk)=sqrt(sum((Mind(:,ii).'-
transf{jj,kk}).^2));
end
end
[MINBM(ii),~]=min(min(Dist,[],1));
[row,col]=find(Dist==MINBM(ii));
Pos(:,ii)=[row;col];
end

% Absolute coordinates of the BM points closest to the first
point of the rock trajectory
NPoints=zeros(8,2);
for ii=1:size(Pos,2)
NPoints(ii,:)=transf{Pos(1,ii),Pos(2,ii)};
end

```

```

% FRAGMENT HEIGHT (Hf)
% Height of the bench at which the fragment is ejected
% bench height -> from bottom of borehole
h=CS(end); % length of borehole
for jj=1:size(NPoints,1)
    Hf(jj)=h+NPoints(jj,2); %with respect to the ground
end

% FRAGMENT BURDEN (Bf)
for jj=1:size(NPoints,1)
    Bf(jj)=-NPoints(jj,1);
end

% ANGLE FROM THE BH TO THE FRAGMENT (HORIZONTAL PLANE x)
% tg β=Δx/Δy
for ii=1:8
    beta(1,ii)=rad2deg(atan(solM{1,ii}(1,1)./solM{1,ii}(1,2)));
    %Error using atan2 - Not enough input arguments
end

%% 3D MODEL
Absolute coordinates of the BM points closest to the first
point of the rock trajectory
NPoints2=zeros(8,3);
for ii=1:size(Pos,2)
    NPoints2(ii,:)=CoordBM{Pos(1,ii),Pos(2,ii)};
end

% Minimum distance to the trajectory of the borehole.
[~,A]=min(pdist2(ddaux,NPoints2),[],1);
for ii=1:numel(A)
    incr(ii,:)=NPoints2(ii,:)-ddaux(A(ii),:);
    ms(ii)=tan(incr(ii,2)./incr(ii,1));
    angl(ii)=rad2deg(atan(incr(ii,2)./incr(ii,1)));
end

```

```
% Angular difference and rotation.
dang=angl-(90-49.8);
for ii=1:8
    solM{1,ii}=[-solM{1,ii}{:,1}.*cos(deg2rad(90-49.8)) - 
    solM{1,ii}{:,1}.*sin(deg2rad(90-49.8)) 
    solM{1,ii}{:,2}]*rotz(-dang(ii));
end

figure
plot3(B8BH7(:,1),B8BH7(:,2),B8BH7(:,3),'b-');
hold on
plot3(dd(:,1),dd(:,2),dd(:,3),'r-');
daspect([1 1 1]);
for kk=1:size(BM,2)
    DD2=zeros(size(AA1,1),1)+AuxD2(kk);
    pp=(-DD1.*n2n2+DD2.*n1n2)./(n1n1.*n2n2-
    n1n2.^2).*P1+((-DD2.*n1n1+DD1.*n1n2)./(n1n1.*n2n2-
    n1n2.^2)).*P2;
    for jj=2:size(AA1,1)-2
        x0=dd(jj,1); y0=dd(jj,2); z0=dd(jj,3);
        [x,fval] =
        fsolve(@(x)myfun(x,pp(jj,:)),dd(jj,:),BM(jj-
        1,kk),P1P2(jj,:)),[1 1 1]);
        plot3(x0+x(1)*BM(jj-
        1,kk)/sqrt(x(1)^2+x(2)^2+x(3)^2),y0+x(2)*BM(jj-
        1,kk)/sqrt(x(1)^2+x(2)^2+x(3)^2),z0+x(3)*BM(jj-
        1,5)/sqrt(x(1)^2+x(2)^2+x(3)^2),'og');
        hold on
    end
end
plot3(World(:,1),World(:,2),World(:,3),'or');

col=colormap(lines);
for ii=1:7
```

```

plot3(solM{1,ii}{:,1},solM{1,ii}{:,2},solM{1,ii}{:,3}, 'o', '
Color',col(ii,:))

end

view(-49.8-90,0);

set(gca, 'XLabel', []);
set(gca, 'YLabel', []);
set(gca, 'ZLabel', []);

%% PARAMETER CORRELATION

% Determine variable statistics
data(:,1)=tresp'; %response time
data(8,1)=NaN;
data(:,2)=angv0'; %Ejection angle
data(:,3)=beta; %Angle with the line defined by the targets
data(:,4)=vv0; %Initial velocity
data(:,5)=Hf; %Relative position, height
data(:,6)=Bf; %Burden
stats=[mean(data);std(data);std(data)./mean(data);min(data)
;max(data)]; %col3=variation coef.
col_header={'','tresp' '(s)', 'alpha' '(–s)', 'beta'
('–s)', 'v0 (m/s)', 'Hf (m)', 'B (m)'};
row_header={'mean','std','CV','min','max'}';
table_stat=[col_header;[row_header,num2cell(stats)]];

% CORRELATIONS

figure
corrplot(data,'type','Spearman','testR','on','varNames',{ 't
resp','alpha','beta','v0','Hf','B'})'

[H,p]=corr(data,'type','Spearman'); % H are values of R, p
is the pvalue

Function: minf

function H = minf(x,Ur,Uc)
A=[x(1);x(2)];
B=[x(3),x(4);x(5),x(6)];

```

```

n=size(Ur,2);
transf=zeros(2,n);
for ii=1:n
    transf(:,ii)=(Ur(:,ii)-A-B*Uc(:,ii)).^2;
end
H=sum(sum(transf,1));
end

```

2 Function: myfun

```

function F = myfun(x,pp,p0,B,P1P2)
F = [pp(1)-p0(1)-(B./sqrt(x(1).^2+x(2).^2+x(3).^2)).*(x(1)-
P1P2(1));
      pp(2)-p0(2)-(B./sqrt(x(1).^2+x(2).^2+x(3).^2)).*(x(2)-
P1P2(2));
      pp(3)-p0(3)-(B./sqrt(x(1).^2+x(2).^2+x(3).^2)).*(x(3)-
P1P2(3))];
end

```

3 Function: funveloc2

```

function err=funveloc2(x,k,D)

%Constants for all trajectories
g=9.81; %gravity
da=1.1614; % air density
S=pi*(D/2).^2; %D=fragment size
m=2721*(4/3)*pi*(D/2).^3; %fragment mass
mu=18.46e-6; % μ coefficient viscosity (air)

%Constants for each rock
tt=k(1,:);
xx=k(2,:);
yy=k(3,:);
x0=k(2,1);
y0=k(3,1);

```

```

% Unknowns
v0x=x(1);
v0y=x(2);

% TIMES
st1=tt(2)-tt(1);
st2=tt(3)-tt(2);
st=st2/100;

Q1=fix(st1/st);
R1=mod(st1,st);
tcal=[tt(1) linspace(tt(1)+R1,tt(2)-st,Q1)
      tt(2):st:(tt(end)+1)];

x=zeros(1,numel(tcal));
y=zeros(1,numel(tcal));
vx=zeros(1,numel(tcal));
vy=zeros(1,numel(tcal));
ax=zeros(1,numel(tcal));
ay=zeros(1,numel(tcal));

[~,idt]=ismembertol(tt,tcal,1e-8);

% EQUATIONS
for i=1:numel(tcal)
    if i==1
        vx(i)=v0x;
        vy(i)=v0y;
        mv(i)=sqrt(vx(i).^2+vy(i).^2);
        Re(i)=da*D*mv(i)/mu;

Cd(i)=(24./Re(i))+((2.6.*Re(i)./5))./(1+(Re(i)./5).^1.52))
+((0.411.*Re(i)./26300).^(-7.94))./(1+(Re(i)./263000).^(-
8)))+((Re(i).^0.08)./461000);
    end
end

```

```

fr(i)=(0.5*da*Cd(i)*S)/m;
ax(i)=-fr(i)*vx(i)*mv(i);
ay(i)=-g-fr(i)*vy(i)*mv(i);
x(i)=x0;
y(i)=y0;

else
    vx(i)=vx(i-1)+ax(i-1)*(tcal(i)-tcal(i-1));
    vy(i)=vy(i-1)+ay(i-1)*(tcal(i)-tcal(i-1));
    mv(i)=sqrt(vx(i).^2+vy(i).^2);
    Re(i)=da*D*mv(i)/mu;

Cd(i)=(24./Re(i))+((2.6.*Re(i)./5))./(1+(Re(i)./5).^1.52))
+((0.411.*Re(i)./26300).^(-7.94))./(1+(Re(i)./263000).^(-
8))+(Re(i).^0.08)./461000;
fr(i)=(0.5*da*Cd(i)*S)/m;
ax(i)=-fr(i)*vx(i)*mv(i);
ay(i)=-g-fr(i)*vy(i)*mv(i);
x(i)=x(i-1)+vx(i)*(tcal(i)-tcal(i-1));
y(i)=y(i-1)+vy(i)*(tcal(i)-tcal(i-1));
end
end
xn=x(idt);
yn=y(idt);
err=sum(sqrt((xn-k(2,:)).^2+(yn-k(3,:)).^2))/numel(tt);
end

```

4 Function: funtrayect2

```

function X=funtrayec2(x,k,D)

%Constants for all trajectories
g=9.81; %gravity
da=1.1614; %air density
S=pi()*(D/2).^2; %D=fragment size
m=2721*(4/3)*pi*(D/2).^3; %fragment mass
mu=18.46e-6; %μ coefficient viscosity (air)

```

```
%Constants for each rock
tt=k(1,:);
xx=k(2,:);
yy=k(3,:);
x0=k(2,1);
y0=k(3,1);

%Unknowns
v0x=x(1);
v0y=x(2);

%TIMES
st1=tt(2)-tt(1);
st2=tt(3)-tt(2);
st=st2/100;

Q1=fix(st1/st);
R1=mod(st1,st);
tcal=[tt(1) linspace(tt(1)+R1,tt(2)-st,Q1)
      tt(2):st:(tt(end)+1)];

x=zeros(1,numel(tcal));
y=zeros(1,numel(tcal));
vx=zeros(1,numel(tcal));
vy=zeros(1,numel(tcal));
ax=zeros(1,numel(tcal));
ay=zeros(1,numel(tcal));

[~,idt]=ismembertol(tt,tcal,1e-8);

% EQUATIONS
for i=1:numel(tcal)
    if i==1
        vx(i)=v0x;
```

```

vy(i)=v0y;
mv(i)=sqrt(vx(i).^2+vy(i).^2);
Re(i)=da*D*mv(i)/mu;

Cd(i)=(24./Re(i))+((2.6.*Re(i)./5))./(1+(Re(i)./5).^1.52))
+((0.411.*Re(i)./26300).^(-7.94))./(1+(Re(i)./263000).^(-
8)))+((Re(i).^0.08)./461000);

fr(i)=(0.5*da*Cd(i)*S)/m;
ax(i)=-fr(i)*vx(i)*mv(i);
ay(i)=-g-fr(i)*vy(i)*mv(i);
x(i)=x0;
y(i)=y0;

else
    vx(i)=vx(i-1)+ax(i-1)*(tcal(i)-tcal(i-1));
    vy(i)=vy(i-1)+ay(i-1)*(tcal(i)-tcal(i-1));
    mv(i)=sqrt(vx(i).^2+vy(i).^2);
    Re(i)=da*D*mv(i)/mu;

    Cd(i)=(24./Re(i))+((2.6.*Re(i)./5))./(1+(Re(i)./5).^1.52))
+((0.411.*Re(i)./26300).^(-7.94))./(1+(Re(i)./263000).^(-
8)))+((Re(i).^0.08)./461000);

    fr(i)=(0.5*da*Cd(i)*S)/m;
    ax(i)=-fr(i)*vx(i)*mv(i);
    ay(i)=-g-fr(i)*vy(i)*mv(i);
    x(i)=x(i-1)+vx(i)*(tcal(i)-tcal(i-1));
    y(i)=y(i-1)+vy(i)*(tcal(i)-tcal(i-1));

end
end
X=[x(idt); y(idt)]';
end

```

5 Function: fundist3

```

function d=fundist3(x,t,x0,y0,D) %Distances
%Constants for all trajectories
g=9.81; %gravity

```

```

da=1.1614; %air density
S=pi()*(D/2).^2; %D=fragment size
m=2721*(4/3)*pi*(D/2).^3; %fragment mass
mu=18.46e-6; %μ coefficient viscosity (air)

%Unknowns
v0x=x(1);
v0y=x(2);
t0=x(3);

%Times
d=zeros(1,numel(t));
for jj=1:numel(t)

if t(jj)>t0
    tcal=t0:0.001:t(jj);
    x=zeros(1,numel(tcal));
    y=zeros(1,numel(tcal));
    vx=zeros(1,numel(tcal));
    vy=zeros(1,numel(tcal));
    ax=zeros(1,numel(tcal));
    ay=zeros(1,numel(tcal));
    Re=zeros(1,numel(tcal));
    mv=zeros(1,numel(tcal));
    Cd=zeros(1,numel(tcal));
    fr=zeros(1,numel(tcal));
    dist=zeros(1,numel(tcal));

    for i=1:numel(tcal)
        if i==1
            vx(i)=v0x;
            vy(i)=v0y;
            mv(i)=sqrt(vx(i).^2+vy(i).^2);
            Re(i)=da*D*mv(i)/mu;
        else
            vx(i)=vx(i-1)+ax(i-1)*dt;
            vy(i)=vy(i-1)+ay(i-1)*dt;
            mv(i)=sqrt(vx(i).^2+vy(i).^2);
            Re(i)=da*D*mv(i)/mu;
        end
        Cd(i)=Cdc*(1+(Re(i)/Re_c)^2);
        fr(i)=Cd(i)*(vx(i).^2+vy(i).^2);
        dist(i)=sqrt((x(i)-x0)^2+(y(i)-y0)^2);
    end
end

```

```

Cd(i)=(24./Re(i))+((2.6.*Re(i)./5))./(1+(Re(i)./5).^1.52))
+((0.411.*Re(i)./26300).^(-7.94))./(1+(Re(i)./263000).^(-
8)))+((Re(i).^0.08)./461000);

fr(i)=(0.5*da*Cd(i)*S)/m;
ax(i)=-fr(i)*vx(i)*mv(i);
ay(i)=-g-fr(i)*vy(i)*mv(i);
x(i)=x0;
y(i)=y0;
dist(i)=0;

else
    vx(i)=vx(i-1)+ax(i-1)*(tcal(i)-tcal(i-1));
    vy(i)=vy(i-1)+ay(i-1)*(tcal(i)-tcal(i-1));
    mv(i)=sqrt(vx(i).^2+vy(i).^2);
    Re(i)=da*D*mv(i)/mu;

Cd(i)=(24./Re(i))+((2.6.*Re(i)./5))./(1+(Re(i)./5).^1.52))
+((0.411.*Re(i)./26300).^(-7.94))./(1+(Re(i)./263000).^(-
8)))+((Re(i).^0.08)./461000);

fr(i)=(0.5*da*Cd(i)*S)/m;
ax(i)=-fr(i)*vx(i)*mv(i);
ay(i)=-g-fr(i)*vy(i)*mv(i);
x(i)=x(i-1)+vx(i)*(tcal(i)-tcal(i-1));
y(i)=y(i-1)+vy(i)*(tcal(i)-tcal(i-1));
dist(i)=dist(i-1)+sqrt((x(i)-x(i-
1)).^2+(y(i)-y(i-1)).^2);

end
end
d(jj)=dist(end);

elseif t(jj)<t0
    tcal=t(jj):0.001:t0;
    x=zeros(1,numel(tcal));
    y=zeros(1,numel(tcal));

```

```

vx=zeros(1,numel(tcal));
vy=zeros(1,numel(tcal));
ax=zeros(1,numel(tcal));
ay=zeros(1,numel(tcal));
Re=zeros(1,numel(tcal));
mv=zeros(1,numel(tcal));
Cd=zeros(1,numel(tcal));
fr=zeros(1,numel(tcal));
dist=zeros(1,numel(tcal));

for i=1:numel(tcal)
    if i==1
        vx(i)=v0x;
        vy(i)=v0y;
        mv(i)=sqrt(vx(i).^2+vy(i).^2);
        Re(i)=da*D*mv(i)/mu;

        Cd(i)=(24./Re(i))+((2.6.*Re(i)./5))./(1+(Re(i)./5).^1.52))
        +((0.411.*Re(i)./26300).^(-7.94))./(1+(Re(i)./263000).^(-
        8)))+((Re(i).^0.08)./461000);
        fr(i)=(0.5*da*Cd(i)*S)/m;
        ax(i)=-fr(i)*vx(i)*mv(i);
        ay(i)=-g-fr(i)*vy(i)*mv(i);
        x(i)=x0;
        y(i)=y0;
        dist(i)=0;
    else
        vx(i)=vx(i-1)+ax(i-1)*(tcal(i)-tcal(i-1));
        vy(i)=vy(i-1)+ay(i-1)*(tcal(i)-tcal(i-1));
        mv(i)=sqrt(vx(i).^2+vy(i).^2);
        Re(i)=da*D*mv(i)/mu;

        Cd(i)=(24./Re(i))+((2.6.*Re(i)./5))./(1+(Re(i)./5).^1.52))
    end
end

```

```

+((0.411.*Re(i)./26300).^(-7.94))./(1+(Re(i)./263000).^(-
8)))+((Re(i).^0.08)./461000);

fr(i)=(0.5*da*Cd(i)*S)/m;
ax(i)=-fr(i)*vx(i)*mv(i);
ay(i)=-g-fr(i)*vy(i)*mv(i);
x(i)=x(i-1)+vx(i)*(tcal(i)-tcal(i-1));
y(i)=y(i-1)+vy(i)*(tcal(i)-tcal(i-1));
dist(i)=dist(i-1)+sqrt((x(i)-x(i-
1)).^2+(y(i)-y(i-1)).^2);

end
end
d(jj)=dist(end);

else
d(jj)=0;
end
end
end

```

6 Function: fundist4

```

function err=fundist4(x,t,x0,y0,D,Dist,W) % minimising the
error sum

%Constants for all trajectories
g=9.81; %gravity
da=1.1614; %air density
S=pi()*(D/2).^2; %D=fragment size
m=2721*(4/3)*pi*(D/2).^3; %fragment mass
mu=18.46e-6; %μ coefficient viscosity (air)

%Unknowns
v0x=x(1);
v0y=x(2);
t0=x(3);

%TIMES
d=zeros(1,numel(t));

```

```

for jj=1:numel(t)

if t(jj)>t0
    tcal=t0:0.001:t(jj);
    x=zeros(1,numel(tcal));
    y=zeros(1,numel(tcal));
    vx=zeros(1,numel(tcal));
    vy=zeros(1,numel(tcal));
    ax=zeros(1,numel(tcal));
    ay=zeros(1,numel(tcal));
    Re=zeros(1,numel(tcal));
    mv=zeros(1,numel(tcal));
    Cd=zeros(1,numel(tcal));
    fr=zeros(1,numel(tcal));
    dist=zeros(1,numel(tcal));

    for i=1:numel(tcal)
        if i==1
            vx(i)=v0x;
            vy(i)=v0y;
            mv(i)=sqrt(vx(i).^2+vy(i).^2);
            Re(i)=da*D*mv(i)/mu;

Cd(i)=(24./Re(i))+((2.6.*Re(i)./5))./(1+(Re(i)./5).^1.52))
+((0.411.*Re(i)./26300).^(-7.94))./(1+(Re(i)./263000).^(-
8)))+((Re(i).^0.08)./461000);

fr(i)=(0.5*da*Cd(i)*S)/m;
ax(i)=-fr(i)*vx(i)*mv(i);
ay(i)=-g-fr(i)*vy(i)*mv(i);
x(i)=x0;
y(i)=y0;
dist(i)=0;

else
    vx(i)=vx(i-1)+ax(i-1)*(tcal(i)-tcal(i-1));

```

```

vy(i)=vy(i-1)+ay(i-1)*(tcal(i)-tcal(i-1));
mv(i)=sqrt(vx(i).^2+vy(i).^2);
Re(i)=da*D*mv(i)/mu;

Cd(i)=(24./Re(i))+((2.6.*Re(i)./5))./(1+(Re(i)./5).^1.52))
+((0.411.*Re(i)./26300).^(-7.94))./(1+(Re(i)./263000).^(-
8)))+((Re(i).^0.08)./461000);

fr(i)=(0.5*da*Cd(i)*S)/m;
ax(i)=-fr(i)*vx(i)*mv(i);
ay(i)=-g-fr(i)*vy(i)*mv(i);
x(i)=x(i-1)+vx(i)*(tcal(i)-tcal(i-1));
y(i)=y(i-1)+vy(i)*(tcal(i)-tcal(i-1));
dist(i)=dist(i-1)+sqrt((x(i)-x(i-
1)).^2+(y(i)-y(i-1)).^2);

elseif t(jj)<t0
    tcal=t(jj):0.001:t0;
    x=zeros(1,numel(tcal));
    y=zeros(1,numel(tcal));
    vx=zeros(1,numel(tcal));
    vy=zeros(1,numel(tcal));
    ax=zeros(1,numel(tcal));
    ay=zeros(1,numel(tcal));
    Re=zeros(1,numel(tcal));
    mv=zeros(1,numel(tcal));
    Cd=zeros(1,numel(tcal));
    fr=zeros(1,numel(tcal));
    dist=zeros(1,numel(tcal));

    for i=1:numel(tcal)
        if i==1

```

```

vx(i)=v0x;
vy(i)=v0y;
mv(i)=sqrt(vx(i).^2+vy(i).^2);
Re(i)=da*D*mv(i)/mu;

Cd(i)=(24./Re(i))+((2.6.*Re(i)./5))./(1+(Re(i)./5).^1.52))
+((0.411.*Re(i)./26300).^(-7.94))./(1+(Re(i)./263000).^(-
8))+(Re(i).^0.08)./461000);

fr(i)=(0.5*da*Cd(i)*S)/m;
ax(i)=-fr(i)*vx(i)*mv(i);
ay(i)=-g-fr(i)*vy(i)*mv(i);
x(i)=x0;
y(i)=y0;
dist(i)=0;

else
    vx(i)=vx(i-1)+ax(i-1)*(tcal(i)-tcal(i-1));
    vy(i)=vy(i-1)+ay(i-1)*(tcal(i)-tcal(i-1));
    mv(i)=sqrt(vx(i).^2+vy(i).^2);
    Re(i)=da*D*mv(i)/mu;

Cd(i)=(24./Re(i))+((2.6.*Re(i)./5))./(1+(Re(i)./5).^1.52))
+((0.411.*Re(i)./26300).^(-7.94))./(1+(Re(i)./263000).^(-
8))+(Re(i).^0.08)./461000);

fr(i)=(0.5*da*Cd(i)*S)/m;
ax(i)=-fr(i)*vx(i)*mv(i);
ay(i)=-g-fr(i)*vy(i)*mv(i);
x(i)=x(i-1)+vx(i)*(tcal(i)-tcal(i-1));
y(i)=y(i-1)+vy(i)*(tcal(i)-tcal(i-1));
dist(i)=dist(i-1)+sqrt((x(i)-x(i-
1)).^2+(y(i)-y(i-1)).^2);
end
end
d(jj)=dist(end);

else

```

```

d(jj)=0;
end
end
err=sum(W.* (Dist-d).^2);
end

```

7 Analysis of response time, initial velocity and ejection angle (α)

```

clear
clc

%% ADJUSTMENT ANALYSIS RESPONSE TIME
%B4-B12
Proced=xlsread('Analisis_trespyv0.xlsx',7,'A2:Q8');
blast=Proced(:,1);
BHnum=Proced(:,2);
BHh=Proced(:,3);
frag=Proced(:,4);
Bf=Proced(:,5);
Hf=Proced(:,6);
Cp=Proced(:,7);
D=Proced(:,8);
tresp=Proced(:,9);
v0z=Proced(:,10);
v0y=Proced(:,11);
tflash=Proced(:,12);
t1=Proced(:,13);
q=Proced(:,14);
H=Proced(:,15);
alpha=Proced(:,16);

v=sqrt(v0z.^2+v0y.^2);
alpha=deg2rad(alpha);

```

```
% Discard fragments that are outside the range [cinf-csup]
and are NaN

k1=[Bf Hf];
k2=[Bf Hf Cp D];
idnan=isnan(tresp(:,1));
idneg=tresp<=0;
id=(idnan | idneg);
tresp(id,:)=[];
v0z(id,:)=[];
v0y(id,:)=[];
v(id,:)=[];
k1(id,:)=[];
k2(id,:)=[];
alpha(id,:)=[];

% MEANS

k1mean=mean(k1);
trespmean=mean(tresp*1000); %ms
vmean=mean(v);

%% RESPONSE TIME ANALYSIS ADJUSTMENT

% k1=[Bf Hf];

%ADJUSTMENT Function 9 - tresp=B^a+H^k
f=@(x,k1) k1(:,1).^x(1)+k1(:,2).^x(2);
[beta1,resid1,[],CovB1,MSE1]=nlinfit(k1,(tresp*1000),f,[0.1
0.1]);
err1=sqrt(diag(CovB1)); %standard error
intert1=abs(beta1')./err1; %tstat
pvalue1=tcdf(-intert1,numel(tresp)-length(beta1));
cil=nlparci(beta1,resid1,'covar',CovB1,'alpha',0.1);
sstot1=sum(((tresp*1000)-mean(tresp*1000)).^2);
ssres1=sum(resid1.^2);
R2_1=1-ssres1/sstot1;
```

```
% ADJUSTMENT Function 15 - tresp=(B/Cp)^a+(H/D)^k
g=@(x,k2)
(k2(:,1)./k2(:,3)).^x(1)+(k2(:,2)./k2(:,4)).^x(2);
[beta2,resnom2,resid2,exitflag2]=lsqcurvefit(g,[1
1],k2,(tresp*1000));
sstot2=sum(((tresp*1000)-mean(tresp*1000)).^2);
ssres2=sum(resid2.^2);
R2_2=1-ssres2/sstot2;

%% VELOCITY ANALYSIS ADJUSTMENT
% k1=[Bf Hf./H];
% ADJUSTMENT Own Function - V=(aH^2+bH+c)B^d
h=@(x,k1)
(x(1).*k1(:,2).^2+x(2).*k1(:,2)+x(3)).*k1(:,1).^x(4);
[beta3,resid3,[],CovB3,MSE3]=nlinfit(k1,v,h,[1 1 1 1]);
err3=sqrt(diag(CovB3)); % Standard error
intert3=abs(beta3')./err3; %tstat
pvalue3=tcdf(-intert3,numel(v)-length(beta3));
ci3=nlparci(beta3,resid3,'covar',CovB3,'alpha',0.1);
sstot3=sum((v)-mean(v)).^2;
ssres3=sum(resid3.^2);
R2_3=1-ssres3/sstot3;

%ADJUSTMENT Own Function - V=a*H^2+b*H+c
j=@(x,k1) x(1).*k1(:,2).^2+x(2).*k1(:,2)+x(3);
[beta6,resid6,[],CovB6,MSE6]=nlinfit(k1,v,j,[1 1 1]);
err6=sqrt(diag(CovB6)); %Standard error
intert6=abs(beta6')./err6; %tstat
pvalue6=tcdf(-intert6,numel(v)-length(beta6));
ci6=nlparci(beta6,resid6,'covar',CovB6,'alpha',0.1);
sstot6=sum((v)-mean(v)).^2;
ssres6=sum(resid6.^2);
R2_6=1-ssres6/sstot6;
```

```

%% ANALYSIS EJECTION ANGLE ( $\alpha$ )
% ADJUSTMENT Own Function -  $\sin(\alpha) = v_0 y / ((aH^2 + bH + c) B^d)$ 
% k1=[Bf Hf./H v0y];
l=@(x,k1)
k1(:,3)./(x(1).*k1(:,2).^2+x(2).*k1(:,2)+x(3)).*k1(:,1).^x
(4))
[beta5,resid5,[],CovB5,MSE5]=nlinfit(k1,sin(alpha),l,[1 1 1
1]);
sstot5=sum(((sin(alpha))-mean(sin(alpha))).^2);
ssres5=sum(resid5.^2);
R2_5=1-ssres5/sstot5;

% ADJUSTMENT Own Function -  $\sin(\alpha) = v_0 y / ((aH^2 + bH + c) B^d)$ 
% k1=[Bf Hf./H v0y];
l=@(x,k1)
k1(:,3)./(x(1).*k1(:,2).^2+x(2).*k1(:,2)+x(3)).*k1(:,1).^x
(4))
[beta4,resid4,[],CovB4,MSE4]=nlinfit(k1,sin(alpha),l,[1 1 1
1]);
sstot4=sum(((sin(alpha))-mean(sin(alpha))).^2);
ssres4=sum(resid4.^2);
R2_4=1-ssres4/sstot4;

% ADJUSTMENT Own Function -  $\cos(\alpha) = v_0 z / ((aH^2 + bH + c) B^d)$ 
% k1=[Bf Hf./H v0z];
m=@(x,k1)
k1(:,3)./(x(1).*k1(:,2).^2+x(2).*k1(:,2)+x(3)).*k1(:,1).^x
(4))
[beta7,resid7,[],CovB7,MSE7]=nlinfit(k1,cos(alpha),m,[1 1 1
1]);
sstot7=sum(((cos(alpha))-mean(cos(alpha))).^2);
ssres7=sum(resid7.^2);
R2_7=1-ssres7/sstot7;

```

8 Correlations

```

clear
clc

%% ADJUSTMENT. CORRELATIONS
%B4-B12
Proced=xlsread('Correlaciones',1,'A2:Q45');
% Discard fragments that are outside the [cinf-csup] range
and are NaN
idnan=isnan(Proced(:,9));
idneg=Proced(:,9)<=0;
id=(idnan | idneg);
Proced(id,:)=[];

blast=Proced(:,1);
BHnum=Proced(:,2);
BHh=Proced(:,3);
frag=Proced(:,4);
Bf=Proced(:,5);
Hf=Proced(:,6);
Cp=Proced(:,7);
D=Proced(:,8);
tresp=Proced(:,9);
v0x=Proced(:,10);
v0y=Proced(:,11);
tflash=Proced(:,12);
t1=Proced(:,13);
q=Proced(:,14);
angv0=Proced(:,15);
beta=Proced(:,16);

v0=sqrt(v0x.^2+v0y.^2);

%% PARAMETER CORRELATION

```

```
% Determine variable statistics
data(:,1)=tresp; %Response time
data(:,2)=angv0; %Ejection angle
data(:,3)=beta; %Angle with the line defined by the targets
data(:,4)=v0; %Initial velocity
data(:,5)=Hf; %Relative position. Height
data(:,6)=Bf; %Burden
stats=[mean(data);std(data);std(data)./mean(data);min(data)
;max(data)]; %col3=variation coef.
col_header={'','tresp' '(s)', 'alpha' '(–s)', 'beta' '(–s)', 'v0 (m/s)', 'Hf (m)', 'B (m)'};
row_header={'mean','std','CV','min','max'}';
table_stat=[col_header;[row_header,num2cell(stats)]];
```

% CORRELATIONS

```
figure
corrplot(data,'type','Spearman','testR','on','varNames',{ 't
resp','alpha','beta','v0','Hf','B'})
```

[H,p]=corr(data,'type','Spearman'); %H are values of R, p is pvalue

9 Azimuth calculation

```
% Coordinates.
World=[150.25    169.52    654.63
151.69    174.11    644.16
154.55    175.62    642.89
158.98    177.94    642.54
162.51    179.62    642.55
166.6     183.54    642.58
170.84    185.34    642.57
174.76    189.01    643.37];
```

```
World=World-World(1,:);
x=World(:,1); y=World(:,2); z=World(:,3);
plot(x,y,'.');
```

```
daspect([1 1 1])
```

```
% Adjusting a straight line
```

```
F=fit(x,y,'poly1');
```

```
az=90-atand(F.p1);
```

10 Initial velocity as a quadratic function

```
h_b4=[11.71 11.26 7.86 6.25 5.21 2.25]./13.25.*100;
```

```
b_b4=[3.17 3.41 4.37 4.97 5.63 7.87];
```

```
v_b4=[20.45 24.45 27.00 26.86 26.23 16.91];
```

```
h_b6=[12.09 11.02 7.70 6.66 5.32 3.16]./12.69.*100;
```

```
b_b6=[2.11 2.86 4.02 4.08 4.48 5.05];
```

```
v_b6=[15.12 19.64 18.12 17.05 16.40 14.19];
```

```
h_b8=[13.90 12.86 11.01 10.06 8.87 7.87 6.37  
4.90]./15.36.*100;
```

```
b_b8=[3.90 3.74 4.16 4.14 4.04 3.93 4.09  
3.95];
```

```
v_b8=[10.47 11.21 12.41 11.83 11.49 8.66 6.04  
5.87];
```

```
h_b10=[14.03 12.95 11.63 10.03 9.00 7.29 5.51  
3.44]./14.46.*100;
```

```
b_b10=[3.37 3.61 3.79 3.80 3.88 3.69 4.10  
4.63];
```

```
v_b10=[7.13 9.30 11.09 13.19 14.21 15.39 14.12  
10.76];
```

```
h_b11=[11.87 10.41 8.60 6.25 5.45 4.57  
2.82]./14.15.*100;
```

```
b_b11=[4.15 5.22 5.53 6.00 5.83 5.86 6.19];
```

```
v_b11=[12.00 12.60 13.67 13.94 12.79 10.45 6.13];
```

```

h_b12=[13.74      11.92      9.23      7.83      6.69      4.97      4.01
3.30]./13.72.*100;
b_b12=[2.25  3.81      5.25      5.26      5.01      5.20      5.32
5.53];
v_b12=[7.02  6.95      7.12      8.11      8.03      6.06      5.21
3.55];

```

```

fprb1=fittype('a+b*x+c*x^2','ind','x');
opts=fitoptions('Method','NonlinearLeastSquares','Robust','
off','StartPoint',[1 1 1]);
[f_b4,gf_b4,o]=fit((h_b4)',(v_b4'),fprb1,opts);
fprb1=fittype('a+b*x+c*x^2','ind','x');
opts=fitoptions('Method','NonlinearLeastSquares','Robust','
off','StartPoint',[1 1 1]);
[f_b6,gf_b6,o]=fit((h_b6)',(v_b6'),fprb1,opts);
fprb1=fittype('a+b*x+c*x^2','ind','x');
opts=fitoptions('Method','NonlinearLeastSquares','Robust','
off','StartPoint',[1 1 1]);
[f_b8,gf_b8,o]=fit((h_b8)',(v_b8'),fprb1,opts);
fprb1=fittype('a+b*x+c*x^2','ind','x');
opts=fitoptions('Method','NonlinearLeastSquares','Robust','
off','StartPoint',[1 1 1]);
[f_b10,gf_b10,o]=fit((h_b10)',(v_b10'),fprb1,opts);
fprb1=fittype('a+b*x+c*x^2','ind','x');
opts=fitoptions('Method','NonlinearLeastSquares','Robust','
off','StartPoint',[1 1 1]);
[f_b11,gf_b11,o]=fit((h_b11)',(v_b11'),fprb1,opts);
fprb1=fittype('a+b*x+c*x^2','ind','x');
opts=fitoptions('Method','NonlinearLeastSquares','Robust','
off','StartPoint',[1 1 1]);
[f_b12,gf_b12,o]=fit((h_b12)',(v_b12'),fprb1,opts);

```

```
figure
hold on
plot(h_b4,v_b4,'b*')
plot(h_b6,v_b6,'r*')
plot(h_b8,v_b8,'g*')
plot(h_b10,v_b10,'m*')
plot(h_b11,v_b11,'k*')
plot(h_b12,v_b12,'c*')

plot(f_b4,'--b')
plot(f_b6,'--r')
plot(f_b8,'--g')
plot(f_b10,'--m')
plot(f_b11,'--k')
plot(f_b12,'--c')
ylabel('Initial velocity (m/s)')
xlabel('Rock height/Bench height (%)')
xlim([10 100])
legend('B4','B6','B8','B10','B11','B12')
```